Spectroscopic Signatures of Isomerization

by

Joshua Herschel Goldblum Baraban

B.S./M.S. Yale University (2006)

Submitted to the Department of Chemistry
in partial fulfillment of the requirements for the degree of

Doctor of Philosophy

at the

MASSACHUSETTS INSTITUTE OF TECHNOLOGY

September 2013

© Massachusetts Institute of Technology 2013. All rights reserved.

Author .....
Department of Chemistry
July 22, 2013

Certified by .....
Robert W. Field
Haslam and Dewey Professor of Chemistry
Thesis Supervisor

Accepted by .....
Robert W. Field
Chairman, Departmental Committee on Graduate Students

This doctoral thesis has been examined by a Committee of the Department of Chemistry as follows:

Professor Robert G. Griffin .....
Chairman, Thesis Committee

Professor Troy Van Voorhis .....
Member, Thesis Committee

Professor Robert W. Field .....
Thesis Supervisor

Spectroscopic Signatures of Isomerization

by

Joshua Herschel Goldblum Baraban

Submitted to the Department of Chemistry
on July 22, 2013, in partial fulfillment of the
requirements for the degree of
Doctor of Philosophy

Abstract

This thesis explores spectroscopic signatures of isomerization, especially new patterns that emerge and report on chemically relevant portions of the potential energy surface, such as the transition state. The most important new pattern discovered is the "isomerization dip", a sharp decrease in the vibrational level spacings, or effective frequency, in modes that project along the reaction coordinate as the transition state is approached. A pattern-breaking perturbation, a K-staggering analogous to a tunneling splitting, is also found in barrier-proximal states. These concepts are demonstrated by the experimental and theoretical analysis of *cis-trans* isomerization in S_1 acetylene (C_2H_2), including the near complete observation and assignment of the level structure from the potential minimum up to the transition state energy. The $\tilde{A}$-$\tilde{X}$ spectrum has been recorded in supersonic jets and molecular beams by laser induced fluorescence and H atom action detection, using double resonance techniques where appropriate to access and simplify portions of the S_1 manifold. Two major *ab initio* calculations have been undertaken to aid in understanding the experimental results, both relying on high-level electronic structure calculations. The large-amplitude dynamics and delocalized wavefunctions of the isomerizing system have been investigated by a reduced dimension discrete variable representation calculation. The anharmonic force fields of both conformers have been calculated by vibrational perturbation theory, and that of the *trans* conformer determined by fitting an effective Hamiltonian to the observed levels. The analysis of these results has led us to propose a method for extracting the transition state energy, and potentially other characteristics, from the frequency domain spectrum.

Thesis Supervisor: Robert W. Field
Title: Haslam and Dewey Professor of Chemistry

Acknowledgments

I would like to thank my advisor, Bob Field, for all of his encouragement and support, and for a wonderful time in his research group. Bob deserves the credit for my growth as a scientist over the last 6 years, and I know that his behind the scenes contributions to my graduate school experience far outnumber those that I'm aware of explicitly. I always enjoyed our discussions of science, spectroscopy and molecules, and I learned a lot from his advice, not to mention his *menschlich* example. I couldn't have asked for a better research supervisor, who granted and fostered independence, while also providing opportunities. Many of the group theses I've read acknowledge an unusual virtue of Bob's; mine is that he is a connoisseur of children's books, a hobby that benefited my kids and me. Thank you, Bob.

Prof. John Stanton (UT-Austin) was practically my second advisor, especially for the theoretical aspects of my graduate work. Ever since I asked John my first question, collaborating with him has been fantastic - fun, helpful, and enlightening on a wide variety of topics. I'm also grateful to John for hosting me a number of times in sunny Austin, and those visits certainly catalyzed a lot of the progress made in this thesis.

Prof. Anthony Merer (UBC, IAMS) is behind all the recent advances in understanding the $\tilde{A}$-$\tilde{X}$ band system of C_2H_2, and the work in this thesis is no exception. It was a privilege to collaborate with him, and interacting with him taught me a great deal. I can only hope I absorbed a small fraction of his attention to detail, perseverance, and simultaneous command of so many aspects of a research problem.

Dr. Adam Steeves preceded me on the S_1 acetylene project, launched me on the study of the *cis-trans* isomerization problem, and provided excellent and much-appreciated mentoring until his graduation. Since then he has continued to provide much sage advice, and the results and insights from his thesis work are the foundation for what I have accomplished.

My main co-workers during graduate school were three undergraduate students (UROPs): Annelise Beck, Bryan Changala, and Julia Berk.

Annelise Beck was already a veteran Field group UROP when I arrived. We worked together on the beginnings of the apparatus used for the experiments described in this thesis, as well as on the DVR calculations, in the short time before she graduated.

Bryan Changala merits special mention. He started out with the sort of work undergraduates usually do, but he quickly became a full-fledged partner in all aspects of the research process, due to his incredible array of talents and his dedication. I was extremely fortunate to work with Bryan for almost 4 years, during which time he not only played an instrumental role in much of the work in this thesis, but also branched out to his own independent contributions towards our overarching goal. It has been a great pleasure to work alongside him, and I wish him the best of luck in graduate school and beyond.

Julia Berk joined the project close to the end of my time at MIT, but nevertheless took part in some of the late-breaking developments. She put in a tremendously helpful effort recording, processing and assigning spectra, and I'm also grateful to her for not being afraid to question our old ingrained lab habits.

My Field group "class" consisted of Tony Colombo, Barratt Park, Yan Zhou, David Grimes (once removed?), and Josh Middaugh (Green group). I'd like to thank them all because, among many other things, I really enjoyed working with them. Tony and Barratt were my neighbors in the middle section of the office, and I could consistently turn to them for a thoughtful opinion, a helping hand, or a good joke. Yan and David and I frequently swapped experimental tips, optics, other parts, or just wildly different perspectives. Josh brought an engineering viewpoint that was good to have around, and I often consulted him (after Tony, usually) when a responsible, practical opinion was deemed necessary.

Many other Field group members, past and present, contributed to my graduate school experience in one way or another. Thanks very much to Prof. Wilton Virgo, Dr. Kyle Bittinger, Dr. Kirill Kuyanov-Prozument, Dr. Hans Bechtel, Dr. Mike McCarthy, Dr. Steve Coy, Prof. Kevin Lehmann, Dr. Vladimir Petrović, Rachel Shaver, Monika Ciuba, Jun Jiang, Peter Richter, and Prof. Pat Vaccaro. Peter Giunta de-

serves special thanks for keeping everything running smoothly. Thank you as well to many collaborators on matters large and small: Dr. Jon Hougen, Prof. Mark Child, Bernadette Broderick, Prof. Arthur Suits, Prof. John Muenter, Asaf Shimshovitz, Prof. David Tannor, Kai Golibrzuch, Dr. Pranav Shirhatti, Prof. Alec Wodtke, Devin Matthews, Dr. Takatoshi Ichino, Dr. Michael Harding, Danielle Larese, Prof. Francesco Iachello, Dr. Neil Reilly, and Dr. Sharly Fleischer.

Funding for this project came from the U. S. Department of Energy. I also received a National Science Foundation Graduate Research Fellowship, and I am particularly grateful for support from the David A. Johnson Fellowship.

I'd like to thank Scott Wade, the Chemistry building manager, for his receptive ear and prompt attention to our perennial problems in the Building 6 basement. Dr. Gang Liu (Electronics Repair) saved me on several occasions by repairing irreplaceable equipment, and inevitably taught me something about how things work and/or how to fix them. Andy Gallant (Central Machine Shop) patiently helped me design, refine and fix any number of pieces of lab equipment.

I want to thank my family for everything - my parents, brothers, and in-laws all helped out in many tangible and intangible ways. Last, but certainly not least, a heartfelt thank you to my wife Mara, and to our children Ayelet, Meena, and Moshe.

Contents

List of Figures

List of Tables

Chapter 1

Introduction

Chemical reactions consist of three parts: reactants, products, and whatever happens in between. While tools for studying reactants, products, and even intermediates are well developed, information about the reaction pathways through phase space is usually inferred rather than directly measured. A convenient simplification is to construct a potential energy surface for the reacting system, whereby points can be characterized topographically. Minima and horizontal asymptotes correspond to reactants, products, and intermediates, while local maxima and saddle points separate the distinct chemical species. Saddle points, often referred to "transition states", are of particular importance for reaction kinetics because they lie at the highest point on the lowest energy path from reactants to products. Despite their importance, transition states have not been amenable to study by the techniques that yield detailed information about the minima. The goal of this thesis, in the broadest sense, is to address this chemical problem by answering a double-ended spectroscopic question - how does the presence of an energetically accessible reaction pathway affect the spectrum of a molecule and can we characterize that path, particularly the transition state, from information contained in the spectrum?

Spectroscopy and patterns are inextricably linked. Obtaining information from any spectral feature is predicated on placing it in some context, so that its characteristics (position, intensity, width, lineshape) can be interpreted. In most cases, much or all of this process is automatic; in other words, the experimentalist has prior

knowledge of what paradigm pertains to the spectrum to be studied. For example, the chemistry student who records an infrared spectrum knows that the peaks observed correspond to bond vibrations, and can then use that information to identify the molecules present in the sample. Even in advanced applications of spectroscopy, the basic model that should be applied to the data is not often in doubt, once the spectrum has been recorded and assigned. Perhaps the main reason for this is that simple quantum mechanical problems solved long ago (to list a few: the hydrogen atom, harmonic and Morse oscillators, rigid rotor) provide the basis for understanding the spectra associated with electronic, vibrational, and rotational degrees of freedom, respectively.

When we consider the spectroscopy of chemically reactive systems, however, we find ourselves in uncharted territory. The simplest chemically relevant problem, an asymmetric double minimum, cannot easily be considered as an extension of any of the classic quantum mechanical examples, especially in the region of interest proximal to the transition state. The approach taken in this work has been to examine the spectrum of a prototypical molecule capable of isomerization, beginning at the lower minimum and progressing upwards in energy towards the transition state. In the course of this investigation, the limits of traditional spectroscopic models are reached and new models are developed out of necessity, which turn out to be intimately related to the properties of the transition state.

It is important to note that our primary goal is new *understanding* of a spectrum and what information it contains about molecular dynamics. Higher sensitivity and resolution, often benchmarks of spectroscopic success, may be prerequisites but not necessarily sufficient to learn something qualitatively new. Similarly, in theoretical calculations or modeling of data, the focus is on matching experiment with sufficient precision in order to understand what the spectrum is telling us. Recognizing a new spectroscopic pattern and its meaning is a process that requires examining a large and varied data set in great detail. A challenge of this approach is that it is not possible to predict what new results will translate into "progress" and outline a specific, long-term research plan or experimental design in advance. The research direction of this

thesis therefore consisted of constant evaluation of our current understanding of the patterns in the spectrum and their meaning. The individual research units described in the chapters outlined below were conceived and carried out on an almost *ad hoc* basis, according to our assessment at any given time. Only in hindsight does it appear that they led along a clear path from the initial questions to the final conclusions.

1.1 Thesis Outline

- The remainder of this Introduction provides some background on our system of choice, S_1 C_2H_2, the first singlet electronically excited state of acetylene, and the *cis-trans* isomerization it supports. The essential experimental elements used in this work are also briefly described.

- Chapter 2 documents the first experimental observation of *cis* S_1 C_2H_2, along with the evidence for this unexpected assignment, given the forbidden nature of the $\tilde{A}\ ^1A_2 \leftarrow \tilde{X}\ ^1\Sigma_g^+$ electronic transition. A surprising K-staggering is found in the rotational structure of the *cis* $3^1 6^1$ vibrational level, somewhat analogous to the well-known tunneling splitting in NH_3.

- Chapter 3 describes a reduced dimension Discrete Variable Representation (DVR) calculation performed to calculate the energy levels and wavefunctions of S_1 C_2H_2, intended to explore whether the effects of isomerization could lead to the appearance of S_1 *cis* levels in the spectrum. Other aspects of *cis-trans* interactions were also investigated using the results of the calculation, which was the first *ab initio* work to use a level of theory adequate to obtain accurate agreement with experiment for all of the vibrational frequencies.

- Chapter 4 contains the analysis of infrared-ultraviolet (IR-UV) double resonance laser induced fluorescence (LIF) experiments that accessed the *ungerade* vibrational states of S_1 C_2H_2 from $45800 - 46550$ cm^{-1}. Several new subbands of transitions to *cis* levels were observed, in addition to a significant new portion of the *trans* vibrational manifold.

- Chapter 5 reports experimental and *ab initio* anharmonic force fields of the *cis* and *trans* conformers of S_1 C_2H_2, based partially on the data collected in Chapter 4. Building on these force fields, it is possible to model the entire *trans* vibrational manifold simultaneously, instead of piecemeal. The results of this global fit point to extensions of the model that enable incorporation of vibrational levels that are significantly affected by the isomerization. This eventually leads to an understanding of the effect of the transition state on the spectrum, discussed in the following chapter.

- Chapter 6 identifies a new spectroscopic pattern that heralds the approach to the transition state, a dip in the effective vibrational frequency that appears at the saddle point energy. This concept is justified theoretically and used to explain the unusual vibrational level structure of *trans* S_1 C_2H_2 at high vibrational excitation. It is further proposed that this dip phenomenon is quite general for saddle points on potential energy surfaces, and could be used to extract the important input parameters to transition state theory from experimental spectra.

- Chapter 7 presents spectra and assignments in the near-barrier region of S_1 C_2H_2, detected either by LIF or by H atom action resonantly enhanced multiphoton ionization (REMPI) spectroscopy. Particularly noteworthy are the K-staggering rotational perturbations, which become increasingly common and large in magnitude as the transition state energy is approached.

1.2 Acetylene

Before providing some necessary background on the relevant electronic states of acetylene, it seems appropriate to explain briefly why this molecule is a good candidate for investigating the core questions of this thesis. If all of the states of the reacting system are to be spectroscopically accessible, it is necessary for the system to be completely bound, which requires a non-bond-breaking unimolecular isomerization. (We

will see, however, that there is a strong relationship between the spectroscopic patterns found in dissociative and non-dissociative chemical processes.) As a tetratomic, acetylene is one of the smallest molecules that can support a conformational change between qualitatively different shapes, making it appropriate for our purposes. Other convenient characteristics include that it is a permanent gas, and its linear symmetric structure composed of light atoms simplifies the spectrum. Consequently, acetylene has been the object of many physical chemistry and spectroscopic studies too numerous to list, and the wealth of information available in the literature makes it yet more attractive for new experiments and calculations.

The following is intended to introduce some salient features of spectroscopic study of the *cis-trans* isomerization in S_1 C_2H_2. The topics touched on here are expanded upon, with references to the literature, where appropriate in subsequent chapters. For those new to the subject, the series of papers by Ingold and King [1] is a good place to begin.

1.2.1 S_0 and S_1 C_2H_2

The S_0 $\tilde{X}$ $^1\Sigma_g^+$ ground electronic state of acetylene is a linear, closed shell, centrosymmetric molecule, containing a C≡C triple bond. Its five vibrational modes are listed in Table 1.1, and its ground state rotational constant is 1.1766 cm^{-1}. Using the most naive possible estimate of $2B$ for line spacings, the spectral density is on the order of 100× less than our laser resolution. This sparseness of lines is decidedly not the case in reality for the electronic spectrum.

Table 1.1: Vibrational Modes of $\tilde{X}$ C_2H_2

Mode	Symmetry	Frequency (cm^{-1})	Motion
ν_1	σ_g^+	3372.87	sym. CH str.
ν_2	σ_g^+	1974.32	CC str.
ν_3	σ_u^+	3288.68	antisym. CH str.
ν_4	π_g	612.098	*trans* bend
ν_5	π_u	726.835	*cis* bend

When one of the π-electrons of the triple bond is excited to an antibonding π^* orbital, the resulting $^1\Sigma_u^-$ configuration is unstable with respect to both *cis* and *trans* bending [2]. The S_1 $\tilde{A}$ *cis* $^1A_2$ and *trans* ^1A_u conformers thus formed are near-prolate asymmetric tops, whose geometries and vibrational frequencies are listed in Tables 3.1 and 5.1. As nonlinear molecules, the S_1 conformers have 6 vibrational normal modes, numbered differently than the S_0 vibrations. The only complex correspondence is that the doubly degenerate ν_4'' and ν_5'' vibrations in S_0 become the a-axis rotation and the *trans*-bend ν_3', and the torsion ν_4' and *cis*-bend ν_6', respectively. The K_a angular momentum projection quantum number of the excited state then corresponds to the vibrational angular momentum ℓ of the ground state.

The complications associated with the large change in geometry and the descent in symmetry extend to the selection rules of the $\tilde{A}$-$\tilde{X}$ band system. Ordinarily, the electronic symmetries would dictate a c-axis transition, with a corresponding selection rule of $K_a' - \ell'' = \pm 1$. The small reorientation of the principal axis system, known as "axis switching" [3], relaxes this restriction, as do the Coriolis interactions found between states containing quanta of ν_4' and ν_6'. These Coriolis interactions also often interfere with the distinction between a/b symmetries, but g/u symmetry is still maintained, such that transitions are vibrationally $g \leftrightarrow g$ or $u \leftrightarrow u$. The symmetry aspects of the $\tilde{A}$-$\tilde{X}$ system can be worked out in the unified framework of Complete Nuclear Permutation and Inversion symmetry groups [4], and a useful illustration (in equivalent rigid point group notation) can be found in Fig. 2-3.

The redeeming feature of the large geometry change in the $\tilde{A}$-$\tilde{X}$ band system is the extensive Franck-Condon (FC) envelope it causes. Despite the low overall strength of the band system, it is possible to access more than the usual number of vibrational states, and therefore larger swathes of the potential energy surface. In fact, the maximum of the Franck-Condon distribution lies among states even higher in energy than the range studied thus far, with other detection considerations, such as quantum yield, coming into play before FC activity dies out. The FC active modes are those that oppose the change in equilibrium geometry: the CC stretch ν_2, because of the change in bond order and therefore length, and the *trans* bend ν_4''/ν_3', often

abbreviated "V" in the literature. It is worth noting that the $\tilde{A}$-$\tilde{X}$ system does not, strictly speaking, obey the separation between electronic and vibrational parts of the wavefunction behind the Franck-Condon principle, and in fact the electronic transition $\Sigma_u^- \leftarrow \Sigma_g^+$ would be forbidden. Distortion into *trans*-bent geometries leads to an allowed transition, but the transition remains forbidden in *cis* bent geometries. The variation of the electronic transition moment μ with geometry is illustrated in Fig. 3-7.

The *cis* and *trans* S_1 conformers mentioned above lie approximately 2500 cm^{-1} apart in energy, with *trans* below *cis*. The transition state between them lies about 5000 cm^{-1} above the *trans* minimum, and has a nearly half-linear planar structure. Somewhat surprisingly, torsional excitation appears to have little to do with this particular *cis-trans* isomerization. The local maximum at linearity is far above the energies considered in this thesis, although some early signs of quasilinear behavior are observed with excitation in ν_3'.

One important spectroscopic concept critical to understanding S_0 and S_1 C_2H_2 is that of a polyad, a group of strongly interacting states all of which must be treated simultaneously [5]. Two or more vibrational modes with near integer frequency ratios will generally lead to polyads, but different types of resonant interactions can lead to very different polyad behavior. Polyads in the ground state of acetylene have been treated extensively [6, 7]. In the S_1 excited state, the two low frequency bends, ν_4' and ν_6' have near identical frequencies and a large K_{4466} interaction matrix element, resulting in the bending B^n polyads, where $n = v_4 + v_6$ is the approximately conserved vibrational quantum number. The structures of these polyads, and particularly their anomalous evolution as a function of energy, are central to this thesis.

Two other phenomena that affect the $\tilde{A}$-$\tilde{X}$ spectrum, and are therefore tangentially related to the topic of this thesis, are intersystem crossing and predissociation. Intersystem crossing in C_2H_2 has been studied extensively by the Field group, and is reviewed in [8, 9]. For the purposes of analyzing the $\tilde{A}$-$\tilde{X}$ band system, spin-orbit interaction with three low-lying triplet electronic states causes line splittings, lifetime variation, quantum beats, and small rotational perturbations. Predissociation refers

to the possibility of fragmentation into C_2H+H, which occurs ~ 3900 cm^{-1} above the *trans* zero point level. The primary consequence is a severe drop in the fluorescence quantum yield, making LIF detection difficult. Some lifetime broadening would be expected, but surprisingly little is observed. This implies some selectivity in the pathway(s) to fragmentation. Below the threshold for production of $\tilde{A}$ C_2H, dissociation must proceed via intersystem crossing and/or internal conversion to S_0. The details of the mechanism(s) are not completely understood, despite previous experimental and theoretical study. Some new preliminary insights will be discussed in Ch. 7, based on new assignments that force reinterpretation of older data, and on our new high resolution H atom action spectra.

1.3 Experimental Apparatus

1.3.1 Vacuum System and Molecular Sources

All of the supersonic jet/molecular beam experiments described in this thesis were performed in an 8″ diameter cylindrical vacuum chamber, equipped with a diffusion pump (Varian, VHS-6) that was backed with a mechanical belt pump (Welch, 1397). The chamber would reach an ultimate vacuum of around 1×10^{-6} torr, rising to no more than 1 millitorr under gas load.

For molecular sources, pulsed nozzles were employed, based on two major types. Most commonly used was a solenoid valve (General Valve, Series 9, $0.5 - 1$ mm orifice), operated at 20 Hz, which produced the coldest rotational and vibrational temperatures. A Jordan valve (C-211 PSV, Jordan TOF) that produced rotationally cold but vibrationally warmer samples, was used when searching for hot bands, also operated at 20 Hz. Results from attempting to heat either valve type were mixed, and eventually a pyrolysis nozzle (based on that used by the Ellison group, UC-Boulder) was used to produce vibrationally hot, rotationally cold molecular beams, by passing a jet expansion through a SiC tube heated to $>$ 1000K. Acetylene was expanded through these nozzles either neat or seeded in He or Ar, with backing pressures

ranging from $1 - 4$ atm.

The REMPI experiments required a differentially pumped system for the microchannel plate (MCP) detector. A second chamber, separated from the first by a slide valve, was constructed for this purpose, with a small turbopump (Varian, V-250). This second chamber easily achieved vacuum of 5×10^{-7} torr, and remained significantly below 10^{-5} torr under load. A skimmer was mounted on the source chamber side of the slide valve, and velocity map imaging style ion optics were attached on the detector chamber side. These consisted of a repeller, extractor and ground plate held in place by alumina rods (eV Parts, Kimball Physics). The MCP detector (C-701, Jordan TOF) was placed at the other end of the detector chamber after a field-free drift region approximately 9" in length. The differentially pumped chamber could be equipped with a fast ion gauge (Beam Dynamics) for monitoring the molecular beam. A simple but essential piece of the REMPI chamber was a port above the interaction region for a beam tool to guarantee the overlap of the (focused) lasers. This consisted of a 1/4" diameter aluminum rod with 1/32" and 1/16" holes drilled in it, which could be raised and lowered through a Cajon tube fitting.

1.3.2 Lasers and Detection

The spectra obtained in this thesis were produced by scanning a tunable dye laser equipped with an intracavity etalon (Lambda Physik, FL3002E). The visible laser output was frequency doubled in β-barium borate (BBO) to produce UV light. A stray reflection of the fundamental was directed through a heated Te_2 absorption cell for frequency calibration. The dye laser was pumped by the third harmonic (355 nm) of a Q-switched solid state Nd:YAG laser (Spectra Physics, PRO-270), operating at 20 Hz. The laser triggering and other timing delays for the apparatus were controlled by SRS and BNC delay generators.

IR light for double resonance experiments was produced by difference frequency generation (DFG) as follows. A second tunable dye laser (FL2002) was pumped with the second harmonic (532 nm) of the same pump laser to produce 750-800 nm light. This beam was combined in a $LiNbO_3$ crystal (Spectra Physics, WEX) with the

Nd:YAG fundamental (1064 nm), generating IR light around 3 μm. The WEX output could be amplified in a second $LiNbO_3$ crystal by optical parametric amplification, again using 1064 nm. A simple photoacoustic cell was used to find acetylene IR lines. Because of the optical table layout and the fact that the IR and UV lasers used the same pump laser, the UV light required a 30 foot delay line to ensure proper temporal coincidence of the laser pulses at the interaction region.

For the H atom REMPI experiments, a third tunable dye laser (Cobra-Stretch, Sirah GmbH) was used to generate the 243.135 nm light that ionized H atoms by 2+1 REMPI. This laser was pumped by the third harmonic of a separate Nd:YAG laser, and frequency doubled in BBO. A wavemeter (Wavemaster, Coherent) was used to verify the laser wavenumber (20564.74 cm^{-1}). In these experiments the photolysis and the REMPI laser beams were focused into the interaction region by 50 and 30 cm lenses, respectively. A 2″ UV-enhanced aluminum spherical mirror (Thorlabs) retroreflected the REMPI laser, greatly enhancing the 2+1 H atom signal. Under these same conditions, the $C_2H_2^+$ signal from $1 + 1$ REMPI could also be obtained from the time of flight spectrum recorded by the MCP detector.

LIF detection was accomplished by use of a 2″ head-on photomultiplier tube (R375, Hamamatsu). Scattered light was virtually eliminated by the combination of a series of 4 iris baffles (SM1 components, Thorlabs) in long arms off of the source chamber, Brewster windows, and filtering the PMT input with dichroic mirrors (for example, ArF 45° HR @ 193 nm, used for rejection @ 220 nm), and colored glass filters (UG-5 or UG-11). Telescoping collection optics were mounted inside the chamber using a lens tube similar to that used for the baffle system.

All data was collected on a digital oscilloscope (LeCroy) and transferred to a computer operating a LabView VI that controlled the data acquisition and laser scanning. The averaged oscilloscope traces were also saved for post-processing, if necessary. Weaker signals were amplified with a fast preamplifier (DHPVA-200, Femto), which increased the dynamic range of the spectra. Auxiliary data (photodiode signals for monitoring laser power and Te_2 transmission) were sent to boxcar integrators (SRS) and then transferred by GPIB to the computer.

Chapter 2

Cis-trans isomerization in the S_1 state of acetylene: identification of cis-well vibrational levels

Abstract

A systematic analysis of the S_1-trans (^1A_u) state of acetylene, using IR-UV double resonance along with one-photon fluorescence excitation spectra, has allowed assignment of at least part of every single vibrational state or polyad up to a vibrational energy of 4200 cm^{-1}. Four observed vibrational levels remain unassigned, for which no place can be found in the level structure of the trans-well. The most prominent of these lies at 46175 cm^{-1}. Its ^{13}C isotope shift, exceptionally long radiative lifetime, unexpected rotational selection rules and lack of significant Zeeman effect, combined with the fact that no other singlet electronic states are expected at this energy, indicate that it is a vibrational level of the S_1-cis isomer ($^1A_2$). Guided by *ab initio* calculations [10] of the cis-well vibrational frequencies, the vibrational assignments of these four levels can be established from their vibrational symmetries together with the ^{13}C isotope shift of the 46175 cm^{-1} level (assigned here as cis-$3^1 6^1$). The S_1-cis zero-point level is deduced to lie near 44900 cm^{-1}, and the ν_6 vibrational frequency of the S_1-cis well is found to be roughly 565 cm^{-1}; these values are in remarkably good agreement with the results of recent *ab initio* calculations. The 46175 cm^{-1} vibrational level is found to have a 3.9 cm^{-1} staggering of its K-rotational structure as a result of quantum mechanical tunneling through the isomerization barrier. Such tunneling does not give rise to ammonia-type inversion doubling, because the cis and trans isomers are not equivalent; instead the odd-K rotational levels of a given vibrational level are systematically shifted relative to the even-K rotational levels, leading to a staggering of the K-structure. These various observations represent the first

definite assignment of an isomer of acetylene that was previously thought to be unobservable, as well as the first high resolution spectroscopic results describing cis-trans isomerization.

The results in this chapter have been published in the Journal of Chemical Physics [11].

2.1 Introduction

The concept of cis-trans (geometric) isomerism in certain organic compounds was first recognized by van 't Hoff in 1874. [12] Isomers of this type differ only in the arrangement of the substituents at a carbon-carbon double bond, but do not interconvert because the potential energy barrier to internal rotation about the double bond is far too high to be surmounted at ordinary temperatures. In some cases the cis and trans isomers have very different properties. The classic example [12–15] is the pair of butenedioic acids, maleic acid and fumaric acid. In the cis isomer (maleic acid) internal hydrogen bonding can occur between the two carboxylic acid groups, whereas in the trans isomer the hydrogen bonding must occur between adjacent molecules, leading to a much higher melting point. In quantum terms these molecules represent two minima at different energies on the same potential energy surface, separated by a large potential barrier.

Low lying vibrational levels of the two isomers will have energy level patterns that are characteristic of rigid molecules, though their vibrational frequencies will differ to some extent. Near the isomerization barrier the vibrational structures of the two isomers must merge into a single large amplitude pattern, since the vibrational motion must encompass both isomeric forms. Exactly how the vibrational level structure evolves in this non-symmetric double minimum situation has not been fully established, though the basic ideas follow from the many studies that have been made of simpler, symmetric potential barrier situations such as internal rotation [16] and ammonia-type inversion. [17–21]

One of the simplest systems that possesses cis and trans isomers is the first excited singlet electronic state (S_1) of acetylene, C_2H_2. *Ab initio* calculations [22–32] predict

that the trans isomer is the more stable, with the cis isomer lying about 2700 cm^{-1} higher, and the barrier to isomerization (saddle point) about 2000 cm^{-1} higher still. Transitions from the $^1\Sigma_g^+$ ground electronic state to levels of the cis-well are forbidden by the electric dipole selection rules, being $^1A_2 - ^1A_1$ in the C_{2v} point group. On the other hand transitions to levels of the trans-well are dipole-allowed ($^1A_u - ^1A_g$ in the C_{2h} point group), and their analysis provided one of the first examples of a molecule changing its point group on electronic excitation. [1, 33, 34] Acetylene is light enough that the vibrational structure of the trans-well [35–37] is not impossibly dense at the energy of the isomerization barrier, which makes it possible to recognize and interpret irregularities that encode the isomerism. Furthermore, there is the possibility that cis-well levels can tunnel through the barrier, pick up some intensity by interaction with nearby trans-well levels, and appear weakly in the absorption spectrum.

The analyses of Refs. [1, 33–37] characterized the Franck-Condon allowed levels of the ^1A_u upper state, assigning them to progressions in the ν_2 (C=C stretch) and ν_3 (trans-bend) vibrations. The *ungerade* fundamentals, ν_4 (torsion), ν_5 (C-H antisymmetric stretch) and ν_6 (cis-bend), were established later by analysis of IR-UV double resonance spectra. [38, 39] More recently, jet-cooled excitation spectra [40] have revealed a number of new combination levels involving the low-lying bending vibrations, ν_4 and ν_6. The energies of these new levels could not be explained easily in terms of the known fundamental frequencies. To clarify the assignments of these levels we undertook a systematic analysis of the level structure of the ^1A_u (S_1-trans) well [41–44] using IR-UV double resonance and one-photon fluorescence excitation spectra. The unexpected positions of the new combination levels turned out to result from unusually strong Darling-Dennison resonance between the ν_4 and ν_6 vibrations. [41, 43] In the end, a very complete picture of the energy level pattern emerged. Together with data from other workers, [1, 33–39] some part of every vibrational polyad (or isolated vibrational level which is not part of a polyad) predicted up to a vibrational energy of 4200 cm^{-1} has now been securely identified.

Four observed vibrational levels, for which there was no place in the level structure of the S_1-trans well, [43] remained unassigned in the energy range up to 4200 cm^{-1}.

These levels lie at 45610, 45735, 46114 and 46175 cm^{-1}. For the level at 46175 cm^{-1} (3977 cm^{-1} above the trans-well origin), the evidence is now clear that it belongs to the cis-well; this level forms the main subject of this paper. The evidence is less complete for the other three vibrational levels but, taken as a whole, the evidence for all four levels adds up to a consistent picture.

2.2 Experimental Details

The spectra of $^{12}C_2H_2$ and $^{12}C^{13}CH_2$ used for this paper are the same as those reported in Refs. [41–43]. Full details were given in Ref. [41], so that only a brief summary is needed here.

Laser-induced fluorescence excitation spectra of pure acetylene were recorded using an unskimmed free jet expansion from a General Valve series 9 pulsed valve, with 0.5 mm orifice diameter and ∼200 kPa backing pressure. A Lambda Physik 3002E pulsed dye laser, frequency-doubled in a β-barium borate crystal, provided the laser radiation, which was detected by a Hamamatsu R331 photomultiplier. $^{130}Te_2$ vapor was used for frequency calibration. [45]

For the IR-UV double resonance experiments, infrared radiation was obtained by difference frequency generation in a $LiNbO_3$ crystal: an injection-seeded Nd:YAG laser (Spectra-Physics PRO-270), operating at 1064 nm, and a tunable dye laser (Lambda-Physik FL2002), operating in the range 740-790 nm, provided the pumping. The IR output was amplified in a second $LiNbO_3$ crystal to about 3 mJ/pulse. The observed acetylene line widths are about 0.09 cm^{-1}.

Laser excitation spectra of $^{13}C_2H_2$ in the region near 46200 cm^{-1} were recorded in a static room-temperature cell. The output of a Lambda-Physik FL2002 dye laser, pumped by an XeCl excimer laser, and operating with Coumarin 440 and 450 dyes, was frequency-doubled in a β-barium borate crystal. The sample of $^{13}C_2H_2$ (MSD Isotopes, 98% enriched) was subjected to several freeze-pump-thaw cycles for further purification, and its fluorescence was recorded by a Hamamatsu R331 photomultiplier. Calibration was again provided by $^{130}Te_2$ vapor. [45]

2.3 Background and Discovery of the 46175 cm^{-1} Vibrational State

The S_1-trans well has its zero-point level at 42197.57 cm^{-1}. [35] Its vibrational assignments are simple to make at low energy, but by 46000 cm^{-1} the density of the level structure is at the point where the assignments of the weaker bands are not always obvious, for various reasons. At low vibrational energy the fact that the low-lying bending vibrations, ν_4 and ν_6 have almost the same frequency (764.9 and 768.3 cm^{-1}, respectively [38]) causes the vibrational structure to form polyads, in each of which the sum of the v_4 and v_6 quantum numbers is constant. However the overtones of the ν_4 and ν_6 modes suffer from strong Darling-Dennison resonance, [41] which causes the energy range of each vibrational polyad to expand vastly as the vibrational quantum numbers increase. For example, the $K' = 1$ levels of the $v_4 + v_6 = 5$ pure-bending polyad (which we abbreviate as B^5) are spread out over 400 cm^{-1}. The combination levels formed by the bending vibrations and the totally symmetric vibrations form similar polyads. There is often considerable overlap between the various polyads, and because anharmonic resonances can occur between them, [43] the structure becomes increasingly complicated. A further problem is created by the half-linear structure of the molecule at the cis-trans isomerization barrier. [26] In such a half-linear structure, one end of the molecule has a CCH bond angle of about 120° while the CCH group at the other end is nearly linear. The minimum energy pathway to isomerization does not lie along any one of the vibrational normal coordinates, but rather along a combination of two coordinates, Q_3 (trans-bend), and Q_6 (cis-bend). The result is huge diagonal cross-anharmonicity (x_{36}) in levels where both ν_3 and ν_6 are excited, [43, 46] which causes the energy spread of the vibrational polyads to increase even more. A final problem is that, because of poor $\tilde{A}$–$\tilde{X}$ Franck-Condon factors and $\tilde{A}$-state predissociation effects, some of the expected vibrational bands at higher energy are unobservably weak, which prevents complete sampling of the vibrational manifold.

Both the IR-UV double resonance and the one-photon fluorescence excitation spec-

tra reach this point of complexity at an excitation energy of about 46000 cm^{-1}. The IR-UV double resonance spectrum is particularly challenging because 15 significantly interacting vibrational levels are expected to lie in the region 45800–46200 cm^{-1}. We have invested considerable effort (as yet unpublished) into assigning the states in this region, and find that the $K' = 0 - 2$ levels of all 15 vibrational levels should lie below 46150 cm^{-1}, with the exception of some of the components of the B^5 polyad. The double resonance spectrum in the region 46160–46240 cm^{-1}, as recorded via the Q branch of the infra-red $(\nu_3 + \nu_4)''$ combination band at 3897 cm^{-1}, is shown in the top part of Fig. 2-1. The structure of the B^5 polyad can be predicted accurately (± 2 cm^{-1}) from calculations based on the lower energy bending polyads. [41] Three of its sub-bands can be assigned at once from the calculations, and two unrelated Coriolis-induced sub-bands, with $K' = 3$ and 4, can also be recognized. This leaves two moderately strong low-K sub-bands unassigned, a $K' = 0$ sub-band at 46175.4 cm^{-1} and a $K' = 2$ sub-band at 46227.1 cm^{-1}. Assuming that their upper states belong to the same vibrational level, and recalling that the K-structure of an asymmetric top is described by the energy level expression $[A-\frac{1}{2}(B+C)]K^2$, their separation gives the rotational constant $A-\frac{1}{2}(B+C) = 12.94$ cm^{-1}, which is a typical value for the vibrational levels of the S_1-trans well. Nevertheless there is no place for these levels in the vibrational manifold of the S_1-trans well, since every level expected in this region is accounted for. (As we show below, this value of $A-\frac{1}{2}(B+C)$ is also consistent with a level of the S_1-cis well.)

The one-photon fluorescence excitation spectrum in the same wavenumber region is illustrated in the lower part of Fig. 2-1. Most of the bands near this region come from the severely overlapped $2^1 3^1 B^2$ and $3^1 B^4$ polyads. Detailed calculations based on vibrational parameters obtained in fits of lower energy polyads, which take the Coriolis and Darling-Dennison interactions into account, have led to unambiguous assignments for the components of these two polyads. [43] All of the observed bands are now accounted for except for a moderately strong $K' = 1$ sub-band at 46192.2 cm^{-1}. As Fig. 2-1 shows, this band lies 3.9 cm^{-1} from the position that would be expected for it on the assumption that it belongs to the same vibrational state as

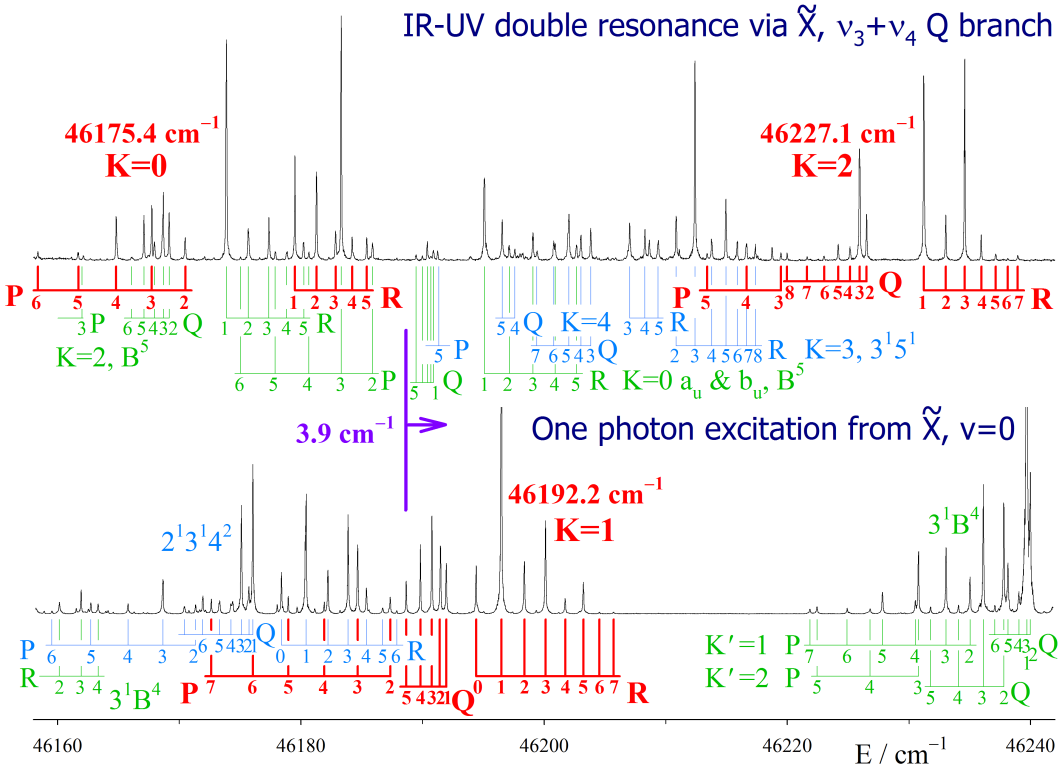

Figure 2-1: Upper trace: IR-UV double resonance spectrum of acetylene in the region $46160-46240$ cm^{-1} recorded via the Q branch of the $(\nu_3+\nu_4)''$ band. Two sub-bands, with $K' = 0$ and 2, which cannot be fitted into the manifold of the S_1-trans state, occur at 46175.4 and 46227.1 cm^{-1}. Lower trace: One-photon excitation spectrum of acetylene in the same wavenumber range. A $K' = 1$ sub-band at 46192.2 cm^{-1} lies 3.9 cm^{-1} above the expected position of the $K' = 1$ sub-band of the upper trace. In both spectra the assignments of the underlying trans-well rotational structure are shown in blue and green.

the unassigned levels of the double resonance spectrum. However such an assumption violates the $g-u$ symmetry selection rules if the vibrational state involved is localized in the S_1-trans well (^1A_u). Upper states reached in one-photon excitation from the $^1\Sigma_g^+$ ground vibrational level must have *gerade* vibrational symmetry, while upper states reached in double resonance via the $(\nu_3+\nu_4)''$ level (which has Π_u symmetry) must be vibrationally *ungerade*. Rotational levels with different values of K in the same vibrational state cannot have different $g-u$ symmetry. The conclusion is either that the $K'=1$ level does not belong to the same vibrational state as the $K'=0$ and 2 levels or that it is not localized in the S_1-trans well. As we show in the next Section, the second alternative is the correct one.

This Section has concentrated exclusively on the 46175 cm^{-1} vibrational level where, as we shall see, the evidence is very strong that this level belongs to the S_1-cis well. Similar accounts can be given for the 45610, 45735 and 46114 cm^{-1} levels, though the data are not as complete. Those levels are discussed in Sec. 2.5.

2.4 Assignment of the 46175 cm^{-1} State to the S_1-cis Electronic State

2.4.1 ^{13}C Isotope shifts

Several lines of evidence, in addition to the fact that there is no place for them in the manifold of the S_1-trans well, indicate that the unassigned levels of Fig. 2-1 belong to the S_1-cis well. The strongest argument is based on the carbon isotope shifts of the $K'=1$ level at 46192.2 cm^{-1}, which are illustrated in Fig. 2-2.

Figure 2-2 contains two spectra, both covering the region $46184.5-46210$ cm^{-1}. The upper trace is the spectrum of jet-cooled acetylene, where most of the features are due to $^{12}C_2H_2$, though some very weak lines of $H^{12}C^{13}CH$, present in natural abundance, also appear. The lower trace is the excitation spectrum of $^{13}C_2H_2$, recorded at room temperature in a static cell. The strong saturated lines in this spectrum are high-J lines from the tail of the very intense 3_0^4, $K=1-0$ band at 46260 cm^{-1};

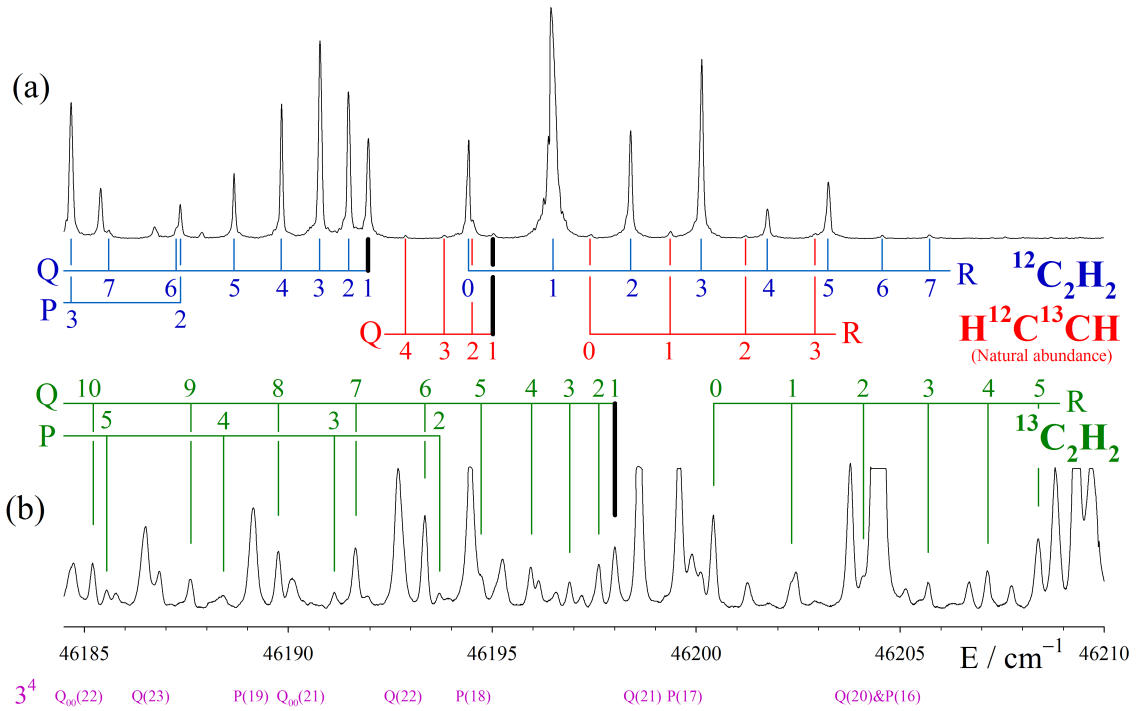

Figure 2-2: (a)Jet-cooled excitation spectrum of the 46192 cm^{-1} ($K' = 1$) sub-band of $^{12}C_2H_2$. Some weak lines of $H^{12}C^{13}CH$, present in natural abundance (2.216%, due to the two equivalent carbon atoms and 1.108% natural abundance of ^{13}C), are also seen. (b) Room temperature excitation spectrum of $^{13}C_2H_2$ in the same wavenumber range. The strong lines, which have been artificially truncated, are high-J Q and P lines from the very intense 3^4, $K' = 1$ sub-band at 46260 cm^{-1}. The assignments of some of them are marked below the wavenumber scale. The tie lines above the spectrum give the assignments of the $^{13}C_2H_2$ isotopomer of the 46192 cm^{-1} band. To make the isotope shifts more visible, the Q(1) tie line has been thickened for the three isotopomers.

some of the line assignments are marked at the bottom of the figure. The tie-lines located between the two traces display the rotational assignments of the $K' = 1$ band at 46192 cm^{-1} ($^{12}C_2H_2$) and the corresponding bands of H^{12}C^{13}CH and $^{13}C_2H_2$. It is immediately clear that the isotope shift for $^{13}C_2H_2$ is almost exactly twice that for H^{12}C^{13}CH, confirming that the bands of all three isotopomers have the same vibrational assignment; also that the bands shift to higher frequency with increasing ^{13}C substitution. The actual isotope shifts are $\Delta\nu$ ($^{12}C_2H_2$ − H^{12}C^{13}CH) = −3.03 cm^{-1} and $\Delta\nu$ ($^{12}C_2H_2$ − $^{13}C_2H_2$) = −6.13 cm^{-1}.

The $^{12}C_2H_2$ − H^{12}C^{13}CH isotope shifts for the trans-well vibrations ν_1 − ν_4 were determined in Ref. [43], where the shifts per quantum were given as ν_1: 3.8 cm^{-1}; ν_2: 23.4 cm^{-1}; ν_3: 5.3 cm^{-1} and ν_4: 0.9 cm^{-1}. (The shifts for ν_5 and ν_6 should be similar to those of ν_1 and ν_4 as can be seen from the results of recent *ab initio* calculations, [10] given in Table 2.1.) The isotope shift of the zero-point level is roughly −6.8 cm^{-1}, which means that the vibrational contribution to the $^{12}C_2H_2$ − H^{12}C^{13}CH isotope shift of the 46192 cm^{-1} band would be about 3.8 cm^{-1} if it belongs to the trans-well. The upper state of the 46192 cm^{-1} band must be a combination level if it belongs to the trans-well, since it lies 3980 cm^{-1} above the zero-point level. Given the known values of the fundamental frequencies and their isotope shifts, from Table 2.1, it is clear that no trans-well combination level at an energy of 3980 cm^{-1} can have such a small vibrational contribution to its $^{12}C_2H_2$ − H^{12}C^{13}CH isotope shift. On the other hand, if the level belongs to the potential well of a different S_1 conformer, for which the minimum lies above that of the trans-well, the vibrational contribution to its isotope shift should be smaller, since the level will lie lower in its potential well. In this context we note that recent *ab initio* calculations [10] predict that the zero-point level of the S_1-cis well lies at 44856 ± 50 cm^{-1}, which is about 2700 cm^{-1} above the zero-point level of the S_1-trans well. Assuming that the 46192 cm^{-1} level belongs to the S_1-cis well, its observed isotope shift matches the expected shift very convincingly, but we defer discussion of it until after the vibrational assignments have been considered (Sec. 2.5).

The assigned lines of the 46192 cm^{-1} band and its isotopomer partners are listed

in Table 2.2, along with the lines of the $K' = 0 - 1$ and $2 - 1$ sub-bands.

Table 2.1: $^{12}C_2H_2$ – $H^{12}C^{13}CH$ isotopomer shifts-per-quantum for the trans-well vibrations of the S_1 state of acetylene, calculated *ab initio* [10] for harmonic vibrations. Values in cm^{-1}. The frequencies given in the left column are the observed fundamentals of S_1-trans $^{12}C_2H_2$.

Vibration	$\Delta\nu$ ($^{12}C_2H_2$ – $^{12}C^{13}CH_2$)
ν_1 (a_g, 2880.1 cm^{-1})	4.0
ν_2 (a_g, 1386.9)	25.9
ν_3 (a_g, 1047.6)	6.2
ν_4 (a_u, 764.9)	1.1
ν_5 (b_u, 2857.5)	5.5
ν_6 (b_u, 768.3)	1.2

2.4.2 Rotational structure of transitions to the S_1-cis well

We have not yet recorded IR-UV double resonance spectra of $^{13}C_2H_2$, and therefore cannot show from isotope data alone that the unassigned $K' = 0 - 2$ levels of Fig. 2-1 belong to the same vibrational state, though the lifetime data (see Section 2.4.4, below) strongly suggest that they do. It was noted in Section 2.3 that, if these three K' levels belong to a single vibrational state of the trans-well, the $K' = 1$ levels should not appear in the one-photon fluorescence excitation spectrum if the $K' = 0$ and 2 levels appear in the IR-UV double resonance spectrum. However group theory arguments show that the appearance of the $K' = 1$ levels in the one-photon spectrum is precisely what must happen if the levels belong to a single vibrational state of the cis-well.

Table 2.2: Assigned lines of the 46175 cm^{-1} band (cis-$3^1 6^1$) and its isotopic counterparts. Values in cm^{-1}. * = blended line

	K = 0 - 1		K = 1 - 0			K = 2 - 1		
J	R	P	R	Q	P	R	Q	P
0			46194.42					
1	46179.51		46196.46	46191.96		46231.21		
2	46181.28	46170.5	46198.39	46191.48	46187.36	46233.02	46226.51	
3	46182.86	46167.73	46200.12	46190.77	46184.68	46234.58	46225.93	46219.47
4	46184.21	46164.81	46201.74	46189.83	46181.92	46235.94	46225.14	46216.65*
5	46185.41	46161.71	46203.23	46188.67	46178.97	46237.13	46224.18	46213.39
6		46158.38	46204.55	46187.25		46238.11	46223.02	
7			46205.72	46185.6		46238.94	46221.62	

Isotopic bands, $K = 1 - 0$

	$H^{12}C^{13}CH$		$^{13}C_2H_2$		
J	R	Q	R	Q	P
0	46197.4		46200.44		
1	46199.36	46195.02	46202.35	46198.26	
2	46201.21	46194.51	46204.08	46197.62	46193.73
3	46202.91	46193.82	46205.7	46196.91	46191.13
4	46204.50*	46192.87	46207.14	46195.95	46188.41
5			46208.38	46194.75	46185.55
6			46209.69*	46193.36	46182.55*
7			46210.51	46191.65	46179.32
8			46211.31	46189.77	46175.98
9			46211.99	46187.6	46172.43
10			46212.42	46185.21	46168.78
11			46212.75*	46182.55*	46164.93
12			46212.75*	46179.74	46160.93
13				46176.70*	46156.76
14					46152.3

It is not necessary to go beyond rigid-molecule considerations to understand the group theory arguments. In essence the difference between the cis and trans isomers is that in C_{2v} symmetry the rovibronic wave functions can transform like all four symmetry species, A_1, A_2, B_1 and B_2, in any given vibronic state, while in C_{2h} symmetry they can only transform as A_g and B_g in a *gerade* vibronic state or A_u and B_u in an ungerade vibronic state. Looking up the species of the rotational levels of asymmetric tops in different point groups,[47] it is easy to show that the observed R and P branch structure of the $K' = 0$ sub-band in the double resonance spectra of Fig. 2-1 will result if the upper state is ${}^{e}A_2 \times {}^{v}B_2 = {}^{ev}B_1$ in C_{2v} symmetry or ${}^{e}A_u \times {}^{v}B_u = {}^{ev}B_g$ in C_{2h} symmetry. Figure 2-3 is an energy level diagram that shows the branch structures that arise in these two cases in fluorescence excitation spectra from the zero-point level of the ground state and in double resonance spectra via the Q branch of $(\nu_3 + \nu_4)''$ (Π_u). The figure shows that a B_u upper vibrational state in C_{2h} symmetry will give only $K = 0 - 1$ and $2 - 1$ sub-bands in double resonance from $(\nu_3 + \nu_4)''$, according to the C-type selection rule, $K' - l'' = \pm 1$, though a weaker axis-switching or Coriolis-induced $K = 1 - 1$ sub-band may be observable given the right circumstances (dashed lines in the figure). However, there will be no transitions from the ground vibrational state of the molecule. In contrast, a B_2 upper vibrational state in C_{2v} symmetry will give $K = 0 - 1$ and $2 - 1$ sub-bands in double resonance and a $K = 1 - 0$ sub-band in one-photon excitation.

The important result is that, for cis-well upper states, bands involving even-K' and odd-K' levels cannot appear in the same spectrum. For trans-well upper states all K' levels (subject to the line strengths given by the direction cosine matrix elements) will appear either in the one-photon spectrum or in the double resonance spectrum, but not both.

2.4.3 Tunneling effects and *K*-staggering

Rigid-molecule arguments, as just described, will be valid up to about the energy of the cis-trans isomerization barrier. Even below that energy, effects arising from tunneling through the barrier will start to become noticeable. Exactly how the levels

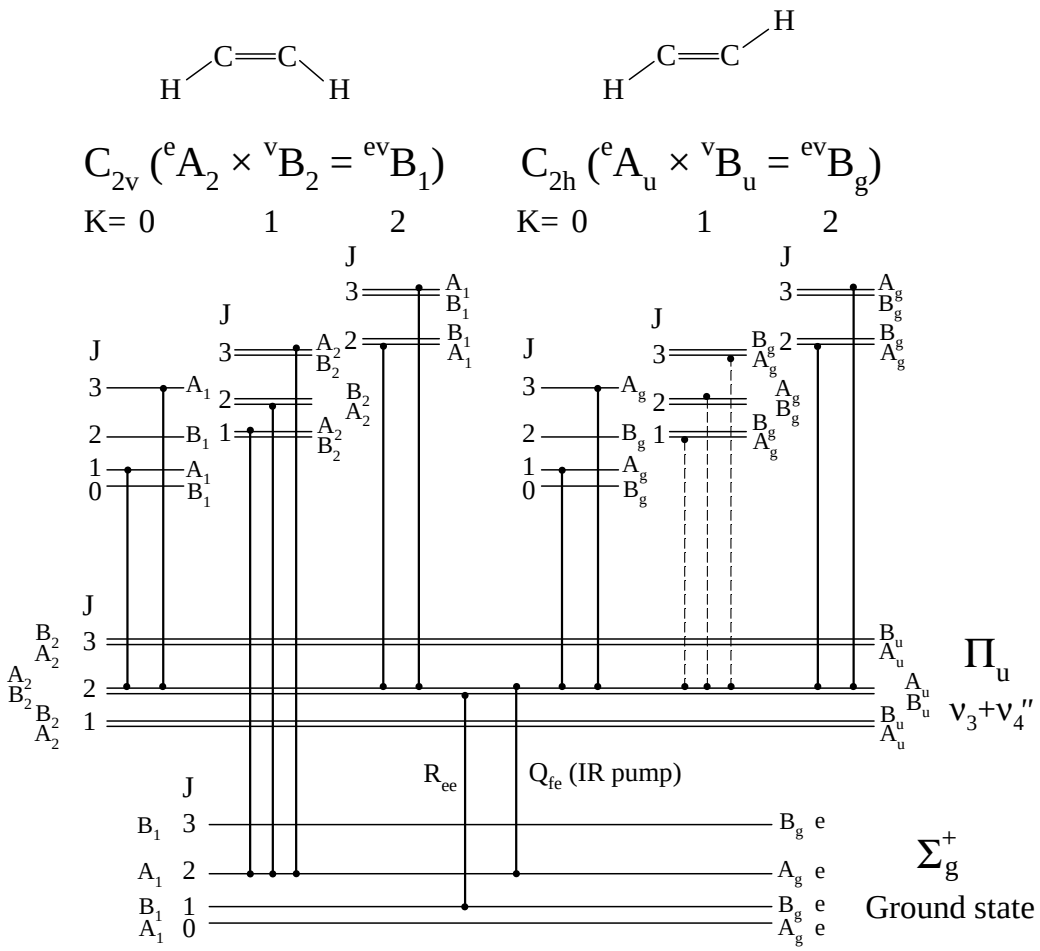

Figure 2-3: Energy level diagram showing the rotational structure expected for the 46175 cm^{-1} state in one-photon excitation and in IR-UV double resonance via the Q branch of the $(\nu_3 + \nu_4)''$ level. Left side: assuming it belongs to the S_1-cis well. Right side: assuming it belongs to the S_1-trans well. The ground state and the $(\nu_3 + \nu_4)''$ level (lower part of the figure) are common to the two parts of the diagram. The symmetry species given for them are reductions of the linear molecule species onto the point groups C_{2v} and C_{2h}.

behave will depend on the mechanism of the cis-trans isomerization. It is not the purpose of this paper to go into the details of the permutation-inversion group theory that is required to describe the observed tunneling effects,[48] but essentially there are three possible mechanisms, requiring description by three different permutation-inversion groups. The energy level patterns are predicted to be different in these three cases.

The mechanism that has received most attention [4, 49] treats the torsion as the only large amplitude coordinate, which leads to isomerization by internal rotation, as in H_2O_2. For C_2H_2 the *ab initio* results predict [26] that the molecule is half-linear at the isomerization barrier, which implies a second mechanism where the large amplitude motions leading to isomerization are local CCH bends, one at each end of the molecule, with the molecule always remaining planar. Naturally, the barrier to internal rotation goes to zero when the molecule is half-linear. This leads to a third mechanism in which the internal rotation is added to the two local bends to give a complete description of the isomerization; embodying three large amplitude coordinates, the permutation-inversion group required [48] is of order 32.

Assuming the C_2H_2 molecule remains planar, with the isomerization occurring exclusively through the local bends, the predicted level pattern is that even-K levels go with one of the two tunneling components of a vibrational state and odd-K levels go with the other. [48] No actual splittings will be observed, but instead there will be a staggering of odd-K levels versus even-K levels. At energies close to the barrier, where internal rotation must also be considered, there will be three tunneling components for each vibrational state, resulting in a further staggering of the $K = 2, 6, 10, \ldots$ levels versus the $K = 0, 4, 8, \ldots$ levels. (There is no further staggering of the odd-K levels.) The level shifts associated with this additional staggering mechanism will probably not be significant until quite close to the isomerization barrier.

The K structure pattern of the levels in Fig. 2-1 appears to be an example in which staggering is observed. The S_1-trans isomer has very large Coriolis interaction between its ν_4 and ν_6 vibrations because of the near-degeneracy of their frequencies. On the other hand, *ab initio* calculation of the S_1-cis well frequencies (summarized in

Table 2.3) indicates a different situation, where the corresponding two frequencies are nearly 250 cm^{-1} apart;[10] therefore there will be only minimal Coriolis interaction in the S_1-cis isomer. Consequently, we can expect the S_1-cis vibrational states to behave as unperturbed asymmetric tops, so that the rotational constant $A-\frac{1}{2}(B+C)$ derived from the $K' = 0$ and 2 levels in Fig. 2-1 truly reflects the molecular geometry. Taking r(CC) = 1.3423 , r(CH) = 1.0983 and θ(CCH) = 132.62°, from Ref. [10], we calculate $A-\frac{1}{2}(B+C)$ for the cis isomer to be 12.79 cm^{-1}. This is very close to the observed value, 12.94 cm^{-1}, derived from Fig. 2-1, which suggests that the internal rotation tunneling mechanism is not important for this vibrational state. As the arrow in Fig. 2-1 indicates, the $K' = 1$ level lies 3.9 cm^{-1} above where the asymmetric top energy formula predicts. Since the centrifugal distortion constant Δ_K calculated from the *ab initio* potential is only 0.00826 cm^{-1}, and there is no reason to suspect that the 46175 cm^{-1} level is significantly perturbed, our interpretation is that this 3.9 cm^{-1} shift represents the staggering of the K structure that results from tunneling through the isomerization barrier.

Table 2.3: *Ab initio*-calculated harmonic vibrational frequencies of the S_1-cis state of C_2H_2.

	Harmonic frequencies			calc. isotope shift [10]
	Ref. [26]	Ref. [31]	Ref. [10]	$^{12}C_2H_2 - {}^{12}C^{13}CH_2$
ν_1 CH sym stretch (a_1)	3049	3094	2997	5.5
ν_2 CC stretch (a_1)	1659	1577	1583	29.1
ν_3 sym bend (a_1)	816	812	806	0.6
ν_4 torsion (a_2)	704	860	817	4.3
ν_5 CH antisym stretch (b_2)	2996	3044	2942	4.5
ν_6 antisym bend (b2)	441	677	572	3.7

Experimentally the ν_6 frequency is estimated, from the energy difference between the $3^1 6^1$ and 3^1 levels (i.e. not corrected for anharmonicity), to be 565 cm^{-1}.

2.4.4 Lifetime and quantum beat measurements

In contrast to the nearby levels of the S_1-trans well, which have upper state lifetimes of about 300 ns, the $K' = 1$ upper level of the 46192 cm^{-1} band has a radiative lifetime of at least 2 μs (for $J' = 1e$). (This is approximately the longest lifetime that

we can measure with our collection optics before the molecules leave the detection region.) The lifetimes of the $K' = 0$ and 2 levels of the double resonance spectrum shown in Fig. 2-1 have not been measured directly but, from spectra recorded with the detection gated at different delay times, are found to be much longer than those of the surrounding vibrational levels. This result strongly suggests that all three unassigned upper levels belong to the same vibrational level, and also provides clear evidence that the upper level is metastable, as expected for a level of the S_1-cis well, where the electronic transition to the ground state is forbidden, being $^1A_2 - {}^1A_1$ in C_{2v} symmetry.

Nevertheless, many of the rotational levels of the S_1-trans isomer are perturbed by triplet states, and have lifetimes longer than 1 μs. [50, 51] It must then be asked if the 46192 cm^{-1} level could be a triplet level. At this energy only the T_3 state has vibrational structure that is sparse enough for spin-orbit interaction to induce a transition to one complete isolated triplet vibrational level. Even so, the rotational structure might be expected to show triplet splittings and possibly local perturbations in such a case. The deciding factor is the rotational magnetic moment, which should be large for a triplet state. [50] We have recorded Zeeman quantum beats from a number of vibrational bands in this region, and find that the pattern given by the 46192 cm^{-1} level is similar to those given by most of the securely-assigned S_1-trans levels in the region. The observed $|g|$-factor for the R(0) line is only 0.089, which means that the upper state has principally singlet character.

Interestingly, spectra of the $K' = 1$ level at 46192 cm^{-1} and the S_1-trans $3^1 6^4$, $K' = 1$ level at 46087 cm^{-1} have been recorded using the technique of surface electron ejection by laser-excited metastables (SEELEM). [52] (N.B.: these levels are not correctly assigned vibrationally in Ref. [52], as that paper was published before detailed calculations of the polyad structure [43] had established the vibrational assignments.) SEELEM spectra are observed when a metastable species is excited by laser excitation, and travels for a time that is huge compared to a typical radiative lifetime, before striking a metal surface and causing the emission of an electron. The vertical excitation energy of the metastable must be larger than the work function of

the metal. In the experiments of Ref. [52], the travel time was 300 μs, and the metal used was gold, which has a work function of 41000 cm^{-1}. *Ab initio* calculations [31] predict that the only metastable triplet state of C_2H_2 lying high enough in energy to give SEELEM intensity is the T_3 state. The metastable T_1 and T_2 states lie too low to give SEELEM intensity though, since their levels form a near-continuum at 46000 cm^{-1}, they presumably contribute to the observed magnetic moments of the 46192 and 46087 cm^{-1} levels (the 46087 cm^{-1} level has $|g| \sim 0.01$). The 46192 cm^{-1} band gives a strong, clean SEELEM spectrum, where the rotational intensity pattern closely follows that of the laser excitation spectrum. [52] In contrast the much stronger 46087 cm^{-1} band gives only a weak disorganized SEELEM spectrum. At present it is not clear why the SEELEM intensities of the two bands are so different; if it should prove that C_2H_2 in its S_1-cis state lives long enough to contribute directly to the SEELEM intensity, SEELEM spectroscopy could possibly provide a method to identify other S_1-cis levels in the laser excitation spectrum.

2.5 Vibrational Assignments of the cis Well States

As discussed at the end of Sec. 2.1, the 46175 cm^{-1} vibrational level is the best-characterized of the observed states that do not fit into the vibrational manifold of the S_1-trans well. Assuming that this state belongs to the S_1-cis well, it must have B_2 vibrational symmetry, while its small ^{13}C isotope shifts imply that it lies quite low in the potential well, probably below 2000 cm^{-1}.

The other three vibrational levels that we have found, which do not fit into the manifold of the S_1-trans well, all lie below the 46175 cm^{-1} level. They give rise to very weak bands where we do not observe the complete set of $K' = 0 - 2$ rotational levels. The most interesting of these levels appears as a $K' = 0$ sub-band at 45734.7 cm^{-1} and a $K' = 2$ sub-band at 45790.8 cm^{-1}, in double resonance via the ground state $(\nu_3 + \nu_4)''$ level. The assigned lines are listed in Table 2.4. The $K' = 0$ sub-band is a single Q branch in double resonance via the Q branch of $(\nu_3 + \nu_4)''$, but appears as R and P branches in double resonance via the R branch of $(\nu_3 + \nu_4)''$.

This is consistent with A_2 upper state vibrational symmetry. The derived value of $A-\frac{1}{2}(B+C)$ is 14.03 cm^{-1}, from which we can predict the expected position of the corresponding $K' = 1$ sub-band, but nothing is found at this energy in either one-photon fluorescence excitation or double resonance spectra. The $K' = 0$ levels have an exceptionally long fluorescence lifetime, compared to other nearby trans states. This further suggests that they cannot belong to states localized in the S_1-trans well.

The other unassigned vibrational levels appear just as single sub-bands. One of these is a $K' = 1$ sub-band at 45622.7 cm^{-1}, which is found in double resonance via the ν_3'' fundamental. The upper state vibrational symmetry is therefore either A_1 or B_1. However the upper levels of the Q lines lie below the upper levels of the R and P lines, which requires that the vibrational symmetry is A_1, assuming that the asymmetry splitting behaves normally. This assumption appears to be valid, because the asymmetry coefficient, $B-C = 0.073$ cm^{-1}, is only slightly smaller than what would be expected for an unperturbed vibrational level of the S_1-cis well (0.085 cm^{-1}). The intensity of this sub-band appears to come from interaction with the topmost $K = 1$ level of trans-3^1B^3, which lies only 8.1 cm^{-1} below. [43] We have not found the corresponding $K' = 0$ and 2 sub-bands; the $K' = 0$ sub-band should lie near 45610 cm^{-1}.

The other unassigned vibrational level which appears as a single sub-band is a $K' = 0$ level at 46114.0 cm^{-1} that perturbs the $K' = 0$ level of the trans-1^13^1 vibrational state between $J' = 5$ and 6. It is found as a hot band from the ν_4'' fundamental in the one-photon excitation spectra. The perturbation in trans-1^13^1 had been noted in Ref. [40], but no extra lines were observed, and little could be said because of blending in their higher temperature spectra. Our jet-cooled spectra give the branch structures of both states up to $J' = 7$, and show that the perturbing state has A_1 vibrational symmetry. The interaction matrix element between the two states is 0.30 cm^{-1}. We have looked without success for the $K' = 2$ levels of the unassigned state near the corresponding levels of trans-1^13^1.

Table 2.4: (a) Assigned lines of the 45734.7 cm^{-1} band (cis-4^1), observed in IR-UV double resonance via the Q branch of the $(\nu_3 + \nu_4)''$ level. Values in cm^{-1}.

	K= 0 - 1	K= 2 - 1	
J	Q	R	Q
1	45734.57	45795.09	
2	45734.26	45797.02	45790.38
3	45733.79	45798.73	45789.96
4	45733.17		45789.38
5	45732.46		45788.63
6	45731.51		
7	45730.36		
8	45729.08		

(b) Assigned $K' = 1$ upper state energy levels of the 45610 cm^{-1} state (cis-3^1), observed in IR-UV double resonance via R and P lines of the ν_3'' fundamental. Values in cm^{-1}.

J	$K' = 1e$	$K' = 1f$
1	45625.09	45624.98
2	45629.46	45629.23
3	45636.07	45635.61
4	45644.88	45644.14
5	45655.83	

(c) Assigned lines of the trans-$1^1 3^1$, $K = 0 - \nu_4''$ and cis-6^2, $K = 0 - \nu_4''$ bands. Values in cm^{-1}.

J	R		Q		P	
1	45506.31	45507.03	45502	45502.75	45499.84*	45500.59
2	45508.09	45508.77	45501.66*	45502.36	45497.24	45498
3	45509.66	45510.32	45501.08*	45501.78	45494.49	45495.22
4	45511.01	45511.64	45500.34	45500.97*	45491.57	45492.25
5	45512.16	45512.99*	45499.37	45499.99		45488.99
6	45512.99*	45513.74*	45498.16*	45498.81	45484.94	45485.66
7			45496.81	45497.42	45481.47	
8			45495.22*		45477.51	45478.32
9			45493.26			

The trans-$1^1 3^1 - \nu_4''$ band is the higher frequency component at low J values. An avoided crossing with cis-6^2 occurs between $J' = 5$ and 6. Blended lines are marked with an asterisk. The Q(9) line was not included in the least squares fit given in Table 2.5.

Table 2.5: (a) Rotational constants from least squares fitting of the S1-cis bands at 46175, 45735 and 45623 cm^{-1}

State	46175 cm^{-1} (cis-$3^1 6^1$)						45735 cm^{-1} (cis-4^1)		45610 cm^{-1} (cis-3^1)	
Isotopomer	$^{12}C_2H_2$		$H^{12}C^{13}CH$		$^{13}C_2H_2$		$^{12}C_2H_2$		$^{12}C_2H_2$	
T_0(K=0)	46175.362	± 0.023					45734.701	± 0.042		
T_0(K=1)	(46192.206)		46195.239	± 0.026	46198.336	±0.020			45622.67	±0.036
A	14.019	0.01	13.89	fixed	13.76	fixed	15.135	0.011	13.95	fixed
B	1.1258	0.0011	1.0934	0.0033	1.0597	0.0003	1.185	0.002	1.118	0.003
C	1.037	0.0013	1.0086	0.0033	0.9809	0.0004	1.02	fixed	1.045	0.005
Δ_{JK}	0.00074	0.0003								
$T_{odd-even}$	3.906	0.02								
r.m.s.	0.0191		0.0147		0.0174		0.0253		0.0213	

Values in cm^{-1}. Error limits are three standard deviations. Constants not listed were not included in the fits. The parameter $T_{odd-even}$ gives the K-staggering, defined as the distance that the $K' = 1$ level lies above its expected position according to the asymmetric top energy expression. The even and odd K levels were fitted to the same set of rotational constants, except that $T_{odd-even}$ was added to the energy of the $K' = 1$ levels. The parameter $T_0(K = 1)$ is equivalent to $T_0(K = 0)$+A$-\frac{1}{2}$(B+C)+$T_{odd-even}$. The band at 45623 cm^{-1} is the $K = 1 - 0$ sub-band of the cis-3^1_0 band, of which the origin is estimated to lie at 45610 cm^{-1}.

(b) Rotational constants from deperturbation of the interacting trans-$1^1 3^1$, $K = 0$ and cis-6^2, $K = 0$ levels, neglecting asymmetry effects

T_0 (cis-6^2, $K = 0$)	46114.01	± 0.05
(B+C) (cis-6^2, $K = 0$)	1.0853	0.0018
T_0 (trans-$1^1 3^1$, $K = 0$)	46114.51	0.05
(B+C) (trans-$1^1 3^1$, $K = 0$)	1.0716	0.0014
W_{12}	0.296	0.019
r.m.s	0.0151	

Values in cm^{-1}. The interaction matrix element, W_{12}, is assumed to have no J-dependence. The fit was carried out on term values calculated from Table 2.5(c) together with energy levels for ν_4'' from Ref. [35]. Error limits are three standard deviations.

The fact that we do not find the complete $K' = 0 - 2$ level structure for these three bands is disappointing but perhaps not unexpected. The sub-bands that can be observed are quite weak, and there is no reason why all three sub-bands with $K' = 0 - 2$ should have comparable intensities, since levels with even and odd K' values obtain their intensity by interaction with different trans-well vibrational levels. In passing we note that the absence of the complete $K' = 0-2$ level structure for these bands argues against the possibility that the intensity comes from vibronic coupling with higher-lying electronic states. If the intensity comes through vibronic coupling, we would not expect to see a K-dependence of the observed intensities.

To obtain the vibrational assignments of these states we must be guided partially by the *ab initio* calculations [10, 26, 31] of the cis-well vibrational frequencies and their isotope shifts, which are summarized in Table 2.3. This table shows that we do not need to consider the two CH stretching vibrations, ν_1 and ν_5 because they will lie near 2900 cm^{-1}, while the CC stretching vibration, ν_2 will have much too large an isotope shift for the 46175 cm^{-1} state. The key lies in the 45735 cm^{-1} state, which has A_2 vibrational symmetry. The only vibrational states with A_2 symmetry expected below 2000 cm^{-1} are the torsional fundamental, 4^1, and the combination levels $3^1 4^1$ and $4^1 6^2$. If the 45735 cm^{-1} state is 4^1, which is calculated to have a vibrational energy of close to 800 cm^{-1}, the zero-point level of the S_1-cis well will lie near 44900 cm^{-1}. If the 45735 cm^{-1} state is one of the combination levels, the S_1-cis zero-point level will lie at least 800 cm^{-1} lower. The most recent *ab initio* calculations of Ref. [10] give the energy of the S_1-cis zero-point level as 44856 $\pm$ 50 cm^{-1}. Since the probable uncertainty in this value is far smaller than 800 cm^{-1}, the only reasonable assignment is that the 45735 cm^{-1} level is the torsional fundamental, 4^1. Given this assignment, it is clear that there is excellent agreement between the calculations and the observed spectrum; both predict the S_1-cis zero-point level to lie near 44900 cm^{-1}.

Returning to the 46175 cm^{-1} level, which has B_2 vibrational symmetry, this level is now known to have about 1300 cm^{-1} of vibrational energy. The only possible B_2 states below about 2000 cm^{-1} are 6^1, $3^1 6^1$ and 6^3. Of these an assignment as $3^1 6^1$

gives good agreement with the calculated frequencies.

The lower of the two A_1 levels, at 45610 cm^{-1}, must then be the ν_3 fundamental. Its energy allows the cis-ν_6 frequency to be estimated roughly as $46175 - 45610 = 565$ cm^{-1}. Although this value agrees remarkably well with the harmonic frequency calculation of Ref. [10], this agreement must be to a large extent fortuitous, because the levels 3^1 and $3^1 6^1$ lie on the cis-well pathway to the isomerization barrier, and must suffer very considerably from anharmonicity, in similar fashion to the corresponding trans-well levels. [43] We note that the anharmonicity constant x_{36} for the S_1-cis state is calculated *ab initio* [53] to have the exceptionally large value of -54.2 cm^{-1}.

The upper of the two A_1 levels, at 46114.0 cm^{-1} (a vibrational energy of approximately 1200 cm^{-1}), then fits as the overtone 6^2. In principle it would be possible to estimate the position of the zero-point level from this assignment, but in the presence of such strong anharmonic effects such an estimate would be of dubious value. Figure 4 shows the observed and predicted vibrational level structure of the S_1 state of acetylene, as presently understood, up to a vibrational energy of about 5000 cm^{-1} (near the energy of the isomerization saddle point). The Franck-Condon allowed trans levels, [1, 33–37] which are responsible for the strong bands in the absorption spectrum, are shown in the columns based on ν_2 and ν_3. Some further trans levels based on ν_1 and ν_5 surround them, while the trans bending levels and their combinations with ν_2 and ν_3 fill most of the rest of the figure. At the far right are the observed cis-well levels and their assignments. It is interesting that, of the six expected lowest-lying vibrational levels of the cis isomer, all have been observed except for the zero-point level and the 6^1 level.

As for the isotope shift of the 46175 cm^{-1} level ($3^1 6^1$), the calculated vibrational contribution to its $^{12}C_2H_2 - H^{12}C^{13}CH$ shift (from Table 2.3) is 4.3 cm^{-1}. Assuming that the isotope shift of the zero-point level is the same as that of the trans-well, -6.8 cm^{-1}, the calculated $^{12}C_2H_2 - H^{12}C^{13}CH$ shift is -2.5 cm^{-1}, which is to be compared to the observed -3.03 cm^{-1}.

The rotational constants derived from least squares fits to the lines of the various S_1-cis well bands are given in Table 2.5.

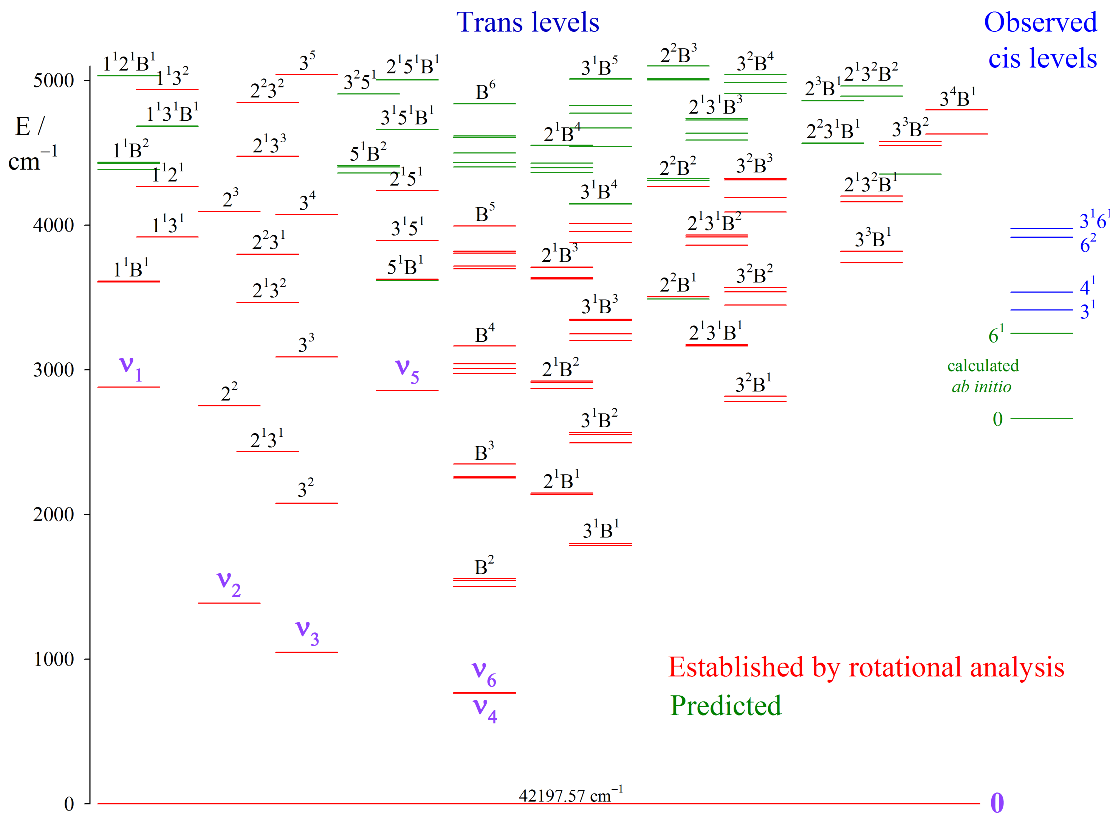

Figure 2-4: Observed and predicted $K = 0$ levels of the S_1 state of C_2H_2 up to a vibrational energy of 5000 cm^{-1}. Red lines indicate vibrational levels of the trans isomer which have been established by rotational analysis; the four observed cis well vibrational levels (at the right hand side of the figure) are indicated by blue lines. Green lines indicate the positions predicted for as-yet-unassigned or unobserved states. The diagram is complete for the trans isomer to 5000 cm^{-1}; a few predicted states above that energy are shown if they belong to polyads that extend below 5000 cm^{-1}.

2.6 On the Origin of the *K*-Staggering

One of the most interesting results of this work is the observation of an even-odd staggering in the K-structure of the cis-$3^1 6^1$ level, which indicates that tunneling through the cis-trans isomerization barrier takes place. Both the DVR calculations of Ref. [10] and the group theory considerations of Ref. [48] predict that such a staggering should occur, but it is not immediately obvious why it arises. A qualitative discussion may help to clarify its origin.

Assume initially that the only vibrational motions possible for C_2H_2 are CCH bending motions at the two ends of the molecule, and that it always remains planar. Cis-trans isomerization can take place if one of the CCH bending angles is reversed. Next assume that C_2H_2 is in an electronic state where the equilibrium configuration is cis-bent, and there is no potential minimum at the trans configuration. It is no longer possible to reverse just one of the CCH bending angles, but if both of the CCH bending angles are reversed at the same time, the cis-bent planar C_2H_2 molecule is converted into another, equivalent, cis-bent planar configuration. This new configuration will have exactly the same energy states as the original configuration. If the potential energy barrier between these two cis configurations is small, such that the molecule can tunnel through it, one has the possibility of inversion-like doubling of the vibrational levels of the two configurations, just as in the familiar case of NH_3. [17–21] Unlike NH_3, though, one can take acetylene back to its original configuration by a C_2 rotation about the inertial a-axis, which means that the new configuration is the same as the original one. Since there is only one possible configuration, the energy states of the second configuration must be thrown away.

Detailed examination of their effects on the various molecule-fixed coordinates [48] shows that the reversal of the CCH bending angles and the C_2 rotation about the a-axis are inextricably linked. To be exact, when these two operations are carried out in sequence, it looks as though nothing has happened to the molecule, or in other words that the identity operation has been carried out. However point group arguments do not apply if tunneling occurs. In the language of extended permutation-inversion

groups this identity is a limited identity (i.e. limited to the non-tunneling situation), because the coordinates corresponding to the two operations, individually, have not returned to their original values. [54] This complicates the throwing away process. The limited identity is one of the symmetry operations of the extended permutation-inversion group. Symmetry arguments [48] show that even-K_a and odd-K_a rotational functions are, respectively, symmetric and antisymmetric under this limited identity operation; the same applies to the sum and difference inversion-like tunneling functions. Also, acceptable rotation-tunneling product functions must be symmetric under this limited identity operation. The result is that the acceptable states (which are not thrown away) are those with even-K_a belonging to the symmetric (sum) tunneling component, and those with odd-K_a belonging to the antisymmetric (difference) tunneling component. In essence the K-staggering in the cis-$3^1 6^1$ vibrational level is what remains of the energy level pattern of the cis-to-cis inversion-like tunneling doubling after half the K-structure in each component has been thrown away. There is no K-staggering in vibrational levels of NH_3, where all K values are present in both inversion components.

The S_1 state of acetylene has cis and trans isomers occurring on the same electronic potential surface, but with a large potential maximum at the linear configuration. In this case the possibility of reversing both CCH bending angles in the two isomers leads to four potential minima, two cis and two trans. These are illustrated in Fig. 3a of Ref. [31], Fig. 1 of Ref. [10] and Fig. 4 of Ref. [48]. When the molecule in one of the cis wells tunnels through the interconversion barrier to the other cis well, it passes across one of the trans wells, but since the energy level structure of the cis wells is quite different from that of the trans wells, there is no inversion-like doubling between the cis and trans isomers as a result of tunneling through the barrier, because the cis and trans isomers are not equivalent. The cis-to-cis inversion-like doubling, giving rise to K-staggering, must still occur, but there will be no splittings. There will be a corresponding trans-to-trans inversion-like doubling, with similar K-staggering in the trans-well levels. More detail is given in Ref. [48], which includes a discussion of the additional staggering that occurs when tunneling through the isomerization barrier

as a result of internal rotation must also be considered.

It may be argued that the K-staggering in C_2H_2 should not be compared with the inversion of NH_3, but rather with the level pattern of a triatomic molecule such as H_2O when it has sufficient bending excitation to become linear. In the H_2O case the K-structure changes smoothly at the barrier to linearity from an asymmetric top pattern to a linear molecule pattern, and there are no discontinuities that alternate with K. However this is not what happens in C_2H_2, where the level pattern is like that of NH_3, but with the even-K levels missing in one inversion component of a vibrational level, and odd-K levels missing in the other.

2.7 Discussion

This work illustrates for the first time some of the high resolution spectroscopic signatures of cis-trans isomerization. The state involved, the S_1 state of acetylene, is well suited for a study of this type because its vibrational structure is comparatively sparse near the cis-trans saddle point, and the bands can be observed in transitions from a different electronic state where no cis-trans isomerism is possible, thereby simplifying the analysis.

To summarize, transitions from the ground electronic state of acetylene are allowed to the lower energy (trans) isomer of the S_1 state, but not to the cis isomer, which lies about 2700 cm^{-1} higher. The interconversion barrier (saddle point) lies about 2000 cm^{-1} still higher in energy, with the transition state being half-linear. [26] The isomerization coordinate which carries the shape of the molecule from that of the trans isomer to that of the transition state is a linear combination of two normal coordinates, Q_3 (trans bend) and Q_6 (cis bend). Very large higher-order cross-terms between Q_3 and Q_6 are therefore needed in the potential function in order to represent the minimum energy pathway along the isomerization coordinate. As a result, the vibrational levels that involve excitation of both ν_3 and ν_6 are highly anharmonic. [43, 46] Very detailed analyses of the level structure of the trans-well are required in order to identify each level [43] and, so far, every expected level of the trans-well has been

accounted for up to a vibrational energy of 4200 cm^{-1}. A few weak extra bands at lower energy are left over. The upper states of these extra bands do not belong to a triplet electronic state, because they are observed to have only small Zeeman effects; their carbon isotope shifts are not compatible with their energy relative to the zero-point level of the trans isomer; *ab initio* calculations predict no other singlet electronic states in this energy region, [31] and the upper states have extremely long lifetimes, indicating that they are metastable. The conclusion is that these extra vibrational levels belong to the S_1-cis isomer, and comparison with the results of *ab initio* calculations [10, 55] strongly supports this conclusion.

The upper state of the most obvious cis-well band assigned so far is cis-$3^1 6^1$ (46175 cm^{-1}). This is not altogether surprising because the isomerization pathway in the cis isomer is also a combination of Q_3 and Q_6, where these coordinates are the symmetric and antisymmetric in-plane bends. The cis-$3^1 6^1$ state lies only about 700 cm^{-1} below the interconversion barrier, and has a high probability of tunneling through it. The tunneling has two consequences. One is that the cis-$3^1 6^1$ state can interact with levels of the trans-well close by in energy, and thereby obtain appreciable absorption intensity. As discussed in the previous section, the other is that its K structure shows a staggering of the odd-K levels versus the even-K levels, [48] amounting to no less than 3.9 cm^{-1}.

As yet no K-staggerings have been identified in trans-well levels. The reason for this is that the bending states of the trans isomer suffer from strong Coriolis and Darling-Dennison resonance, so that it is difficult to establish the zero-order positions of the K-rotational levels. Nevertheless the progressive breakdown of the simple Coriolis plus Darling-Dennison model for the higher bending combination polyads of the trans isomer [43] must reflect the onset of K-staggerings. Not every predicted level near the energy of the interconversion barrier will show K-staggerings, of course; the magnitudes of these staggerings will depend on the specific vibrational quantum numbers, and on how effectively the molecule in a particular state can tunnel through the barrier.

In addition to this even-odd K-staggering arising from local-bend tunneling, there

will be a further staggering of the $K = 2, 6, 10, ...$ levels versus the $K = 0, 4, 8, ...$ levels, when tunneling due to internal rotation becomes important near the cis-trans saddle point. [48] Table 2.5 shows that the A rotational constant of the torsional fundamental, cis-4^1, is about 1 cm^{-1} larger than that of cis-$3^1 6^1$, which (as described in Section 2.4.3) is close to the value calculated from the *ab initio* geometric structure. The $K' = 2$ level of cis-4^1 (45790.8 cm^{-1}) lies not far above the upper $K' = 2$ level of trans-$2^2 B^1$ (45777.9 cm^{-1}); [43] thus we cannot rule out the possibility that it has been pushed up by interaction with it. Nevertheless the effects of internal rotation are expected to be magnified on excitation of the torsional vibration and, when only the $K' = 0$ and 2 levels are observed, any staggering due to internal rotation tunneling will appear as a change in the apparent A rotational constant derived from their separation. [48] Therefore it is not impossible that there is a K-staggering of about 4 cm^{-1} due to internal rotation tunneling in the cis-4^1 vibrational level. Nothing can be said in this instance about possible staggering due to the local-bend tunneling (odd-K versus even-K) since the $K' = 1$ level of cis-4^1 has not been located.

A number which could be of some significance is the interaction matrix element between the cis-6^2 and trans-$1^1 3^1$ levels, which is found, from the minimum rotational level separation at the perturbation between them, to be 0.30 cm^{-1}. (See Table 2.5.) In a simple model this matrix element would be the product of an electronic factor, a cis-to-cis tunneling matrix element and a cis-trans vibrational overlap integral, divided by a cis-trans energy denominator. It will be instructive to attempt to reproduce this number by *ab initio* calculation.

The vibrational energy level pattern expected at higher energies can be predicted roughly from the DVR calculations reported in Ref. [10]. Those states which have many quanta of ν_3 and ν_6 will show progressively larger K-staggerings, which will rapidly become so large that it will be difficult to associate a given set of even-K levels with a corresponding set of odd-K levels. Their vibrational wave functions, instead of being mostly localized either in the two cis-wells or in the two trans-wells, will have amplitude in all four wells, and the mixed state vibrational characters of the even- and odd-K levels will become increasingly different. The assignment of approximate

vibration-rotation quantum numbers will require very detailed calculations. Since the barrier to internal rotation vanishes at the half-linear transition state, there will be a further staggering of the $K = 2, 6, 10, ...$ levels versus the $K = 0, 4, 8, ...$ levels, as just described. In contrast, the progressions that do not involve the bending vibrations will continue normally, as at lower energy, barring minor perturbations and resonances.

The level pattern above the interconversion barrier will presumably reorganize itself according to a new basis set, just as the levels of the ν_2 (umbrella) vibration of ammonia above the inversion barrier can be treated as those of a planar molecule vibrating with large amplitude. It would seem that the bending levels of acetylene above the cis-trans isomerization barrier should rearrange themselves into those of a non-linear molecule vibrating with three very large amplitude coordinates. The vibrational wave functions will sample all of the available bending phase space, so that any given level can no longer be labeled specifically as cis or trans. Above the potential maximum at the linear configuration the level pattern will become that of a linear molecule but, at that high energy, interactions with other electronic states will almost certainly obscure the pattern.

In conclusion, the spectrum of a molecule capable of cis-trans isomerization consists of superimposed spectra from the two isomers in the energy region below the interconversion barrier. Those vibrations corresponding to the minimum energy pathway to isomerization are extremely anharmonic, and those levels near the barrier which can tunnel through it display staggerings in their K-rotational structure. At the interconversion barrier the levels merge into a very different-looking large amplitude vibrational pattern. Those vibrations that are not involved in the isomerization path behave normally, so that the spectrum consists of overlapping progressions with different degrees of complexity.

Many aspects of the spectrum are different from those of molecules showing inversion doubling or internal rotation. We are continuing work on the interesting region of the S_1 state of acetylene where the vibrational level pattern is reorganizing itself near the barrier to isomerization.

Chapter 3

Reduced Dimension DVR Study of *cis-trans* Isomerization in the S_1 State of C_2H_2

Abstract

Isomerization between the *cis* and *trans* conformers of the S_1 state of acetylene is studied using a reduced dimension DVR calculation. Existing DVR techniques are combined with a high accuracy potential energy surface and a kinetic energy operator derived from **FG** theory to yield an effective but simple Hamiltonian for treating large amplitude motions. The spectroscopic signatures of the S_1 isomerization are discussed, with emphasis on the vibrational aspects. The presence of a low barrier to isomerization causes distortion of the *trans* vibrational level structure and the appearance of nominally electronically forbidden $\tilde{A}\ ^1A_2 \leftarrow \tilde{X}\ ^1\Sigma_g^+$ transitions to vibrational levels of the *cis* conformer. Both of these effects are modeled in agreement with experimental results, and the underlying mechanisms of tunneling and state mixing are elucidated by use of the calculated vibrational wavefunctions.

The results in this chapter have been published in the Journal of Chemical Physics [10].

3.1 Introduction

The history of the $\tilde{A}$ state of acetylene is full of spectroscopic surprises. Beginning with the discovery that acetylene changes shape from linear to *trans*-bent upon elec-

tronic excitation [1, 33, 34], the $\tilde{A} \leftarrow \tilde{X}$ spectrum has exhibited a string of unexpected phenomena, including axis switching [3], triplet perturbations [51, 56, 57], as well as unusually strong Coriolis interactions and Darling-Dennison resonance between the bending vibrations [38, 41]. Most recently, the comprehensive assignment of the low energy vibrational structure has led to the identification of several "extra" levels. These appear in the spectrum near 3000 cm^{-1} above the ground vibrational state of the *trans* conformer, just as the effective Hamiltonian ($\mathbf{H}^{\text{eff}}$) models developed at lower energy begin to break down [43].

The most probable explanation for these "extra" levels is that they belong to the *cis* conformer of the S_1 state [11]. *Ab initio* calculations have long predicted a *cis* minimum [26, 31, 58], but experimental confirmation has been hard to come by. This is because the S_1-S_0 electronic transition is forbidden in C_{2v} geometries, and any spectroscopic observation of the *cis* conformer is therefore expected to manifest itself in the form of weak transitions or indirect effects, necessarily resulting from vibronic mechanisms.

The purpose of this paper is to investigate theoretically the spectroscopic consequences of the low barrier isomerization process on the $\tilde{A}$ state potential surface. In general, how will the presence of a second distinct accessible minimum distort the vibrational energy level patterns? One detail of particular interest is whether S_1 *cis* states could appear at the observed energies with the intensities observed for the "extra" levels. The calculations in the literature characterize the relevant stationary points on the potential energy surface (PES), but cannot address these questions because of the delocalized nature of the wavefunctions involved in large amplitude motion and the importance of effects like tunneling. Large amplitude dynamics on a reduced dimension S_1 surface have been studied previously by spectral quantization [30, 32], but those calculations focused mainly on the well-known Franck-Condon active progressions in the CC stretching mode, ν_2, and the *trans*-bending mode, ν_3, while revealing little about the weak or forbidden bands that encode the isomerization dynamics.

The method we choose for our treatment uses a reduced dimension Discrete Vari-

able Representation [59]. Since we are investigating an isomerization process, the calculation must be able to treat large amplitude motions that span the two geometries. DVR methods are well-suited to this type of problem because the basis functions are not tied to a single center as they usually are in a variational calculation [60]. Since the half-linear transition state [26] and the Franck-Condon active vibrations are all planar, we can perform a reduced dimension calculation and still expect to capture the essential features of the experimental spectrum. As described in detail below, the calculation is performed in the three dimensions that encompass the CC stretch as well as the *trans* and *cis* bending vibrations.

An important ingredient in our calculation is a high accuracy potential energy surface for an excited electronic state. This work represents the first application of EOM-CCSDT [61] methods to the PES of a polyatomic molecule, and we believe there is great promise in applying such methods to the study of electronically excited states. In fact, we find that this level of theory is necessary to obtain quantitatively acceptable agreement with experiment for this system.

We obtain from our DVR calculation the vibrational eigenstates of the full S_1 potential surface in the three dimensional coordinate space. Since the basis functions are not defined relative to one specific geometry, the eigenfunctions are not predetermined to belong to either the *cis* or *trans* conformer, although they naturally divide themselves in this way at low energy. We therefore expect that the calculated results will contain all of the effects we desire to model: the possible existence of *cis* levels interspersed among those of the *trans* conformer, and any mixings between them that arise from tunneling through the isomerization barrier. Other signatures of the isomerization, such as the distortion of the *trans* level structure, should also be satisfactorily reproduced.

Finally, we note that this method could be generally applicable to other isomerizations, even in larger molecules. It allows for a selective treatment of only the few coordinates relevant to the minimum energy isomerization path, but is still based on a simple and easily understandable Hamiltonian. Its foundation on established DVR methods provides computational efficiency and accuracy.

3.2 Methods

In this section we describe the elements of our method for reduced dimension vibrational DVR calculations. Ours is not the first such calculation, even on acetylene [62, 63], but our approach differs from those of previous authors. We specify significant departures from earlier reduced dimension DVR calculations on acetylene where appropriate.

An important consideration in a reduced dimension calculation is that the qualitative and quantitative accuracy of the results are frequently balanced against the effort required to perform the calculation. In this work we have gone to some lengths in order to obtain quantitatively accurate results, but very useful qualitative results can be had much more easily. Even for spectroscopists, the pattern and assignments of the levels can be valuable even if quantitative agreement with experiment is poor. We demonstrate this point later on in connection with the quality of the potential energy surface and the number of dimensions included in the calculation, which are the two factors that have the greatest impact on the computational cost of the calculation.

It is appropriate to begin our discussion of the details by mentioning that we desire a matrix representation of $H = T + V$, where T and V are expressed in the same basis. We will examine the two parts of the Hamiltonian separately, but first we must digress briefly on the subject of coordinate systems.

3.2.1 Molecule-Fixed Coordinate Systems

The choice of coordinate system for a calculation in the molecular frame is a complicated one. The problem of separating vibration and rotation is exacerbated when large amplitude motions are possible [64], and even remaining in the center of mass frame may not be trivial [62, 63] for molecules larger than triatomics. For acetylene, several different coordinate systems have been used in the literature for various types of calculations [65, 66]. We find the internal coordinates of **FG** theory [67] to be extremely convenient, and recommend them generally. The vibrational phase space is spanned efficiently by these coordinates, especially at low energy, and

the **G** matrix elements [68, 69] derived from them provide a simple way to represent the kinetic energy operator.

In reduced dimension calculations using internal coordinates, one departure that may be necessary from the canonical set of such coordinates for a given molecule concerns their domains. Since the usual set of $3N-6$ coordinates is chosen to uniquely specify all possible geometries (leaving aside linearity for the moment), it may be necessary to change the domain of one or more of the angles. For example, since we do not include the usual torsional coordinate, τ, in our planar acetylene calculation, it is necessary to increase the domain maximum of at least one of the $\angle$CCH valence angle bends from π to 2π in order to allow both *cis* and *trans* geometries. (In this paper τ is defined as zero, except in Table 3.1 where $\tau = \pi$.) Additionally, here both $\angle$CCH bends extend from 0 to 2π, a space that encompasses two *cis* and two *trans* minima. The calculated wavefunctions are therefore rovibrational and can be classified in the G_4 CNPI-MS group, as explained in Sec. 3.3.1.

3.2.2 The Potential Energy Surface

The hallmark of all DVR calculations is the simplicity of the potential energy matrix elements. More generally, any function of coordinates is a diagonal matrix, $\langle\theta_i|\hat{f}(x)|\theta_j\rangle \approx f(x_i)\delta_{ij}$, where the $\{x_i\}$ are the pseudospectral grid points of the DVR basis [70]. Once a reduced set of coordinates has been chosen, only two things remain to be done to express V in the DVR basis: finding the appropriate level of *ab initio* theory at which to calculate the potential energy surface, and deciding how to treat the discarded degrees of freedom when the active coordinates are varied.

Previous theoretical investigations of the S_1 surface encountered difficulties with the harmonic frequencies of the *trans* structure, especially the lowest frequency modes, ν_4 and ν_6 [26, 31]. We report here EOM-CCSDT harmonic frequencies and compare them to EOM-CCSD values and experimental data in Table 3.1. Since we exclude ν_4, the CCSD frequencies seem satisfactory, but still the improved agreement at CCSDT is obvious. Indeed, we were able to obtain qualitatively useful results with a CCSD potential surface, but quantitative agreement requires CCSDT. In light of

this, a reasonable full set of harmonic frequencies appears to be a good criterion for selecting a level of *ab initio* theory. The relatively poor quantitative agreement with experiment obtained in a full dimensional calculation of the vibrational fundamentals using a CCSD surface [71] corroborates this conclusion, as our reduced dimension CCSD vibrational fundamentals for ν_3 and ν_6 are very similar to their results.

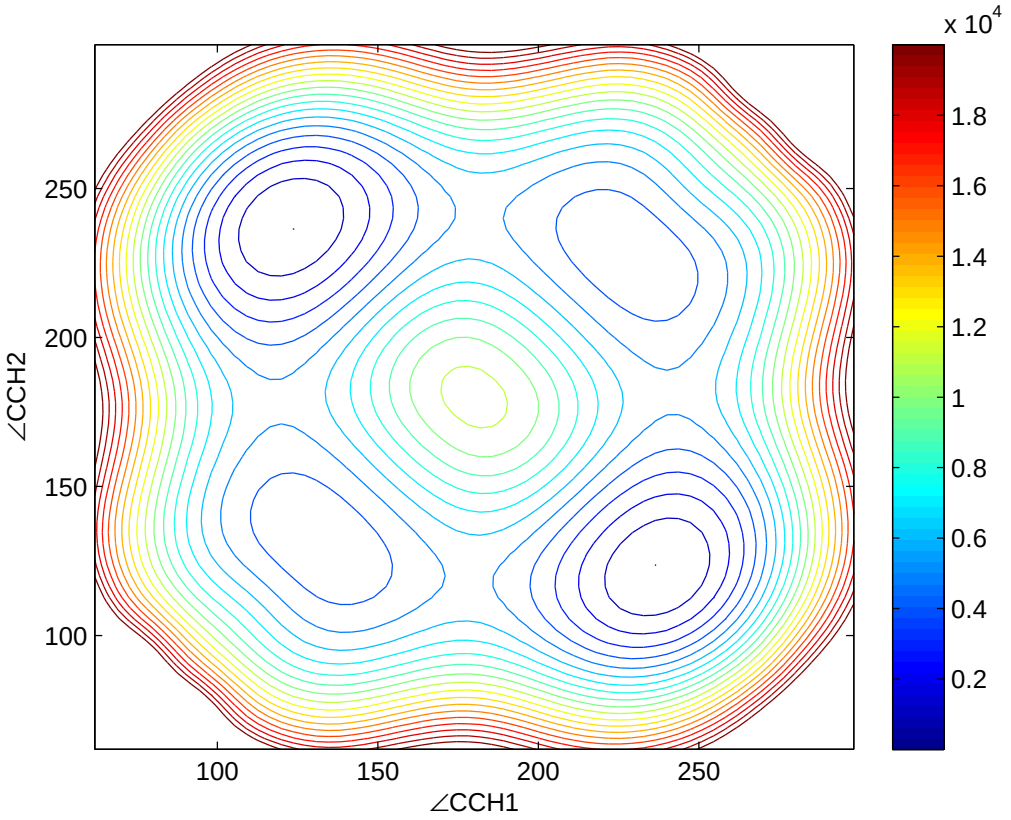

Figure 3-1: A slice of the S_1 PES with R_{CC} and R_{CH} at their *trans* equilibrium values. The *cis* minima are located in the lower left and upper right, and the *trans* minima are in the upper left and lower right. The energy scale is in cm^{-1} and the contour spacing is 10^3 cm^{-1}.

The simplest approach for dealing with the discarded degrees of freedom is to fix them at their equilibrium values. While it is impossible to make absolute generalizations due to the heterogeneous decomposition of the normal modes into the internal coordinates, our experience is that this approximation leads to computed vibrational fundamentals within at worst 10% of the experimental values, but usually signifi-

Table 3.1: Geometries and harmonic frequencies for $\tilde{A}\ ^1A_u\ ^{12}C_2H_2$: Comparison of *ab initio* methods

	CCSD [26]	CCSDT	Expt. [41, 42, 72, 73]
ω_1	3107.7	3053.5	$(3004)^a$
ω_2	1471.4	1424.6	1410.26
ω_3	1106.6	1106.1	1070.34
ω_4	614.6	761.5	764.7
ω_5	3083.7	3031.0	$(2914)^a$
ω_6	745.8	776.5	772.5
$\angle$CCH	123.64	122.09	122.48
R_{CC}	1.3575	1.3743	1.375
R_{CH}	1.0907	1.0963	1.097
T_0	43830	42334	42197.57

Frequencies in cm^{-1}, angles in degrees, and bond lengths in Å.

[a]These harmonic frequencies are less well determined because their overtones have not yet been observed. [42]

cantly better. We would have been satisfied with this approximation except for the Fermi resonance that manifested itself between 2^n6^m and $2^{n-1}6^{m+2}$ in early calculated results, which precluded comparisons with effective Hamiltonian fits to experimental data. We therefore replace R_{CC} with the normal coordinate for ν_2 from the harmonic frequency calculation, which provides a prescription for varying the CH distances as the CC bond length changes.[1] We did also consider vibrational adiabatic potentials, which are commonly used in the literature [62, 63]. However, given the limited return and the enormous computational cost of minimizing the energy at every point on the entire three dimensional grid, we elected not to pursue this option. A fitted surface might be more suitable for addressing this particular issue.

3.2.3 The Kinetic Energy Operator

The kinetic energy operator presents several difficulties. The form of the Laplacian in the chosen coordinate system must be determined, which can be very tricky

[1]The consequences of this substitution for the kinetic energy will be discussed in Section 3.2.3. This is not a major alteration of the calculation; it significantly improves the value obtained for the ν_2 fundamental and otherwise causes only minor changes in the level structure. Results quoted are solely from this version of the calculation, except in Sec. 3.3.4.

[62, 63, 66], especially since singularities in the kinetic energy are possible. Furthermore, expressing the Laplacian in a DVR basis can lead to a non-Hermitian **H**. The kinetic energy operator matrix elements are more complicated than those of V, but we merely need to add matrix representations of differential operators to the trivial matrix representations of functions of coordinates already in our repertoire. Depending on the underlying basis, DVR matrix elements of differential operators can be calculated straightforwardly either via basis transformations to and from a finite basis representation [74], e.g. a harmonic oscillator, or by explicit formulas [75], most commonly based on Fourier functions [76–78]. The selection of an appropriate DVR basis consists primarily of choosing one whose underlying basis functions have the same boundary conditions as the eigenfunctions to be obtained [77].

We use the **G** matrix elements to obtain the kinetic energy operator, taking care to follow Podolsky [79], and also using an explicitly Hermitian form [80] of each term, such that

$$T = \frac{-\hbar^2}{2} g^{1/4} \sum_{i,j} \left(\frac{\partial}{\partial S_i} \right)^{\dagger} g^{-1/2} \mathbf{G}_{ij} \frac{\partial}{\partial S_j} g^{1/4} \tag{3.1}$$

where $g = \det |\mathbf{G}|$ and the S_i are the internal coordinates. Even though the sum extends only over the active coordinates, the determinant g includes $\mathbf{G}_{ij}$ for all pairs of coordinates. It is important to note that although the traditional **FG** matrix solution invokes the approximation of infinitesimal displacements, the coordinates themselves and their **G** matrix elements are valid for motions of any amplitude [67]. We simply represent the functions of coordinates in the $\mathbf{G}_{ij}$ as diagonal matrices instead of evaluating them at a specific geometry. In our planar acetylene calculation we take care to use the kinetic energy matrix elements for the bending of a linear molecule [69], since the torsional angle is not well behaved when planar *cis-trans* isomerization can occur.

Finally, for consistency with our use of the ν_2 normal coordinate when calculating the PES, we also redefine R_{CC} as the CC stretch component of the ν_2 normal coordinate, according to $Q_k = \sum_t \left(L^{-1}\right)_{kt} S_t$, where Q, S, and L are the mass-weighted normal coordinate, an internal coordinate, and the transformation that diagonalizes

GF, respectively [67]. The R_{CH} contributions are still neglected.[2]

3.2.4 Specifics and Practical Considerations

The specifics of our treatment of S_1 acetylene are as follows. We take a subset of the internal coordinates, consisting of the two ∠CCH valence angle bends ($0 \leq \{\phi_1, \phi_2\} \leq 2\pi$) and the C–C bond stretch, which correspond loosely to $\{\nu_2, \nu_3, \nu_6\}$. Our DVR basis is then the direct product basis $\phi_1 \otimes \phi_2 \otimes R_{\mathrm{CC}}$, and we use the sinc DVR basis [77] for the angles, but a harmonic oscillator basis for the bond stretch. The final results were generated using 120 grid points for each of the two bend bases, and 43 points for the stretch basis. The pseudospectral grid points and differential operator matrix elements are available from analytical formulas for the sinc basis, and, for the harmonic oscillator basis, from the diagonalization of the coordinate matrix and the application of the resulting transformation matrix to other operators expressed in the harmonic oscillator basis. We then construct **T** according to Eq. 3.1. We calculate the potential energy for 10 geometries along each coordinate at regular intervals spanning $\{60^\circ \leq \phi_1 \leq 300^\circ, 60^\circ \leq \phi_2 \leq 180^\circ, 1\ \text{Å} \leq R_{\mathrm{CC}} \leq 2\ \text{Å}\}$; the rest of the PES is related to this portion by symmetry. *Ab initio* calculations were performed with the CFOUR program system [81, 82], using the EOM-CCSDT method and the NASA Ames ANO1 basis set. The elements of **V** are found by interpolating the potential energy surface at the DVR grid points using a cubic spline method, after discarding grid points that lie outside the original domain of the *ab initio* surface. This reduced the size of the basis mentioned above to 80×80×34.

In practice, the construction and diagonalization of **H** are accomplished by a basis set contraction (see Eq. 35 of Ref. [60]). The DVR **H** for the 2D $\phi_1 \otimes \phi_2$ space at every value of R_{CC} is diagonalized, and the eigenvectors above a chosen cutoff energy are discarded. (For the results presented here this cutoff energy was 10,000 cm^{-1}, with a minimum of 35 vectors retained per 2D block.) The resulting

[2]This redefinition weights the R_{CC} kinetic energy by the projection of the internal coordinate onto the ν_2 normal mode. The effect is to discard portions of this term that would be included in ν_1 in full dimensionality.

rectangular transformation matrices are used to compress the remaining blocks of the 3D **H**, which are off-diagonal in R_{CC}, prior to the final diagonalization. Applying the rectangular transformation matrices in reverse transforms the final eigenvectors back to the grid point representation.

3.3 Results

Using the method described here, vibrational eigenstates of S_1 acetylene could be obtained up to energies exceeding 15,000 cm^{-1}. For the most part we will limit the discussion to states up to about 5,000 cm^{-1}. In general we will forego itemized examination of the calculated states and instead focus on more broad agreement with experiment and predicted trends, in keeping with the goals stated in the beginning of Section 3.2. Nevertheless, it is worth mentioning that the calculated vibrational fundamentals are within 2% of the experimental values (Table 3.2), despite the neglect of the other dimensions. (The results of an *ab initio* harmonic frequency calculation for the *cis* geometry are given for reference in Table 3.3.)

Table 3.2: DVR vibrational fundamentals for $\tilde{A}\ ^1A_u$ and $\tilde{A}\ ^1A_2$ $^{12}C_2H_2$

	$\tilde{A}\ ^1A_u$		$\tilde{A}\ ^1A_2$	
	Calc.	Expt. [35, 38]	Calc.	Expt. [11]
ν_2	1414.65	1386.9	1489.61	–
ν_3	1033.6	1047.55	789.56	–
ν_6	780.35	768.26	588.35	(565)[a]

Frequencies in cm^{-1}.
[a]Estimated from the energy difference between two observed combination bands.

3.3.1 Symmetry of the Reduced Dimension Eigenstates

Before entering into a more detailed discussion of the calculated states, it is necessary to work out the connections between the symmetries that exist in the coordinate space of the calculation and the true symmetries of the molecule, so as to be able to interpret the wavefunctions. It can be seen in Fig. 3-1 that two *trans* and two *cis*

Table 3.3: *Ab initio* geometry and harmonic frequencies for $\tilde{A}\ ^1A_2\ ^{12}C_2H_2$

ω_1	2997.14
ω_2	1583.22
ω_3	806.09
ω_4	817.5
ω_5	2941.81
ω_6	571.62
$\angle$CCH	132.62
R_{CC}	1.3423
R_{CH}	1.0983
T_0	45155

Frequencies in cm^{-1}, angle in degrees, and bond lengths in Å.

minima exist in the calculation. Each well possesses a twofold symmetry, such that the PES has four equivalent (triangular) quadrants. More generally, the symmetry group of the reduced dimension Hamiltonian is of order four. Reflection across the antidiagonal corresponds generally to the $(12)(ab)$ CNPI symmetry operation [64], but can also be thought of as the C_2^b operation in the C_{2v} point group. Reflection across the diagonal is similarly $(12)(ab)^*$, or the i operation in the C_{2h} point group. This leads to the conclusion that inversion through the center of the coordinate space as depicted in Fig. 3-1 correlates with the E^* operation. Therefore, the eigenstates produced by the calculation will belong to one of the four rovibrational irreducible representations laid out in Table 3.4, as will be illustrated in Fig. 3-2. Accordingly, we expect each calculated vibrational level to appear as a near degenerate pair of eigenstates with different rotational symmetries, except when *cis-trans* interaction causes one member of the pair with a particular rovibrational symmetry to shift. This shift is analogous to the K-staggering that occurs in the experimental spectrum [11].

3.3.2 Agreement with Experiment

The primary difference between the DVR results and the observed levels is that many states are missing due to the reduced dimensionality. Most important, due to the exclusion of ν_4, all bending (B) polyads are represented by a single vibrational

Table 3.4: Rovibrational symmetries of DVR wavefunctions

CNPI-MS [4]	C_{2h}	C_{2v}
$Sa-/As-$	a_g, K_c odd	b_2 oo
$Ss+/Aa+$	a_g, K_c even	a_1 ee
$Ss-/Aa-$	b_u, K_c odd	a_1 oo
$Sa+/As+$	b_u, K_c even	b_2 ee

R_a^π is not an equivalent rotation for the *trans* geometry, and therefore its oe/ee and oo/eo have the same CNPI symmetry. Conversely, the *cis* rotational structure supports all CNPI symmetries, but only oo and ee appear here. The first member of a pair of CNPI-MS labels will be used as a shorthand notation.

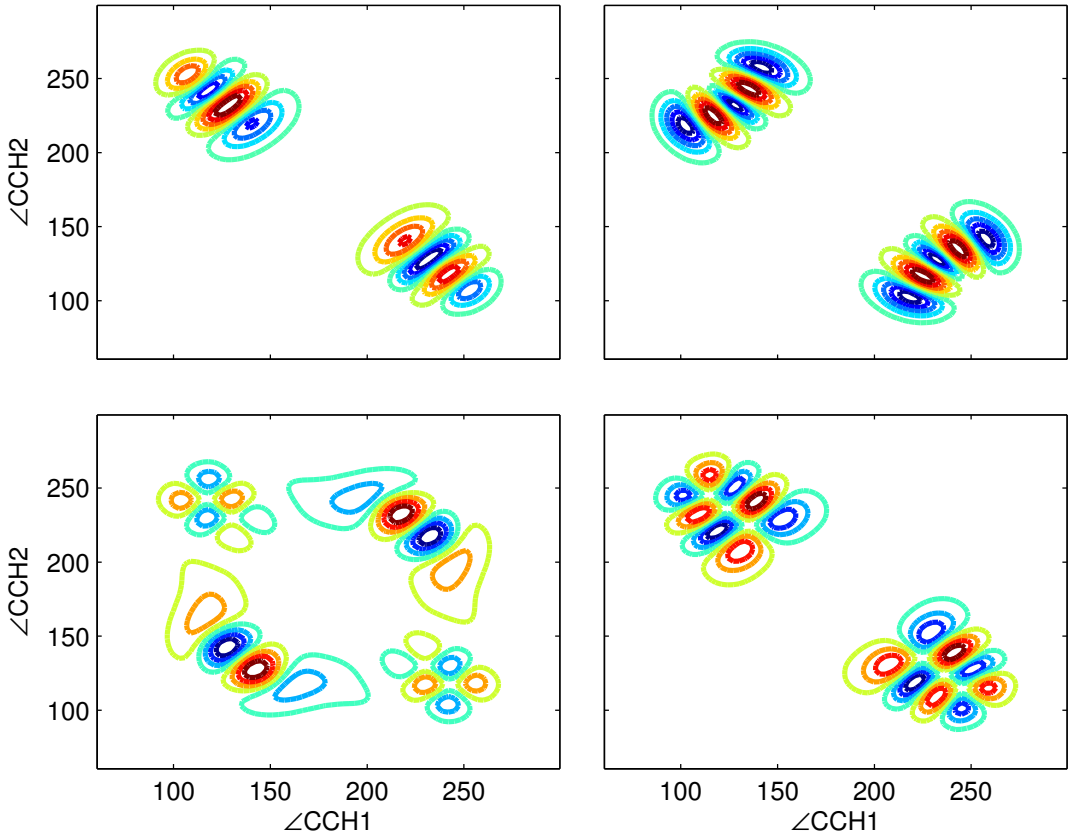

Figure 3-2: Wavefunctions illustrating the 4 symmetries listed in Table 3.4 and the types of levels discussed in Sec. 3.3.2-C. Clockwise from the top left: *trans* 3^3, $Sa-$; *trans* 6^4, $Ss+$; *trans* 3^36^1, $Ss-$; *cis* 6^3, $Sa+$. These states belong to the classes of levels with excitation in only totally symmetric modes, pure bending levels, stretch-bend combination levels, and *cis* levels, respectively. Note that the *cis* 6^3 wavefunction is delocalized over both *cis* and *trans* wells. The nodal patterns for *trans* ν_3 are similar to those obtained by spectral quantization [30, 32].

level, i.e. instead of the $n+1$ vibrational levels in a B^n polyad, the 3D calculation includes only one level, 6^n. States involving quanta in ν_1 and ν_5 are also missing, but less conspicuously.

The simplest illustration of the agreement between calculation and experiment is the juxtaposition of one photon spectra in Fig. 3-3. (The method for computing spectra is described in Sec. 3.A.) The correspondence between individual features is clear at low vibrational energy, not only for the strong Franck-Condon active progressions that can be seen easily in the figure, but also for the weaker bending polyads [41, 43] that have been identified. The comparison does become slightly more complicated at higher energy where the experimental characterization of the level structure is less complete. The onset of predissociation [83] above 46074 cm^{-1} causes many states to essentially disappear from the LIF spectrum, but the simulated spectrum makes no allowance for this effect. Furthermore, the density of states not present in the reduced dimension calculation increases rapidly above the fundamentals of the neglected CH stretching modes (45077.65 and 45054.97 cm^{-1} for ν_1 and ν_5, respectively). Fortunately, these discrepancies do not cause significant difficulties in analyzing the calculated levels and extracting information relevant to the states observed experimentally.

We now proceed with a more detailed comparison of the calculated level structure to that observed experimentally. In the recent experimental literature, the vibrational states are categorized in three groups: states containing excitation only in the totally symmetric modes [40, 42], the pure bending polyads [41], and the stretch-bend combination polyads [43]. We organize our discussion accordingly.

3.3.2.1 Totally Symmetric Modes

The states 2^n3^m are relatively straightforward, and the calculated levels match well with experiment. Values obtained from fitting the groups 2^n and 3^n agree with Table 5 of Ref. [42], with ω_2 and ω_3 approximately 20 cm^{-1} too high and too low, respectively. The parameters x_{22} and x_{33} are close to correct but too small in magnitude, such that the residual for ν_3 changes sign at $3\nu_3$. Even for ν_2, the residuals remain in the

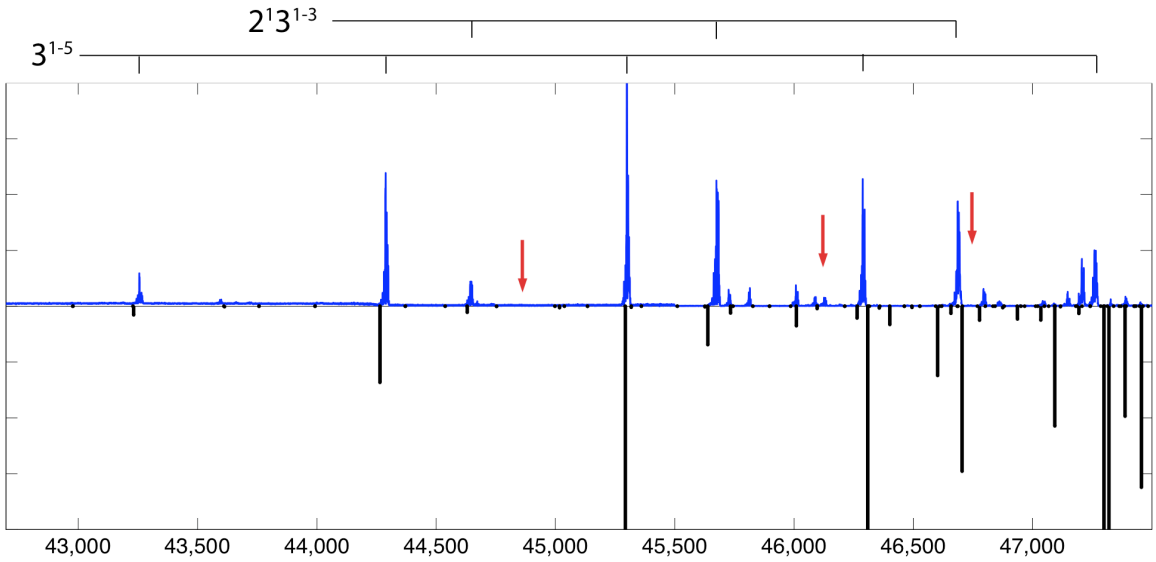

Figure 3-3: Comparison of calculated spectrum (downward) with the one photon LIF [43]. The more intense peaks have been truncated to make the weaker transitions visible. Members of the two main Franck-Condon active progressions are identified for reference. Three arrows mark the approximate positions of (from left to right) the *cis* origin, the C_2H+H dissociation limit, and the zero point energy corrected *cis-trans* barrier.

tens of cm^{-1} over the energy region of interest. The deviations from experiment are presumably due primarily to the neglect of the symmetric CH stretch.

3.3.2.2 Pure Bending States

We next consider the pure bending polyads [41], where the lowest members are nominally the 6^n states that exist in the DVR calculation. Here the comparison is complicated by the omission of the torsion from the calculation, since ν_6 and ν_4 interact very strongly via Coriolis effects and Darling-Dennison resonance. Nevertheless, we find that ω_6 from the DVR is only 8 cm^{-1} higher than the experimental value, and the anharmonicity is once again too small in magnitude. This is undoubtedly due to the surprisingly large contribution of the vibrational angular momentum to the experimental value of x_{66}, an effect absent from the calculation. Overall the bending behavior here is nearly harmonic, as is the case with the deperturbed level structure. As in the previous section, the too high harmonic frequency is presumably due at least in part to the neglect of the CH stretches, since ν_5 is also of b_u symmetry.

3.3.2.3 Stretch-Bend Combination Polyads

The stretch-bend combination polyads demand a more detailed comparison, because a global model that accounts for their vibrational structure has not yet been developed, despite the existence of extensive assignments and rotational analyses [43]. Such a comparison is presented graphically in Fig. 3-4 by plotting the effective frequencies of the bending modes as a function of quanta in ν_3. It can be seen that the calculation reproduces well even the more unusual features of the observed level structure, and the minor differences are due to the disagreement in the diagonal anharmonicities, explained in the previous two sections. The pathological behavior of this set of states is not entirely unexpected, as a combination of ν_3 and ν_6 essentially constitutes the isomerization path coordinate. Excitation in both these modes in either well should promote *cis-trans* tunneling, which will cause mixings as discussed in subsequent sections.

One oddity of particular interest is the dramatic decrease in ω_3^{eff} for the 3^n6^2 series,

illustrated in Fig. 13 of Ref. [43] up to $3^2 6^2$. Our recent high sensitivity spectra have revealed a band that is a promising candidate for $3^3 6^2$, although the assignment has yet to be confirmed by rotational analysis and therefore details regarding it will be communicated later. We nevertheless incorporate it in the figure for comparison with the DVR prediction. We further include the well-known level at 47206 cm^{-1} as $3^4 6^2$, based on the preliminary assignment of $3^3 6^2$ as well as previous discussions [42, 84], in addition to the strong intensity and proximity of $3^4 6^2$ to 3^5 in the calculated spectra. For both of these tentative assignments we find good agreement with the DVR results.

The importance of this sharp decrease in the effective frequencies is that it signals the onset of the *cis-trans* isomerization process as the potential softens approaching the transition state. We now turn our attention to the *cis* minimum of the S_1 state and its vibrational levels.

3.3.3 $^1A_2$ *cis* states

The adiabatic energy separation between the *cis* and *trans* isomers of acetylene is found to be 2659 cm^{-1} based on high-level *ab initio* calculations. Specifically, the effects of valence electron correlation have been included up to the coupled-cluster singles, doubles, triples and quadruples (CCSDTQ) level of theory, using the equation-of-motion (EOM) variant of coupled-cluster theory to treat these excited state isomers. In addition, effects of basis set insufficiency are estimated using extrapolation techniques[3] [86], and contributions due to zero point energies, core correlation and

[3]Because the target of the calculations is associated with an excited electronic state, no HEAT-based protocol exists and the specifics of the calculation warrant explanation. First, the geometries used in the calculations are those from Table 3.1. Contributions to the electronic energy of the ground electronic states at these geometries were evaluated as per the HEAT-456Q protocol. The excitation energies at these geometries were evaluated by extrapolating all-electron EOM-CCSD results obtained with the cc-pCVXZ (X = 5 and 6) basis sets using the formula advocated by Helgaker et al.[85] Contributions of triple and quadruple excitations to the excitation energy were obtained by extrapolating (frozen core) cc-pVDZ and cc-pVTZ EOM-CCSDT results and taking the difference between them and the corresponding EOM-CCSD energies. Quadruple excitations were taken from (frozen core) EOM-CCSDTQ and EOM-CCSDT results. In addition, the zero-point correction is that obtained from the EOM-CCSDT calculations with the ANO1 basis. A smaller contribution comes from scalar relativistic effects, which were obtained by contracting the relaxed EOM-CCSD density matrix obtained with the cc-pCVTZ basis in an all-electron calculation with the appropriate operators. The diagonal Born-Oppenheimer contribution was neglected.

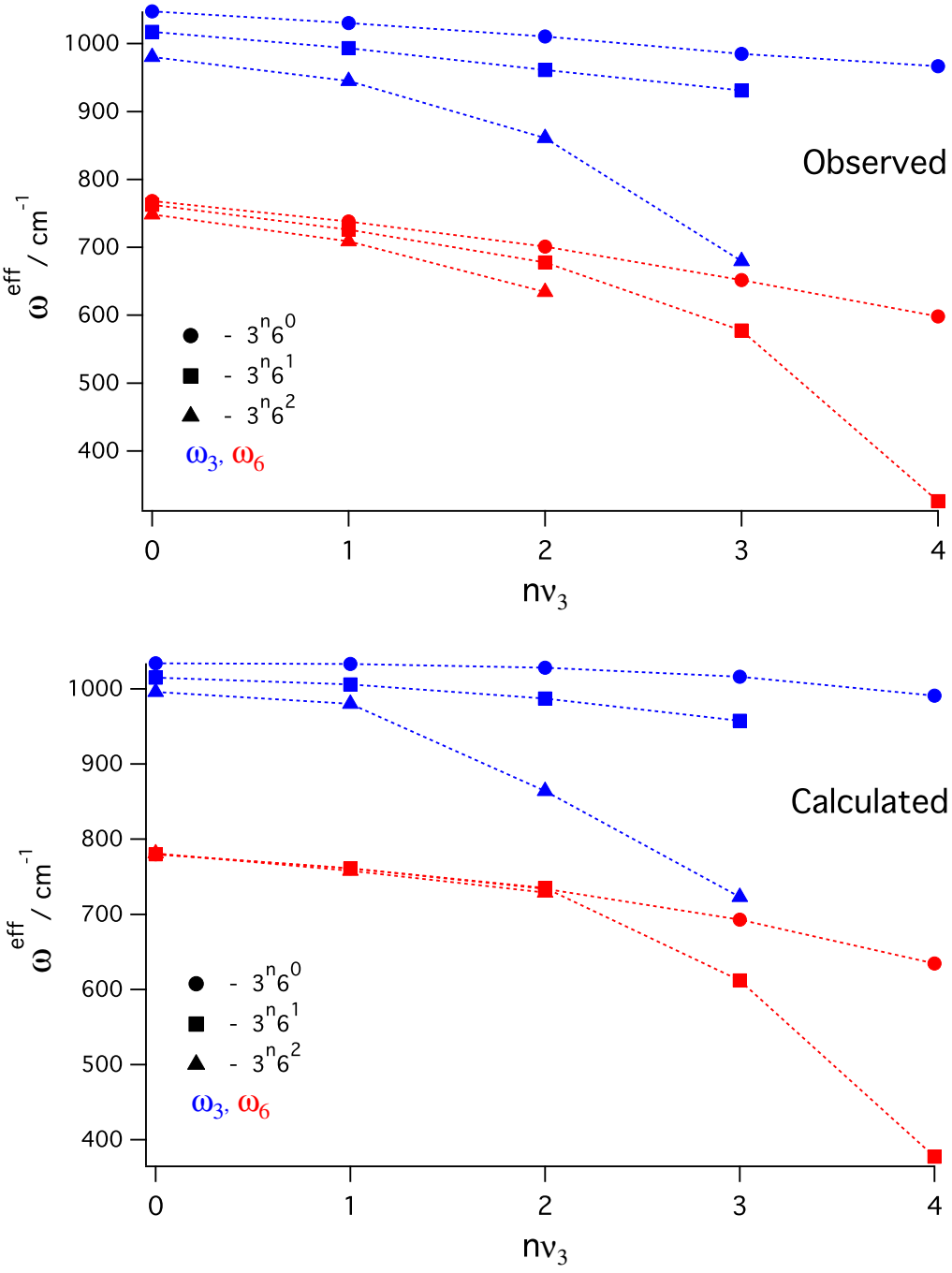

Figure 3-4: Plots of ω_3^{eff} and ω_6^{eff} vs. v_3 derived from the observed and calculated level structure. Different marker styles denote data from different values of v_6. Deperturbed values for T_0 are used, except for the 3^36^2 and 3^46^2 levels, which have not yet been deperturbed. (In those cases the energy of the observed $J = K = 0$ state is used instead.)

scalar relativistic effects are included as well. The final result of these calculations predicts the zero-point level of the *cis* isomer to lie at 44856 cm^{-1}, a calculation that we believe to be in error by no more than 50 cm^{-1}. In passing, we note that the present results are in line with a similar estimate published some time ago by Kállay and Gauss [55] of 44852 cm^{-1}.

At the EOM-CCSDT/ANO1 level of theory used in the DVR, the *cis* ground state lies above that of the *trans* conformer by ∼2820 cm^{-1}, and its vibrational state manifold is consequently less dense at any given energy. We find that all but the lowest-lying states contain at least a few percent *trans* character, using the crude metric $2\int_0^{\pi}\int_{\pi}^{2\pi}\int_0^{\infty}|\psi|^2\ dR_{CC}d\phi_1 d\phi_2$, but even these states are predicted to have non-negligible intensity in one of the four spectra discussed in Ref. [41]. These results are partially summarized in Table 3.5. At higher energy it is frequently the case that one or both rovibrational symmetries interact so strongly with several *trans* states that it is difficult to attach that zero-order assignment to any particular eigenstate. Accordingly, it should be kept in mind that the mixing fractions are probably sensitively dependent on local resonances. Spectral intensity is, as expected, generally correlated with *trans* character, and, as noted earlier, excitation in ν_3 and ν_6 greatly enhances *cis-trans* mixing. An in depth investigation of *cis-trans* interaction and intensity borrowing for a specific level is undertaken in the next section.

3.3.4 Investigation of a Specific *cis* ↔ *trans* Interaction

In order to determine the effects of *cis* states on the *trans* level structure and possible sources for their intensity, we would ideally like to compare the predictions of a model that neglects *cis-trans* mixing to the true spectrum (either calculated or experimental). In the absence of a global $\mathbf{H}^{\text{eff}}$ for the S_1 state, it is difficult to consider the level structure and spectral intensities in terms of a zero-order picture perturbed by the addition of an interaction. However, we can use the DVR to approximate two non-interacting minima by performing two calculations wherein the wavefunctions are restricted to one geometry or the other. The *cis-trans* "interactions" are then calculated by the trick of using the eigenstates of the full PES, $|\psi_i\rangle$, as a complete

Table 3.5: Calculated *cis* levels up to 5,000 cm^{-1}

State[a]	$E - T_0^{trans}$	$E - T_0^{cis}$	% *trans*
0^0	2840.84	0	<0.01
6^1	3429.19	588.35	0.03
3^1	3630.4	789.56	0.05
6^2	4015.4	1174.56	1.61
$3^1 6^{1\,b}$	4161.3	1320.46	5.13
2^1	4330.45	1489.61	0.17
3^2	4417.97	1577.13	16.8
6^3	4576.07	1735.23	25.9
$3^1 6^2$	4664.0	1823.16	45.5
$3^2 6^1$	4883.01	2042.17	34.7
$2^1 6^1$	4919.7	2078.86	2.01

[a]Values given are averaged between *oo* and *ee*.
[b]This level will be discussed in detail in Sec. 3.3.4.

set to find the vibrational overlap integrals between the zero-order *cis* and *trans* wavefunctions

$$ {}^0\langle\varphi_m^{cis}|\varphi_n^{trans}\rangle^0 = \sum_i {}^0\langle\varphi_m^{cis}|\psi_i\rangle\langle\psi_i|\varphi_n^{trans}\rangle^0 \tag{3.2} $$

and the mixing fractions follow from dividing by the zero-order energy differences. (The "true" interaction matrix elements also include an electronic pre-factor, so that we obtain only relative coupling strengths.) Zero-order spectra can also be computed between the $\tilde{X}$ state and the non-interacting sets of S_1 states, which allows for the tracking of intensity borrowing when the interaction is turned on. It should also be noted that this method can aid in assigning highly mixed eigenstates, particularly by inspection of the quantities $\langle\psi_i|\varphi_m^{cis}\rangle^0$ and $\langle\psi_i|\varphi_n^{trans}\rangle^0$.

The results of the above procedure as they apply to *cis* $3^1 6^1$, a state that lies in the region below *trans* 3^4, are discussed in the remainder of this section[4]. The vibrational b_2 symmetry of this state means that its $K = 1$ level interacts with $K = 1$ a_g levels, and that its $K = 0, 2$ levels interact with $K = 0, 2$ b_u levels. The two rotational

[4]The results in Sec. 3.3.4 are based on the first version of the calculation mentioned in Sec. 3.2.2. The zero-order energy ranking of the levels makes it impossible for the second version of the calculation to capture this interaction correctly, since the interacting levels cannot cross. In the first version of the calculation, the *trans* ν_3 fundamental is 1058.8 cm^{-1} (as opposed to 1033.6 cm^{-1}), such that *trans* 3^4 lies considerably higher, and crucially, above rather than below *cis* $3^1 6^1$ in zero-order.

symmetries therefore require parallel but separate analyses, and so we will treat only *oo*, since it appears in the simpler one photon spectrum [11].

The zero-order state of interest is trivially recognized by its nodal pattern (Fig. 3-5a). The eigenstate with this nominal assignment can then be identified (Fig. 3-5b), even though the zero-order state is mixed into several eigenstates. The spectra for the zero-order states and the eigenstates are plotted in Fig. 3-5c-d for 100 cm^{-1} above and below *cis* $3^1 6^1$. These spectra differ in two diagnostically important ways. First, the intensity has been redistributed such that the *cis* state has increased its intensity from essentially nothing to greater than that of *trans* $2^1 3^1 6^2$. This tells us not only that there is *cis-trans* interaction, but also that the intensity of the *cis* state derives entirely from this mixing and not from purely vibronic effects, such as the variation of the electronic transition moment with the nuclear coordinates (Fig. 3-7). Second, the energy level pattern has changed because the interacting states repel one another. Interestingly, although ordinarily no strong resonance would mix *trans* $2^1 3^1 6^2$ and *trans* 3^4, their interactions with a common *cis* state cause them to move apart, an example of indirect mixing.

The explanation for these two phenomena is displayed in Fig. 3-5e-f. We see that *trans* $2^1 3^1 6^2$ has a much larger overlap integral with *cis* $3^1 6^1$, as expected because of its excitation in ν_6, but *trans* 3^4 is near resonant, and consequently the two states have approximately equal mixing angles with *cis* $3^1 6^1$. This provides the *cis* state with significant intensity, and in fact the calculated relative intensities for these three states agree quite well with those observed experimentally. Finally, the vibrational overlaps between the two *trans* states and the *cis* state are in fact of opposite sign, which suggests the possibility of observable interference effects. This three state interaction is currently being investigated experimentally, and early results are so far consistent with the calculation.

3.3.5 Above-Barrier Dynamics

A full dimensional transition state search finds the *cis-trans* barrier height to be 4979 cm^{-1} (Table 3.6). In the reduced dimension PES used in the DVR, the barrier

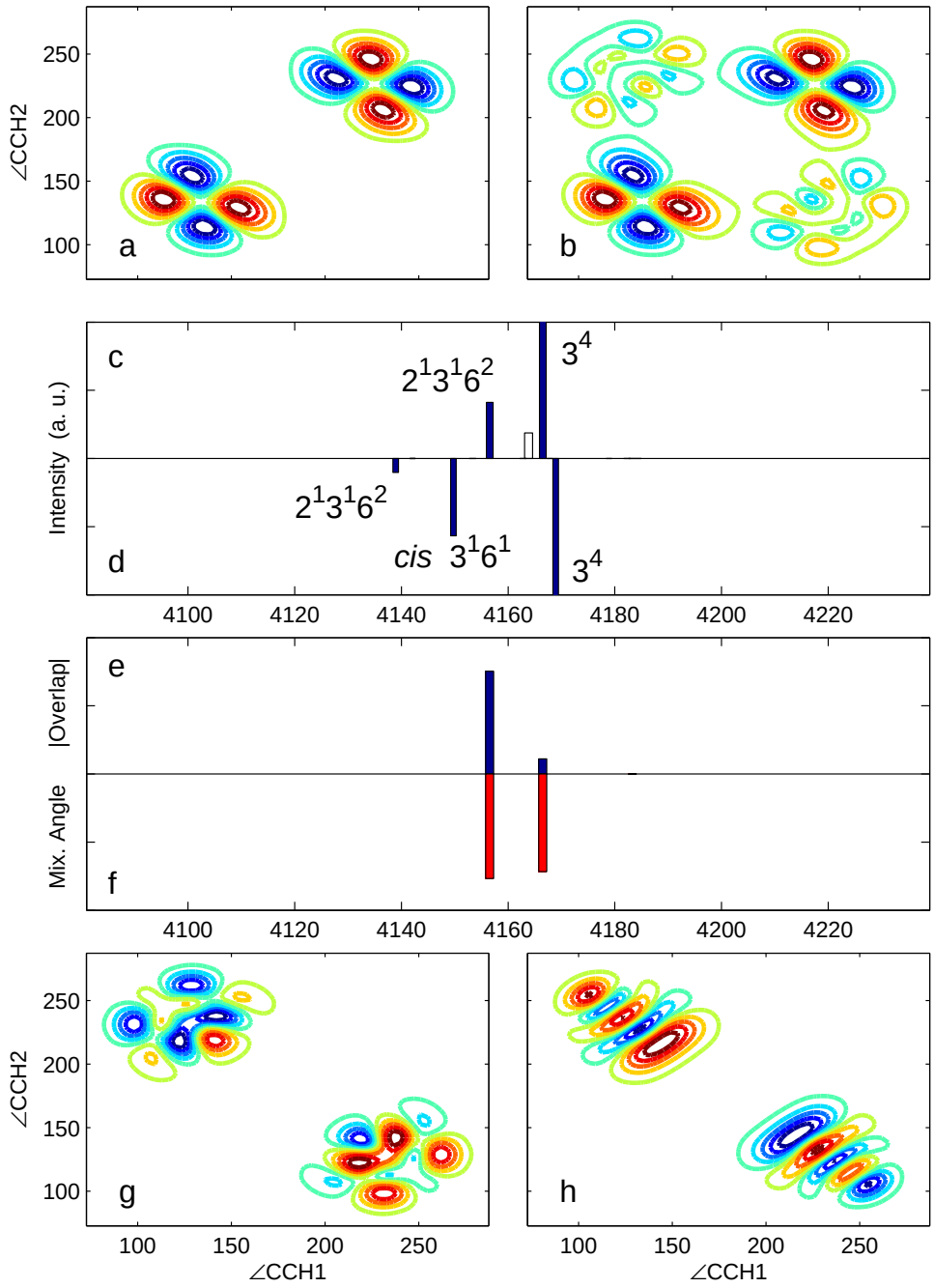

Figure 3-5: Plots depicting the analysis of *cis-trans* mixing and intensity borrowing involving *cis* $3^1 6^1$ *oo*. (a) Zero-order wavefunction of *cis* $3^1 6^1$ *oo*. (b) Eigenstate with nominal assignment of *cis* $3^1 6^1$ *oo*, showing significant *trans* character. (c) Stick spectrum of the zero-order states. The peak of *cis* $3^1 6^1$ *oo* (white) has been multiplied by 10^3. (d) Stick spectrum of the eigenstates, in which intensity has been transferred to *cis* $3^1 6^1$ *oo* from the nearby *trans* states. (The intensity of *trans* 3^4 is off scale in both (c) and (d), and the energy offset between the two spectra is slightly arbitrary.) (e) Magnitudes of vibrational overlaps between the states shown in (c) and *cis* $3^1 6^1$ *oo*. Many other states (not shown) have as large or larger vibrational overlaps with *cis* $3^1 6^1$. (f) Magnitudes of the mixing angles between the states shown in (c) and *cis* $3^1 6^1$ *oo*. These are the largest mixing angles by at least an order of magnitude, belonging to *trans* $2^1 3^1 6^2$ and *trans* 3^4, whose zero-order wavefunctions are shown in (g) and (h), respectively.

height is effectively[5] 5145 cm^{-1}.

Table 3.6: *Ab initio* geometry and harmonic frequencies for $\tilde{A}\ ^1A''\ ^{12}C_2H_2$

ω_1	3405.17
ω_2	2745.18
ω_3	1470.48
ω_4	890.01
ω_5	$886.19i$
ω_6	766.18
$\angle CCH_1$	119.80
$\angle CCH_2$	178.70
R_{CH_1}	1.1147
R_{CH_2}	1.0680
R_{CC}	1.3548
$T_e - T_e^{trans}$	4979

Frequencies in cm^{-1}, angles in degrees, and bond lengths in Å. The transition state geometry is slightly *cis*-bent.

Above this energy, delocalized states begin to appear [30] (Fig. 3-6), but other states unrelated to the isomerization coordinate remain unaffected. Although any conclusions about the above-barrier dynamics would be premature, a cursory analysis of the delocalized wavefunctions shows that they correspond to out of phase combinations of local benders. The elliptical shapes ("ring modes") are therefore similar to Lissajous figures for two equal amplitude oscillations with a phase difference of $\pm\pi/4$ or $\pm 3\pi/4$, unlike the patterns along diagonal or cardinal axes that accompany normal or local mode behavior, respectively (Fig. 3-8). The two differently inclined ring modes are presumably the above-barrier counterparts of *cis* and *trans* bending.

Some states that have amplitude in both wells do not exhibit this ring mode behavior; in our results such states always have nodal patterns in each well that are clearly assignable, indicating that these states are less affected by the isomerization despite their delocalization.

The shapes of the wavefunctions both above and below the barrier to isomeriza-

[5]The reduced dimension potential does not allow the CH bond distances to be different, yet their asymmetry is appreciable (See Table 3.6). Relaxing these bond distances would give a lower, more accurate barrier height.

tion provide some clues about the important resonances in the bending Hamiltonian. Since we do not observe the cross shaped wavefunctions indicative of local modes, we can infer that the K_{3366} Darling–Dennison resonance does not dominate the dynamics. This is in line with the frequency ratio of the two modes being not $2:2$ but rather $\sim 1.3:2$, lying in between the usual ratios for strong Darling–Dennison and Fermi resonance. We find [84] that both types of resonance are necessary in an $\mathbf{H}^{\text{eff}}$ to reproduce the unusual nodal patterns of the below-barrier *trans* well DVR wavefunctions. The presence of both strong Fermi and Darling–Dennison resonance leads to the destruction of any polyad structure in the $\tilde{A}$ state. For fixed values of (v_1, v_2, v_5), all states of a given symmetry can interact via known anharmonic interactions, so the Hamiltonian does not readily block diagonalize according to conserved polyad quantum numbers. Research into this phenomenon and its relation to low barrier isomerization is ongoing.

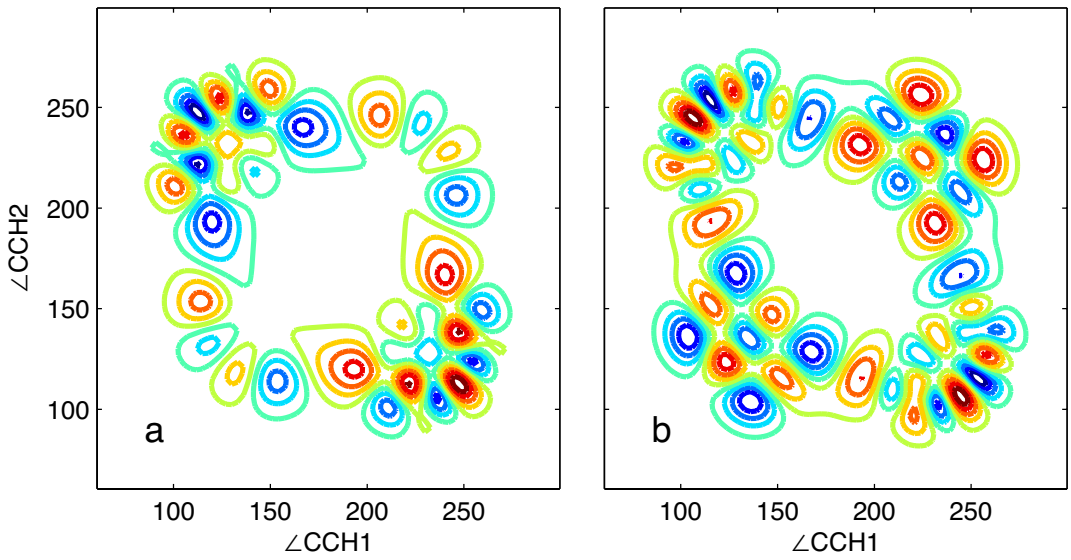

Figure 3-6: Wavefunctions of delocalized states above the isomerization barrier.

3.4 Conclusion

We set out in this paper to investigate the spectroscopic consequences of low barrier *cis-trans* isomerization in S_1 acetylene by calculating the vibrational eigenstates of a high accuracy PES using a reduced dimension DVR method. The calculation reproduces some difficult aspects of the *trans* conformer level structure, which are ultimately due to the isomerization. Another consequence of the isomerization process is that nominally forbidden transitions to the *cis* conformer appear. These transitions occur in our calculation near the observed energies of the "extra" levels in the $\tilde{A} \leftarrow \tilde{X}$ spectrum of acetylene. We find that our reduced dimension DVR calculation agrees with the explanation of these "extra" levels as belonging to the *cis* conformer, and that we are able to explain the intensities of these levels by using the calculated results to investigate *cis-trans* mixings. Although we believe that the reduced dimension DVR method demonstrated here is a powerful approach for studying isomerizing systems, there are interesting aspects of the S_1 C_2H_2 spectrum that it does not address, including strong vibration-rotation interactions and possible multiple pathways to isomerization. We intend to develop a full dimensional treatment for S_1 acetylene to study these effects and enable comparison with the complete set of experimental observations.

Acknowledgments

J. Baraban would like to thank D. Tannor, T. Van Voorhis and A. Merer for helpful discussions, and is grateful for support by an NSF Graduate Research Fellowship. This work was supported at MIT by DOE Grant No. DE-FG0287ER13671.

3.A Computation of $S_1 \leftrightarrow S_0$ Spectra

In order to calculate $\tilde{A} \leftrightarrow \tilde{X}$ spectra, two additional quantities are required beyond the $\tilde{A}$ state vibrational wavefunctions: the electronic transition moment, μ, and the $\tilde{X}$ state vibrational wavefunctions. We calculate the transition moment *ab initio*

over our coordinate grid at the EOM-CCSD/ANO1 level of theory, again using the CFOUR program system [81]. The $\tilde{X}$ state vibrational wavefunctions can be obtained merely by replacing the $\tilde{A}$ state PES with that of the $\tilde{X}$ state and repeating the DVR calculation. This portability of the method is one of its powerful features. Although the results thus obtained for the $\tilde{X}$ state are not worth examining in depth, given the numerous *ab initio* treatments in the literature, we would like to note that the qualitatively important features related to large amplitude motions are simulated correctly by our DVR method. Chief among these is the emergence of the "local-bender" states [63, 87] from the normal modes ν_4'' and ν_5'', as shown in Fig. 3-8.

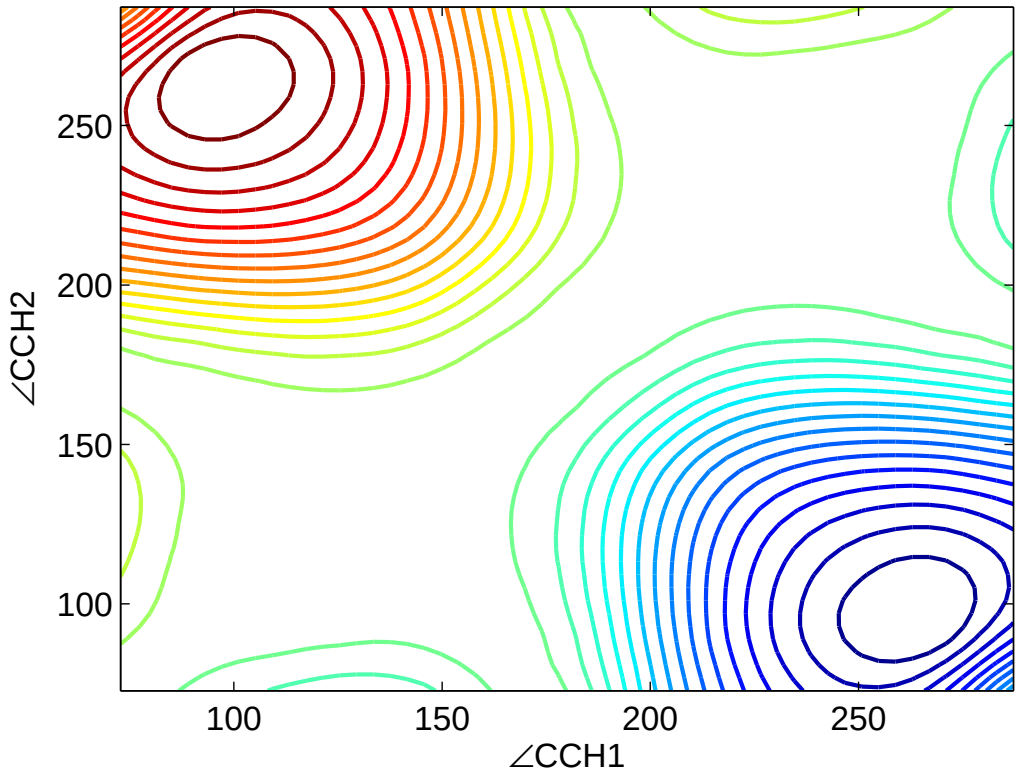

Figure 3-7: The transition moment μ as a function of the bending angles. Note that $\mu = 0$ at all points of C_{2v} symmetry, including linearity. In order for the overall symmetry of μ to be $Ss-$, the quantity used to calculate $\tilde{A} \leftrightarrow \tilde{X}$ spectra must have $Sa-$ symmetry in the DVR coordinate space. Briefly, this requirement arises because the $\tilde{X}$ state DVR wavefunctions are vibrational instead of rovibrational. Adding the rotational symmetry factor necessary to ensure that transitions occur between the same nuclear spin symmetry species includes an extra $Sa-$ in μ.

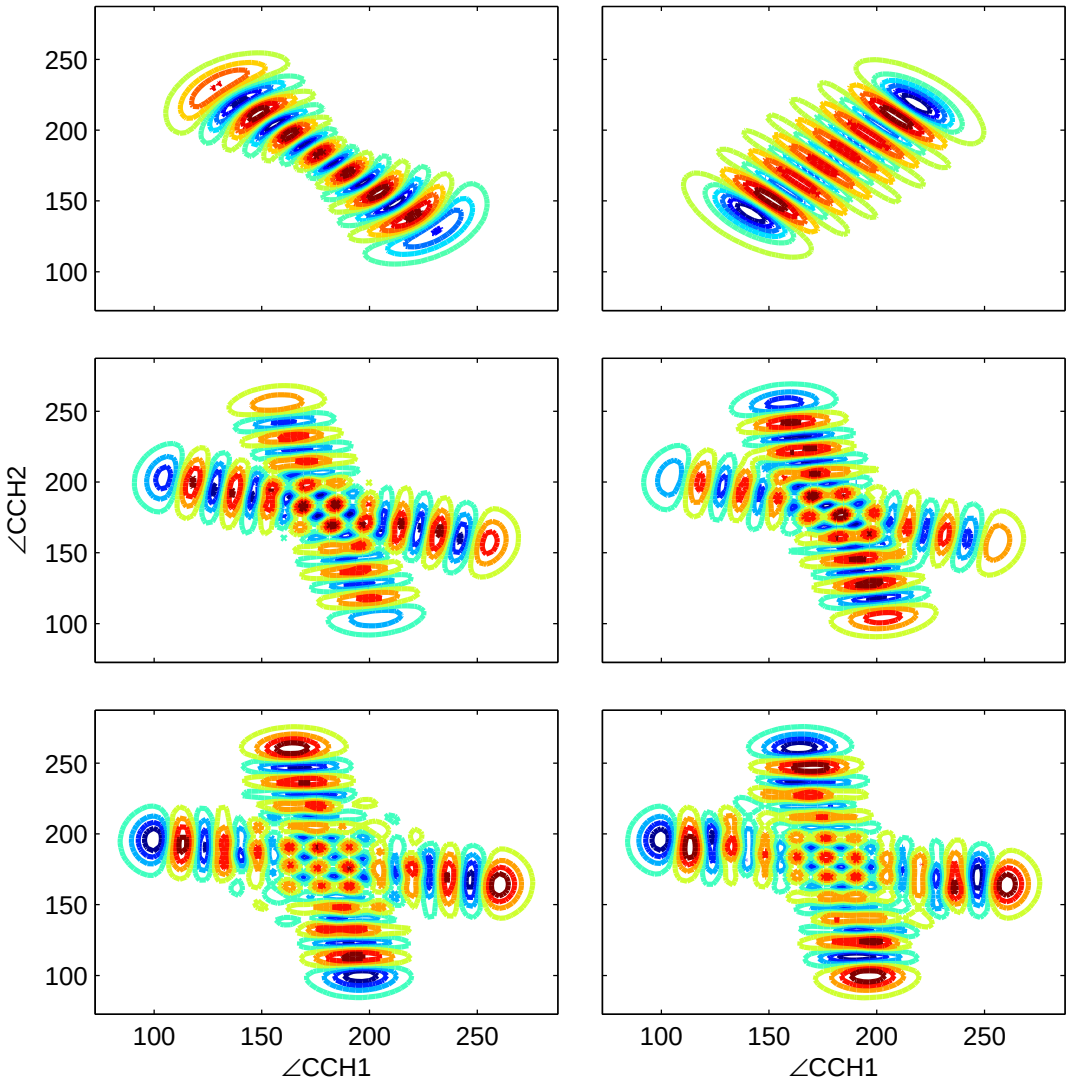

Figure 3-8: From top to bottom, pairs of wavefunctions depicting the evolution from the normal mode limit to the local mode limit in S_0 acetylene from approximately $8,000$ to $12,000$ cm^{-1} of vibrational excitation.

With these two results in hand, we calculate for each pair of eigenstates the spectral intensity $I_{mn} = |\langle m|\mu|n\rangle|^2$, where m and n belong to different electronic states. In order to calculate the product it is necessary to interpolate the transition moment and wavefunctions to a common set of grid points. This process yields all possible upward spectra, including the four necessary to sample experimentally the full rovibrational structure of the $\tilde{A}$ state [41], and also all possible downward spectra (DF/SEP). This wealth of information was of enormous value when analyzing the

calculated results, and we expect it to guide future experiments.

Chapter 4

The $\tilde{A}\ ^1\mathrm{A}_u$ state of acetylene: *ungerade* vibrational levels in the region 45800 – 46550 cm^{-1}

Abstract

The ungerade vibrational levels of the $\tilde{A}\ ^1\mathrm{A}_u$ (S_1-trans) state of C_2H_2 lying in the region $45800 - 46550$ cm^{-1} have been assigned from IR-UV double resonance spectra. The aim has been to classify the complete manifold of S_1-trans levels in this region, so as to facilitate the assignment of the bands of S_1-cis C_2H_2. The rotational structure is complicated because of the overlapping of vibrational polyads with different Coriolis and Darling-Dennison parameters, but assignments have been possible with the help of predictions based on the properties of polyads at lower energy. An important result is that the analysis of the ($1^1 4^1$, $1^1 6^1$) polyad determines the anharmonicity constants x_{14} and x_{16}, which will be needed to proceed to higher energies. Some regions of impressive complexity occur. Among these is the band given by the $3^3 6^1$, $K = 1$ state at 45945 cm^{-1}, where a three-level interaction within the S_1 state is confused by triplet perturbations. Several probable S_1-cis states have been observed, including cis-6^2, $K = 1$; this vibrational level appears to show a K-staggering, of the type that arises when quantum mechanical tunnelling through the barrier to cis-trans isomerization is possible. The total number of identified cis vibrational states is now 6 out of an expected 10 up to the energies discussed in this paper.

The results in this chapter have been published in the FASE special issue of Molecular Physics [88].

4.1 Introduction

It has been known for nearly 60 years [1, 33, 34] that the first absorption transition in the electronic spectrum of acetylene, $\tilde{A}\ ^1\mathrm{A}_u - \tilde{X}\ ^1\Sigma_g^+$, goes from the ground state (where the molecule is linear) to an excited state where the molecule is trans-bent (point group C_{2h}). Some years after the first analyses, *ab initio* calculations [26, 28–31, 89] showed that the excited electronic state, $\tilde{A}$, also supports a potential minimum corresponding to a cis-bent structure. Because the $\tilde{A}$ state of the cis-bent structure transforms as $^1\mathrm{A}_2$ in the C_{2v} point group, it was thought that transitions from the ground state to it would never be observable, since $^1\mathrm{A}_2 - {}^1\Sigma_g^+$ electronic transitions are forbidden by the electric dipole selection rules. Nevertheless, a recent detailed study of the vibrational structure of the $^1\mathrm{A}_u - {}^1\Sigma_g^+$ system [43] has identified some weak bands going to levels which cannot be fitted into the manifold of the $^1\mathrm{A}_u$ (S_1-trans) state. The $^{13}\mathrm{C}$ isotope shifts, upper state lifetimes and rotational structures of these bands confirm that they belong to the $^1\mathrm{A}_2$ (S_1-cis) state. [11]

The discovery of the S_1-cis state of acetylene opens up the very interesting possibility of studying the spectroscopic signature of cis-trans isomerization at high resolution. In the S_1 state of $\mathrm{C}_2\mathrm{H}_2$ the trans conformer is the more stable, with the separation of the cis and trans zero-point levels being about 2700 cm^{-1}; the barrier to isomerization is calculated to lie about 2300 cm^{-1} above the cis zero-point level. [10] The molecule is predicted [26] to be half-linear at the saddle point, with one of the CCH angles near 120°, and the other near 180°. Since the barrier to isomerization is not unduly high, the vibrational structure is not hopelessly dense at the saddle point, so that many vibrational assignments can be made with some certainty. However, the arguments that lead to these assignments are not trivial.

There are a number of complicating factors. The isomerization pathway, which the molecule follows in going from its trans equilibrium structure to the half-linear structure at the transition state, is a combination of the vibrational normal coordinates Q_3 (trans bend) and Q_6 (cis bend). Since the pathway leads to a saddle point on the potential surface, the result is huge anharmonicity in the combination levels 3^m6^n,

represented by large values of x_{36} and the higher anharmonicity constants. [46, 53] The most severe problem in identifying the levels is that ν_6 is inextricably bound up with ν_4 (torsion) as a result of the vibrational angular momentum, which causes levels of these vibrations to interact by two different mechanisms. The two fundamentals ν_4 and ν_6 lie at 764.9 and 768.3 cm^{-1}, respectively, and interact strongly through both a- and b-axis Coriolis coupling ($\zeta^a_{46} = 0.70, \zeta^b_{46} = 0.71$). [38] In addition to the Coriolis coupling, the overtones also suffer from unusually strong Darling-Dennison resonance ($K_{4466} = -51.7$ cm^{-1}). [41] The result is that the vibrational levels involving ν_4 and ν_6 form polyads of interacting levels, where the levels have the same value of $v_4 + v_6$. These polyads have highly irregular vibrational and rotational structures, which can only be reproduced with detailed numerical simulations. Fortunately, ν'_3 is the principal Franck-Condon active vibration in the electronic transition, [1, 33–36] which means that many of the combination levels 3^m6^n carry sizeable intensities. Also, it turns out that some systematic patterns can be recognized in the various polyads. For example, the structures of those polyads which differ only in their values of $v4 + v6$ can be represented approximately by a single set of effective vibrational and anharmonicity constants. [41] This has been the key to making assignments at progressively higher energies.

The present paper reports analyses of the ungerade vibrational levels in the region $45800 - 46500$ cm^{-1}, as observed in IR-UV double resonance. The objective of the work has been to establish secure assignments of all the trans levels in this region so that any levels left over can confidently be assigned to the cis conformer. The region studied is one of considerable complexity, containing 22 more or less strongly interacting vibrational levels from the trans manifold and 4 levels from the cis manifold. Two of these four are newly identified.

4.2 Experimental details

The rotational selection rule $K' - l'' = \pm 1$ for the electronic transition necessitated two sets of double resonance experiments in order to sample all of the levels with

$K' = 0 - 2$. In one, the ν_3 IR fundamental ($l'' = 0$) gave access to the $K' = 1$ upper levels; in the other, the combination levels $(\nu_3 + \nu_4)''$ and $(\nu_1 + \nu_5)''$ ($l'' = 1$) gave access to the $K' = 0$ and 2 levels.

The $(\nu_3 + \nu_4)''$ and $(\nu_1 + \nu_5)''$-pumped spectra analyzed in this paper are the same as those reported in Refs. [43] and [41]. As Ref. [43] contains the complete experimental details, only a summary of those IR-UV double resonance experiments will be given here. Difference frequency generation in a $LiNbO_3$ crystal pumped by an injection-seeded Nd:YAG laser (Spectra-Physics PRO-270) at 1064 nm and a tunable dye laser (Lambda Physik FL2002) at 740-790 nm produced the IR radiation, which was amplified in a second $LiNbO_3$ crystal to about 3 mJ/pulse. The UV radiation was generated by a second dye laser (Lambda Physik FL3002E) pumped by the third harmonic of an Nd:YAG laser (Spectra-Physics DCR-3). Most of the dye laser output was frequency-doubled in a β-barium borate crystal, while a small portion of the fundamental was passed through a heated $^{130}Te_2$ vapor cell for frequency calibration ($\sigma = 0.02$ cm^{-1}). The IR and UV radiation were sent into a molecular beam chamber where they interacted with an unskimmed jet of neat acetylene expanded through a pulsed valve (General Valve, Series 9) with a backing pressure of 2 atm. The laser-induced fluorescence was observed at an angle mutually perpendicular to the laser path and molecular beam and recorded by a Hamamatsu R331 photomultiplier tube.

The newly recorded ν_3''-pumped spectra were obtained in a separate apparatus from that used in the recording of the $(\nu_3 + \nu_4)''$ and $(\nu_1 + \nu_5)''$-pumped spectra. A single injection-seeded Nd:YAG laser (Spectra-Physics PRO-270) pumped the two tunable dye lasers for both IR and UV generation. The Nd:YAG second harmonic at 532 nm pumped the first dye-laser (Lambda Physik FL2002) operating at 790 nm (LDS 798 dye). As above, this output, along with the Nd:YAG fundamental at 1064 nm, pumped a $LiNbO_3$ crystal producing IR radiation via difference frequency generation. Approximately 1.5 mJ/pulse was achieved through the difference frequency generation alone, and this IR beam was not amplified with a second $LiNbO_3$ crystal. To ensure the resonance of the IR frequency with transitions in the ν_3 fundamental band [90], a photoacoustic cell with 15 torr of neat acetylene gas at room temperature

was monitored before each IR-UV double resonance experiment. The grating-limited IR spectral width was 0.10 cm^{-1}.

The Nd:YAG third harmonic at 355 nm pumped the second dye-laser (Lambda Physik FL3002E) to produce laser radiation over the range 460-470 nm (Coumarin 460 dye). This output was doubled with a β-barium borate crystal and, as above, a small portion of the fundamental was used for $^{130}Te_2$ frequency calibration. An intracavity etalon reduced the spectral width to 0.04 cm^{-1}, and after frequency-doubling, the UV power was approximately 100-200 μJ/pulse. The IR and UV beams were recombined with a dichroic mirror before entering the molecular beam chamber. As a single Nd:YAG laser generated both pulses, their relative arrival times at the chamber could be controlled only through the addition of a delay line in the UV beam path. The length of the delay line was such that the UV pulse arrived 15 ns after the IR pulse.

The molecular beam chamber contained an unskimmed supersonic jet of neat acetylene expanded through one of two pulsed valves (Jordan PSV C-21, $d = 0.5$ mm or General Valve, Series 9, $d = 1.0$ mm). The latter achieved superior vibrational cooling, necessary when single-photon hot-bands obscured overlapping IR-UV double resonance features in the spectrum. In both cases, the jet was backed by a pressure of 1 atm and interacted with the IR-UV radiation about 2 cm from the nozzle. The diffusion pumped chamber achieved an ultimate pressure of 7×10^{-7} torr, while under gas load it rose to $0.5 - 2 \times 10^{-5}$ torr.

A Hamamatsu R375 photomultiplier tube collected the laser-induced fluorescence using f/1.2 collection optics and a UG-11 filter to block laser scatter. Additionally, optical baffles consisting of a set of 3.5 mm aperture irises placed 23 cm from the interaction region and a second set of 5.5 mm aperture irises placed 10 cm from the interaction region were installed in the entrance and exit window arms of the chamber, which significantly reduced laser scatter. The photomultiplier tube signal was split and one line was input to a 30 dB voltage amplifier (Femto DHPVA-200). This was necessary as the fluorescence intensity of levels in the studied energy region range varied over several orders of magnitude. The time-dependent fluorescence signal was recorded for 2 μs after the UV pulse arrival time. For each frequency resolution

element, the fluorescence signal was averaged for 20 laser shots. The integration gate of the time signal could be chosen depending on the fluorescent lifetime of the final state. Typically, the fluorescence signal over the first 0.4 μs after the UV laser pulse was integrated. However, for short-lived states this integration gate had to be moved earlier in time and included the UV laser pulse scatter. In this case, the laser scatter and power fluctuations were small enough not to contribute significantly to the integrated signal noise.

Since the ν_3'' fundamental is a parallel band, IR pumping of individual R and P lines gives J''-selectivity. In contrast, the narrow Q branches of the perpendicular transitions to the $(\nu_3 + \nu_4)''$ and $(\nu_1 + \nu_5)''$ combination levels allow pumping of the $J = 1f - 5f$ levels simultaneously. This speeds up the data acquisition process, but loses the J-selectivity. As a result it was sometimes difficult to be certain of the rotational assignments of weaker lines in dense regions of the Q-pumped IR-UV double resonance spectra.

4.3 Appearance of the spectra

As observed by IR-UV double resonance, the region $45800 - 46500$ cm^{-1} consists of congested overlapping structure centred on the very intense 3^36^1 band at 45938 cm^{-1}, with sparser structure to higher frequency. A survey spectrum is given in Fig. 1 of [43]. The congested region contains 15 vibrational levels from the trans manifold, together with two cis levels. One of the cis levels is cis-3^16^1, which was described in [11]. The trans levels are 3^15^1 and the polyads 3^3B^1, 1^1B^1, 2^1B^3 and B^5. (The notation B^n means n quanta of the bending vibrations, where $n = v_4 + v_6$; a polyad B^n consists of $n + 1$ vibrational levels.) Three of the K states from the B^5 polyad were described in [11, 41], and analyses of the 3^15^1 state [39] and the 3^3B^1 polyad [46] have been reported by other workers, but no previous attempts have been made to assign the remainder of the congested region. The sparse region contains the 2^15^1 state and the polyads 3^2B^3 and $2^13^2B^1$, together with two new cis levels. There are surprising numbers of accidental near-degeneracies among the upper states, which

result in some wickedly complicated spectra.

Because the rotational selection rule $K' - l'' = \pm 1$ requires separate experiments for the even-K and odd-K upper states, no single spectrum can illustrate the complete level pattern. To be sure, many of the K states show up in both spectra when b-axis Coriolis interaction mixes close-lying levels differing in K by one unit, but the intensities of the bands are not representative in those cases. Figure 4-1 gives a stick diagram of the $K' = 0 - 2$ structure in the congested region around 46000 cm^{-1}, as observed in the two spectra, with approximate intensities indicated by the heights of the sticks. A common feature of all the polyads, particularly those with $v_4 + v_6 > 1$, is that the vibrational and rotational structure is much denser at the low frequency extreme than at higher frequencies. This level density effect at low frequency is a consequence of the a-axis Coriolis coupling, which depresses the lower members of the polyad with $K > 0$. Where Darling-Dennison resonance is also present, this density effect is enhanced. The 2^1B^3 polyad, shown in Fig. 4-1, is a good example of this. Figure 4-1 also shows how the congestion of the structure in the 45800 45950 cm^{-1} region results from overlapping of the low frequency extremes of three polyads.

The lower part of Figure 4-1 shows the assignments of the levels to the various polyads. Except in one instance where two $K = 2$ levels are almost degenerate, the assignments are unambiguous, because it has been possible to predict the positions of the levels to within a few cm^{-1}, using data from previous analyses of polyads at lower energy. These predictions are described below.

4.4 Results

As yet, no attempt has been made to fit all of the interacting levels of Fig. 4-1 simultaneously by least squares. Table 4.1 lists rotational constants obtained from band-by-band fitting of the 60 observed K' upper states. It has not been possible to obtain meaningful constants for every K state either because the bands are too weak, or because of perturbations. In the latter cases, a separate discussion of the interactions is given.

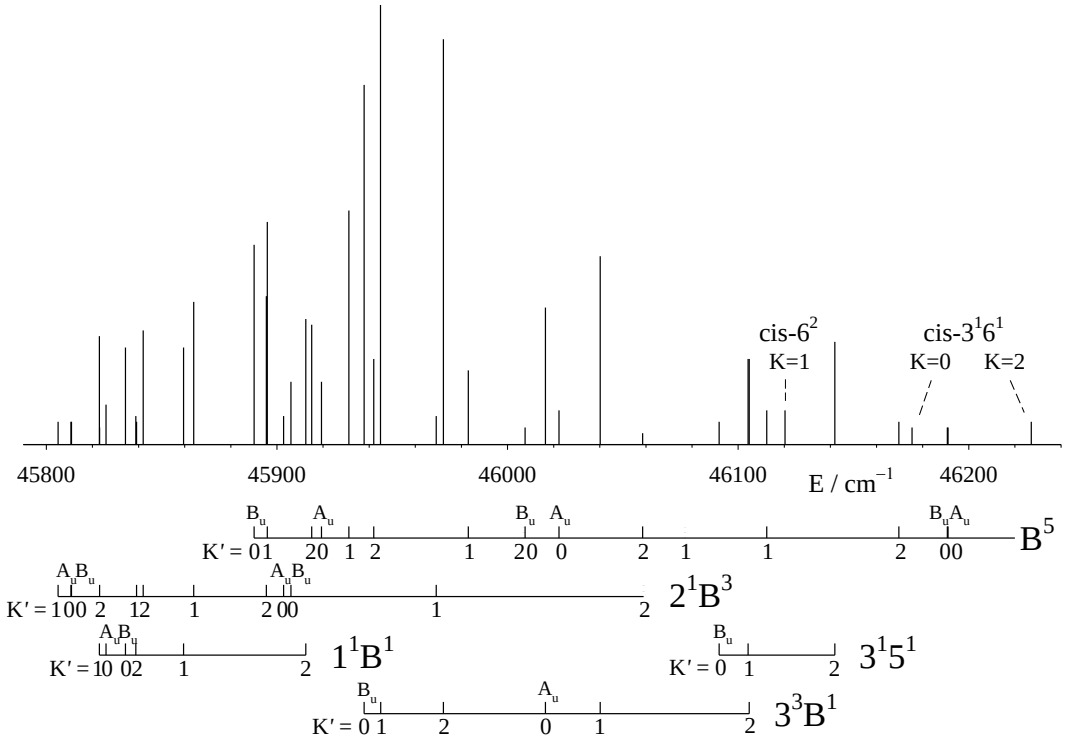

Figure 4-1: Stick diagram of the ungerade $K' = 0 - 2$ levels of the $\tilde{A}\ ^1\mathrm{A}_u$ (S_1-trans) state of $\mathrm{C_2H_2}$ in the region $45800 - 46240$ cm^{-1}, with their assignments, as recorded using IR-UV double resonance via the ν_3'' (σ_u^+) and $(\nu_3+\nu_4)''$ (Π_u) vibrational levels of the ground state. The two spectra have been combined into a single plot. States that could not be found are marked with dotted lines at their predicted positions. Two vibrational levels of the $^1\mathrm{A}_2$ (S_1-cis) state also appear; their positions are indicated with dashed lines.

Table 4.1: C_2H_2, band-by-band analyses of the *ungerade* states in the $45800 - 46500$ cm^{-1} region. Rotational constants (cm^{-1}) are from least squares fittings where a r.m.s. error is given. q is the same as $\frac{1}{2}$(B−C) for $K = 1$ states, and is the coefficient of $J^2(J+1)^2$ in the asymmetry splitting of $K = 2$ states; a positive value of q means e levels above f. D terms are needed where b-axis Coriolis coupling distorts the rotational structure of a state; these D constants do not represent true centrifugal distortion.

	K	T_0[a]	3σ	B	3σ	$10^2 q$	3σ	D	r.m.s.
2^1B^3	1 (I)	45805.09	0.05	0.9353	0.0094	1.13	0.17	$(-1.60 \pm 0.44) \times 10^{-3}$	0.019[b]
2^14^3	0, A_u	45810.66	0.08	1.1335	0.0126			$(0.95 \pm 0.38) \times 10^{-3}$	0.023
2^16^3	0, B_u	45810.86	0.1	1.125	0.0096			$(0.75 \pm 0.16) \times 10^{-3}$	0.040
1^1B^1	1 (I)	45822.99	0.17	0.9328	0.0304	−4.16	1.2	$(-1.6 \pm 1.0) \times 10^{-3}$	0.071
2^1B^3	2 (I)	45823.07	0.18	1.1031	0.0213	0.095	0.091	$(0.79 \pm 0.70) \times 10^{-3}$	0.036
1^14^1	0, A_u	45825.88	0.18	1.1926	0.0294			$(0.30 \pm 0.09) \times 10^{-2}$	0.053
1^16^1	0, B_u	45834.26	0.08	1.1191	0.0092			$(0.95 \pm 0.21) \times 10^{-3}$	0.026
1^1B^1	2 (I)	45838.81	0.07	1.0666	0.0067	0.094	0.032		0.018
2^1B^3	1 (II)	45839.12	0.21	0.613	0.037[c]	0.32	1.45	$(-2.41.2) \times 10^{-3}$	0.085
2^1B^3	2 (II)	45842					See Fig. 4-2		
1^1B^1	1 (II)	45859.53	0.03	1.1053	0.0058	1.03	0.23	$(0.110.20) \times 10^{-3}$	0.013
	K	T_0[a]	3σ	B	3σ	$10^2 q$	3σ	D	r.m.s.

Table 4.1 – continued: C_2H_2, band-by-band analyses of the *ungerade* states in the $45800 - 46500$ cm^{-1} region.

	K	T_0[(a)]	3σ	B	3σ	10^2q	3σ	D	r.m.s.
2^1B^3	1 (III)	45863.9	0.14	1.169	0.0223	0.99	0.77	$(0.370.73) \times 10^{-3}$	0.045
B^5	0, B_u (I)	45890.08	0.03	1.0452	0.0007				0.016
2^1B^3	2 (III)	45895.39	0.07	0.9933	0.0095	-0.29	0.64	$(-0.560.26) \times 10^{-3}$	0.015
B^5	1 (I)	45895.80[(d)]	0.04	1.1028	0.0044	-0.81	0.19	$(0.320.10) \times 10^{-3}$	0.011
2^1B^3	0, A_u (II)	45902.93	0.03	1.0733	0.0039				0.009
2^1B^3	0, B_u (II)	45906.07	0.08	1.1296	0.0153			$(0.65 \pm 0.45) \times 10^{-3}$	0.022
1^1B^1	2 (II)	45912.5	0.15	1.0923	0.0202	-0.016	0.014	$(0.93 \pm 0.55) \times 10^{-3}$	0.032
B^5	2 (I)	45915.11	0.1	1.0005	0.0138	-0.014	0.009	$(-0.58 \pm 0.37) \times 10^{-3}$	0.022
B^5	0, A_u (II)	45919.28	0.1	1.0991	0.0061				0.046
B^5	1 (II)	45931.17	0.023	0.9963	0.0033	-1.87	0.19	$(0.31 \pm 0.09) \times 10^{-3}$	0.010
3^36^1	0, B_u	45937.76	0.02	1.0476	0.0006				0.006
B^5	2 (II)	45942					See Fig. 4-5		
3^36^1	1	45945					See Fig. 4-5		
2^1B^3	1 (IV)	45969.09	0.06	1.0846	0.0100	0.42	0.4	$(0.43 \pm 0.34) \times 10^{-3}$	0.023
3^36^1	2	45972.24	0.05	1.0703	0.0014	-0.0018	0.0027		0.030
	K	T_0[(a)]	3σ	B	3σ	10^2q	3σ	D	r.m.s.

Table 4.1 – continued: C_2H_2, band-by-band analyses of the *ungerade* states in the $45800 - 46500$ cm^{-1} region.

	K	T_0[(a)]	3σ	B	3σ	10^2q	3σ	D	r.m.s.
B^5	1 (III)	45983.006	0.031	1.0786	0.0057	2.18	0.35	$(-0.080.19) \times 10^{-3}$	0.011
B^5	0, B_u (III)	46007.5_8		1.13			only two rotational levels		
3^34^1	0, A_u	46016.36	0.06	1.0863	0.0025				0.028
B^5	0, A_u (IV)	46022.34	0.02	1.1218	0.0012				0.009
3^34^1	1	46040.17	0.05	1.0836	0.0021	−4.83	0.22		0.023
B^5	2, (IV)	46058.6[(e)]		1.057		0.04	very weak band		
3^15^1	0, B_u	46091.75	0.07	1.0743	0.0060				0.027
3^15^1	1	46104.31	0.04	1.0695	0.0022	4.35	0.26		0.016
3^34^1	2	46104.7_8	0.15	1.0793	0.0065	0.060	0.014	perturbed	0.069
B^5	1 (V)	46112.44	0.026	1.1645	0.0019	0.25	0.25		0.015
cis-6^2	1	46120.338	0.018	1.0845	0.0013	5.02	0.15		0.010
3^15^1	2	46141.91	0.03	1.075	0.0009	−0.0024	0.0014		0.020
B^5	2 (V)	46169.68	0.05	1.0906	0.0021	−0.0025	0.0063		0.019
B^5	0, B_u (V)	46190.69	0.01	1.1252	0.0004				0.005
B^5	0, A_u (VI)	46191.01	0.02	1.1256	0.001				0.007
	K	T_0[(a)]	3σ	B	3σ	10^2q	3σ	D	r.m.s.

Table 4.1 – continued: C_2H_2, band-by-band analyses of the *ungerade* states in the $45800 - 46500$ cm^{-1} region.

	K	T_0[(a)]	3σ	B	3σ	10^2q	3σ	D	r.m.s.
3^2B^3	0, B_u (I)	46287.045	0.066	1.0336	0.0023				0.018
3^2B^3	1 (I)	46290.995	0.019	1.0808	0.0013	−0.38	0.16		0.010
B^5	1 (VI)	46292.29		1.113		0	Only three rotational levels		
3^2B^3	2 (I)	46321.686	0.023	1.0423	0.0006	−0.002	0.001		0.011
$2^13^2B^1$	$1e$ (I)[(f)]	46358.8	0.13	1.05	0.008		See Fig. 4-10		0.058
$2^13^2B^1$	0, B_u	46359.3					See Fig. 4-10		
cis-3^2	1	46361.2_8		1.07_9		−0.041	See Fig. 4-10		
$2^13^2B^1$	2 (I)	46380.339	0.068	1.0725	0.0054	−0.035	0.003	$(0.10 \pm 0.08) \times 10^{-3}$	0.024
$2^13^2B^1$	0, A_u	46386.95	0.08	1.0977	0.0047				0.035
3^2B^3	0, A_u (II)	46397.83	0.07	1.0734	0.0023				0.037
cis-4^16^1	1	46407.702	0.036	1.0602	0.0025	−3.32	0.30		0.018
3^2B^3	1 (II)	46413.84	0.02	1.0751	0.001	−3.33	0.12		0.013
$2^13^2B^1$	1 (II)	46415.82	0.02	1.0677	0.0011	−4.13	0.14		0.013
3^2B^3	2 (II)	46430.07	0.08	1.0063	0.0039	−0.027	0.018		0.039
$2^13^2B^1$	2 (II)	46476.107	0.029	1.0725	0.0006	−0.0019	0.0008		0.021
	K	T_0[(a)]	3σ	B	3σ	10^2q	3σ	D	r.m.s.

Table 4.1 – continued: C_2H_2, band-by-band analyses of the *ungerade* states in the $45800 - 46500$ cm^{-1} region.

	K	T_0 [a]	3σ	B	3σ	10^2q	3σ	D	r.m.s.
3^2B^3	1 (III)	46479.619	0.026	1.0484	0.0045	1.24	0.74		0.013
3^2B^3	2 (III)	46500.817	0.037	1.1305	0.0039			$(0.45 \pm 0.08) \times 10^{-3}$	0.010
3^2B^3	0, B_u (III) [g]	46510.969	0.07	1.1193	0.0046			$(-0.10 \pm 0.08) \times 10^{-4}$	0.025
3^2B^3	0, A_u (IV)	46531.11_7	0.11_4	1.1228	0.0183			$(4.6 \pm 5.5) \times 10^{-4}$	0.033
3^2B^3	1 (IV)	46598.4_8		1.09			perturbed		
3^2B^3	2 (IV) [h]	46696.267	0.012	1.0846	0.0004				0.007

(a) The electronic origin of the transition (T_{00}) lies at 42197.57 cm^{-1}. [35]

(b) $H = (-0.125 \pm 0.054) \times 10^{-4}$

(c) Very strong Coriolis interaction with $2^1B^3, K = 2$ (II).

(d) $J = 1$ levels omitted from the fit.

(e) Only four levels; J-assignments not secure. Two $K = 2$ levels predicted at this position: $B^5, K = 2$ (IV) and $2^1B^3, K = 2$ (IV); assigned to B^5 on the basis of intensity.

(f) No attempt has been made to fit the various levels of the 46359 cm^{-1} group, except for the $K = 1e$ levels of $2^13^2B^1$. See text for further details.

(g) This state is perturbed, but it is not easy to pick out the avoided crossings. Many of the states at this energy suffer from triplet perturbations.

(h) The vibrational assignment of this state is not definite, since two other $K = 2$ bands lie nearby (See Table 4.2). An assignment of 5^1B^2 is also possible.

4.4.1 Predictions of the vibrational and rotational structures of the polyads

As indicated above, the assignments of the K states could be made following predictions of the vibrational and rotational structures based on constants derived from polyads at lower energy. It was found in [41] that the pure bending polyads could all be represented with fair accuracy by a single set of vibrational and anharmonicity parameters. This allowed predictions and assignments to be made for the three K states of the B^5 polyad observed in that work, based on the parameters from detailed least squares fitting of the B^1, B^2 and B^3 polyads. In the present work, where the rest of the B^5 polyad has been assigned, the predictions of [41] were used again, and were found to be accurate to within 7 cm^{-1} for all the observed $K = 0 - 2$ states. Greater accuracy should not be expected since it is known that Fermi resonances of the type $\Delta\nu_2 = \pm 1, \Delta\nu_B = \mp 2$ are present. Nevertheless the shifts caused by these resonances are quite small, except in one instance. The lowest $K = 0$, B_u level of the B^5 polyad is predicted to lie 20 cm^{-1} below the corresponding $K = 0$, A_u level, but is found experimentally to lie 29 cm^{-1} below it. It happens that the top $K = 0$, B_u and A_u levels of the 2^1B^3 polyad lie in the gap between the two B^5 levels. Fermi resonance then pushes the B^5, B_u level further down and the B^5, A_u level further up. At the same time, the B_u and A_u levels of the 2^1B^3 polyad, which in the absence of the resonance are predicted to lie in the energy order B_u below A_u, end up with the A_u level 3 cm^{-1} below the B_u level. The resulting level pattern can be understood from Fig. 4-1.

It turns out that the combination stretch-bend polyads behave similarly to the pure bending polyads. For example, from the least squares results for the 3^2, 3^2B^1 and 3^2B^2 level positions [35, 43, 46], it is possible to derive a set of effective vibrational and anharmonicity parameters that gives the basis for a prediction of the 3^2B^3 polyad:

$$
\begin{aligned}
\omega_4 &= 739.93, & x_{44} &= 0.43, \\
\omega_6 &= 712.765, & x_{66} &= -11.715, \\
x_{46} &= 19.38, & K_{4466} &= -66.50 \text{ (all in cm}^{-1}\text{)}; \\
\zeta^a_{46} &= 0.77, & \zeta^b_{46} &= 0.638.
\end{aligned}
\tag{4.1}
$$

Taking the rotational constants from the lower polyads, this set predicts the K levels of the 3^2B^3 polyad to within 10 cm^{-1}. The resulting assignments are clear-cut, except for a pair of bands near 46415 cm^{-1}, where there is a near-degeneracy (to within 2 cm^{-1}) with a level from the $2^13^2B^1$ polyad. It is interesting that the predictions for the 3^2B^3 polyad are not as accurate as those for the B^5 polyad; the levels in question lie closer to the barrier to cis-trans isomerization, and it may be that the effects of tunnelling through it are already evident.

The predictions used in this work were full calculations of the rotational and vibrational structures of the polyads, based on a matrix treatment of the rotation, Coriolis coupling, and Darling-Dennison resonance. The matrix elements have been described in detail in [41], and are not repeated here.

At the start of this work it was not known whether the lowest K states in the 45800 cm^{-1} region belong to the 1^1B^1 polyad or to the 2^1B^3 polyad. The answer was supplied by ab initio calculations [53] of the anharmonicity parameters x_{14} and x_{16}, and confirmed later by arguments of the type just described. For these two parameters, the ab initio results gave -16.1 and -9.8 cm^{-1}, respectively, while the experimental values (taking the 1^1B^1 polyad as the higher of the two, as in Fig. 4-1) are -16.7 and -11.6 cm^{-1}; the alternative assignment, with the 1^1B^1 polyad as the lower of the two, gives x_{14} and x_{16} as -31.9 and -35.0 cm^{-1}, respectively.

4.4.2 $K' = 0 - 2$ levels in the region 45800 − 45880 cm^{-1}

The lowest $K' = 0 - 2$ levels of the 1^1B^1 and 2^1B^3 polyads lie in the region 45800 − 45880 cm^{-1}. The b-axis Coriolis interactions are sufficiently strong that almost every K' state appears in the double resonance spectra from both ν_3'' ($l'' = 0$) and $(\nu_3 + \nu_4)''$ ($l'' = 1$), regardless of its K' value. For both polyads, the lowest level is a $K' = 1$ level, as is frequently the case in the bending polyads when ν_3 is not excited. The next levels in each polyad are a pair of $K' = 0$ levels, with A_u and B_u symmetries. These two $K' = 0$ levels are 8.4 cm^{-1} apart for 1^1B^1, but only 0.2 cm^{-1} apart for 2^1B^3. This difference arises because the 2^1B^3 polyad is subject to Darling-Dennison resonance, whereas the 1^1B^1 polyad is not. The A_u level lies below the B_u level in both polyads, as expected when ν_3 is not excited.

The energy level pattern of the ten lowest levels is illustrated in Fig. 4-2, where the reduced rotational levels are plotted against $J(J+1)$. A remarkably strong b-axis Coriolis interaction occurs between the second $K = 1$ and $K = 2$ levels of the 2^1B^3 polyad (illustrated at the top of the figure). The lower of the two resulting levels has an apparent B rotational constant of 0.6 cm^{-1}, compared to 1.07 cm^{-1} for an unperturbed level. This means that it falls rapidly in energy, relative to the levels nearby, and passes through the $K = 0$, B_u level of 1^1B^1, causing a small perturbation. At $J = 6$ it runs into another interaction, with the lowest $K = 2$ level of the polyad. The corresponding band has a very unusual appearance, with the R branch forming a head at $J'' = 1$ in double resonance via ν_3''. This band is illustrated in Fig. 4-3, where it is labelled 45838 $K = 1$. Fig. 4-3 also shows the band given by the $K = 2$ level which interacts with it. This is labelled 45842 $K = 2$; its branches have unusual spacings at low J. A somewhat similar Coriolis interaction occurs in the B^3 polyad, [41] though not in 3^1B^3.

Two close-lying $K' = 1$ levels at 45860 and 45864 cm^{-1} (1^1B^1, $K = 1$ (II) and 2^1B^3, $K = 1$ (III)) give strong bands in the ν_3 double resonance spectra, but only very weak features in the $(\nu_3 + \nu_4)''$ spectra. (The Roman numeral notation gives the ascending energy order for their K value within the polyad.) The predictions place

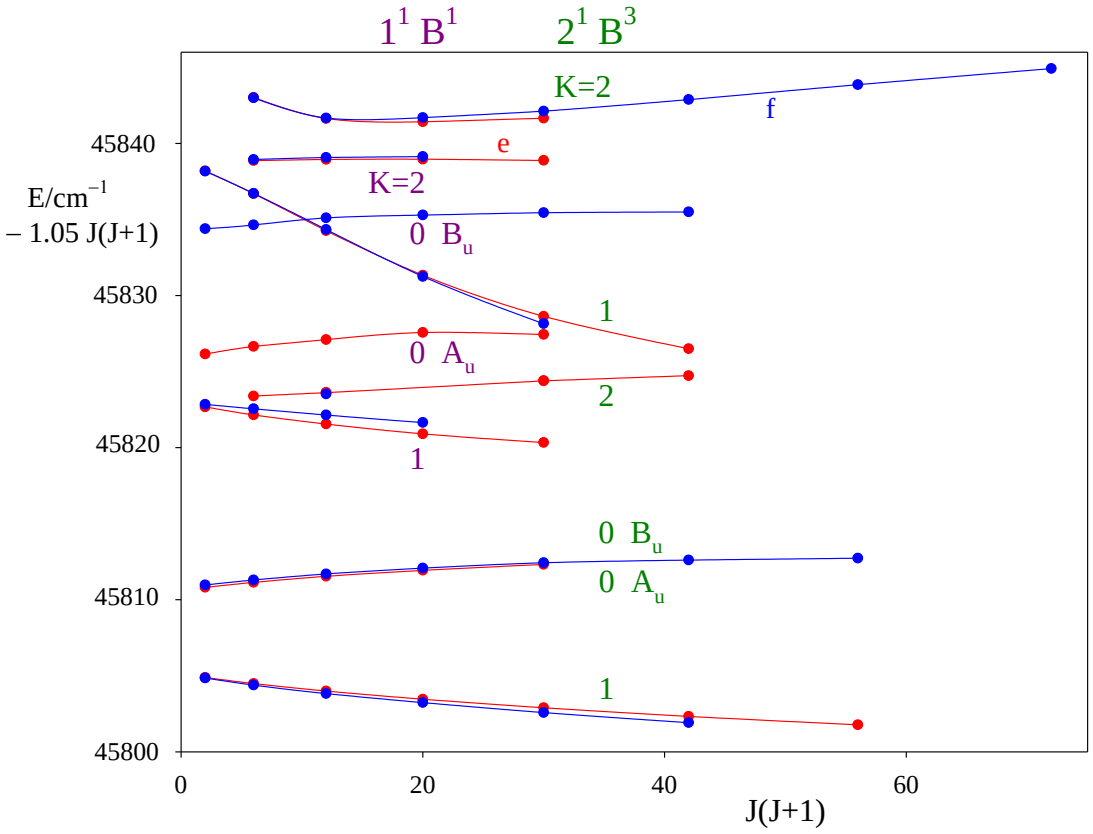

Figure 4-2: Observed energy level structure of the ten states with $K' = 0 - 2$ from the 2^1B^3 and 1^1B^1 polyads in the region $45800 - 45840$ cm^{-1}. The K'-assignments are given in two columns, 1^1B^1 on the left and 2^1B^3 on the right. Rotational levels of e symmetry are shown with open circles and dashed lines; those of f symmetry are shown with full circles and solid lines. (In the color version, levels of e symmetry are coloured red, and levels of f symmetry are coloured blue.) A strong b-axis Coriolis interaction occurs between the upper $K' = 1$ and 2 states of the 2^1B^3 polyad. The 2^16^3 state ($K = 0$, B_u) lies 0.2 cm^{-1} above the 2^14^3 state ($K = 0$, A_u), and has an essentially identical B value.

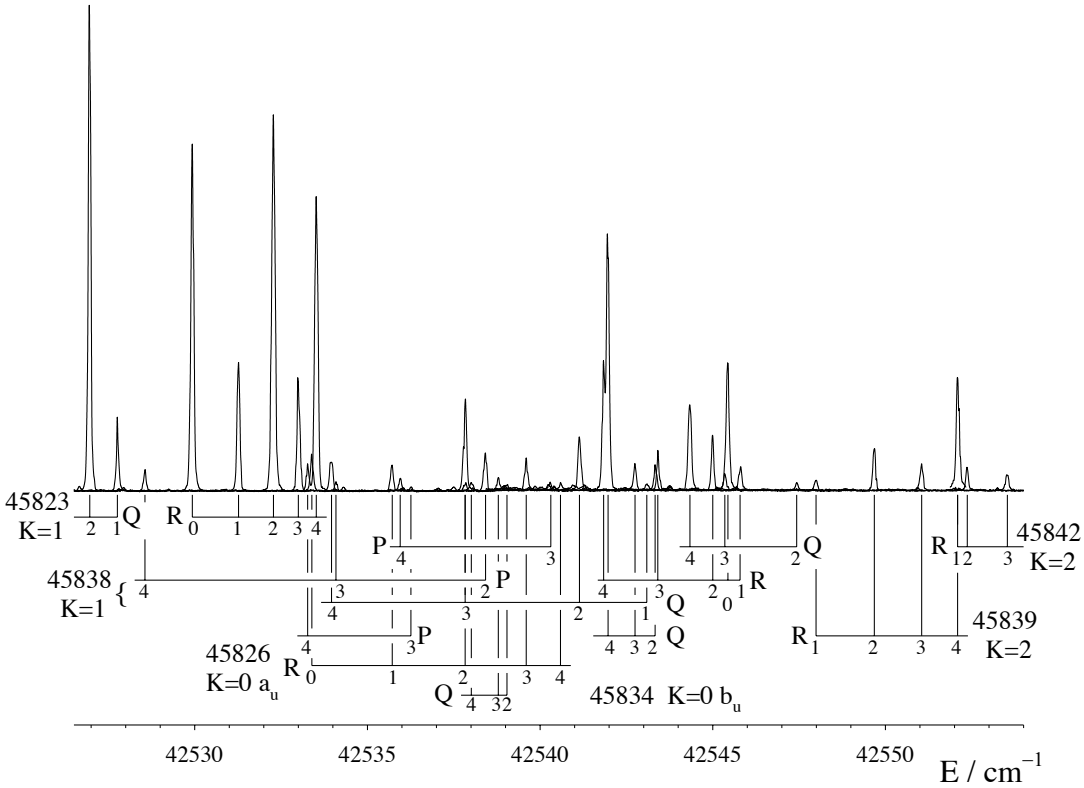

Figure 4-3: IR-UV double resonance spectrum of C_2H_2 in the region $45820 - 45850$ cm^{-1}, as observed via levels of the ν_3'' (σ_u^+) fundamental of the ground state. Five spectra (from $J'' = 0 - 4$) are plotted on top of each other, to give the appearance of a single spectrum. Six bands are shown; they are named according to the energies of their band origins in cm^{-1}, as in Fig. 4-2. Their J assignments are each given on a single horizontal tie-line, except for the 45838 $K' = 1$ band, which is shown on two lines; it has an unusual structure where the R branch forms a head at $J = 1$. The energy scale is that of the UV laser.

the 1^1B^1, $K = 1$ (II) level just 1 cm^{-1} below the 2^1B^3, $K = 1$ (III) level but, since the predictions are accurate only to about ± 4 cm^{-1} for any given level, it was not possible initially to be sure of the assignments. A similar situation occurs with the $K = 2$ levels at 45912 and 45915 cm^{-1}, which can be assigned from the predictions as 1^1B^1, $K = 2$ (II) and B^5, $K = 2$ (I), though without it being possible to decide which is which. However, all the K' states expected in this region have been found, so that we potentially have data for all six of the 1^1B^1, $K = 0 - 2$ states, and can subject these levels to a least squares fit. Interestingly, after examining the various possibilities, the conclusions drawn from the least squares fit are very clear: the lower of the two $K = 1$ levels is 1^1B^1, as is the lower of the two $K = 2$ levels.

4.4.3 $K' = 0 - 2$ levels in the region 45890 − 45990 cm^{-1}

The region $45890 - 45990$ cm^{-1} contains the 3^36^1 level, which gives very intense bands, [46, 91] together with the dense group of levels at the low frequency extreme of the B^5 polyad. It seems that anharmonic resonances transfer intensity from the 3^36^1 level to all the other levels nearby, so that the resulting spectrum is strong but crowded. Fifteen states with $K' = 0 - 2$ are predicted in this region, and all are observed. There are no major perturbations except in the 3^36^1 vibrational level, where all the K' states show small splittings as a result of interaction with the background of triplet levels. The 3^36^1, $K' = 1$ state has a particularly large number of triplet perturbations, and is also involved in a three level interaction with states from the B^5 polyad.

The spectrum given by the 3^36^1, $K' = 1$ state, as seen in double resonance via the $J'' = 0 - 5$ levels of the ν_3'' fundamental, is illustrated in Fig. 4-4. In order not to confuse the patterns, some overlapping lines from the 3^36^1, $K' = 0$ state at 45937 cm^{-1} and the B^5, $K' = 1$ state at 45931 cm^{-1} are shown with dots. In the absence of perturbations, the spectrum would consist of an R, a Q and a P line for each J'' value but, as the figure shows, all the lines are split into several components, usually forming three main groups. A prominent interval of $1 - 2$ cm^{-1} appears in most of the groups of lines. Many of the lines are surrounded by a background of weak unresolved

structure, which may extend for up to 1 cm^{-1}. The background levels are presumably from the triplet manifold, which is expected to be extremely dense at this energy [8]. Most of the lines give extremely long lifetimes (1-3 μs or more), and several exhibit strong zero-field quantum beats. The R(0) line is especially interesting. It consists of two very strong lines, separated by 0.31 cm^{-1}, surrounded by about eight weaker features spread over more than 2 cm^{-1}. The two strong lines have almost exactly the same intensity, which implies that the zero-order $3^3 6^1, J' = 1$ level is to high accuracy degenerate with a background $J' = 1$ level. Combination differences between the components of the R(0) and P(2) lines, which go to the same upper levels, show that the background of weaker features is real. The spacing of these levels gives an idea of how dense the triplet manifold actually is.

The observed upper state energy levels are shown, plotted against $J(J+1)$ and with suitable reduction, in Fig. 4-5. The sizes of the symbols in Fig. 4-5 are rough representations of the intensities of the features in Fig. 4-4. Curves have been drawn through the centres of gravity of the strongest features. These curves show that there is a second zero-order vibrational level of the S_1-trans state in this energy range, and that it undergoes an avoided crossing with $3^3 6^1, K' = 1$ between $J' = 3$ and 4. This second set of rotational levels begins at $J' = 2$, indicating that it belongs to a $K = 2$ state, but the avoided crossing pattern is somewhat unusual, because the slopes of the rotational energy curves are not the same before and after the crossing. As we shall see, the perturbing state is B^5, $K = 2$ (II), which is itself perturbed. The triplet perturbations are clearly associated with the zero-order $3^3 6^1$ state, because at the avoided crossing they transfer from the top set of levels to the next set down, following the state with $3^3 6^1$ character.

A third set of energy levels is shown as a dotted line at the lower right hand side of Fig. 4-5. The upper states have comparatively short lifetimes, closer to the nominal S_1 lifetime of 300 ns, and the lines at higher J values are sharper than those of the interacting $3^3 6^1, K = 1$ and B^5, $K = 2$ (II) states, indicating that they are less affected by the background of triplet levels. This implies that they belong to the S_1 state. The K' value of the upper state is either 3 or 4, depending on whether or not

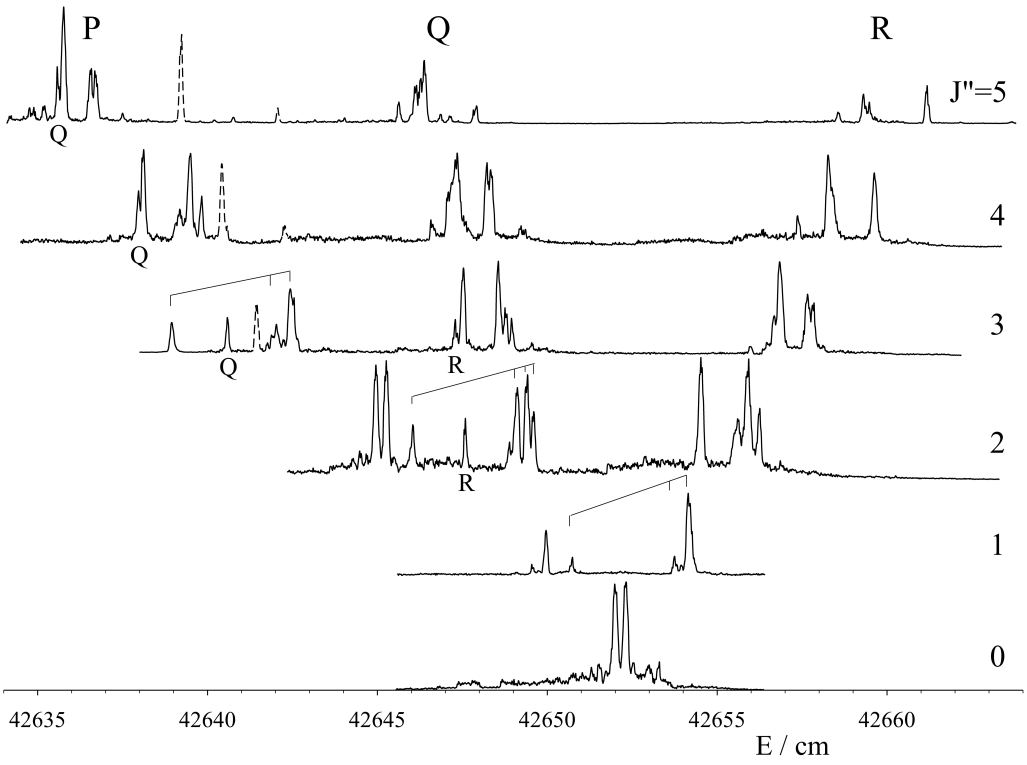

Figure 4-4: IR-UV double resonance spectra of C_2H_2 showing the $\tilde{A}\ ^1A_u$, $3^36^1, K' = 1$ band as seen via the $J'' = 0 - 5$ levels of the ground state ν_3'' (σ_u^+) vibrational level at 3295 cm^{-1}. The $J' = 2$ patterns are indicated by tie-lines in all three branches to indicate the position of the principal perturbing $K' = 2$ state. Some rotational lines marked Q and R belong to the $K' = 3$ state that interacts with the perturbing $K' = 2$ state, causing its energy level pattern to be distorted. For clarity, some Q lines from the $3^36^1, K' = 0$ band and some R lines from the $B^5, K' = 1$ (II) band are shown dashed. The energy scale is that of the UV laser.

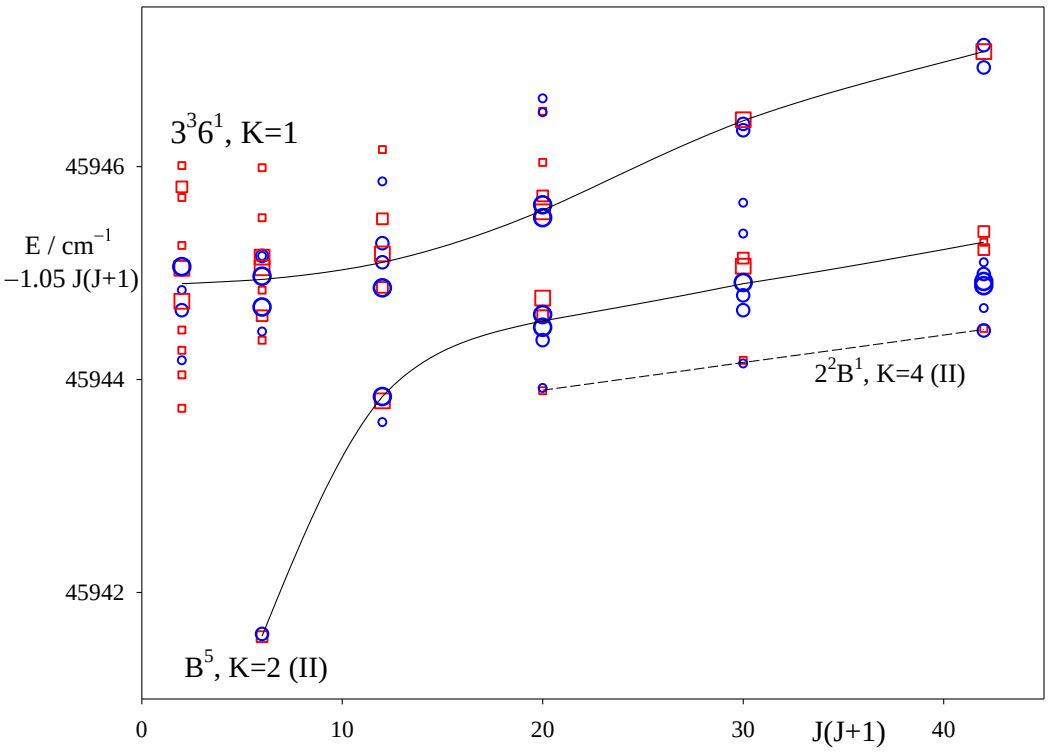

Figure 4-5: Energy levels of the $\tilde{A}\ ^1\mathrm{A}_u$, $3^36^1, K' = 1$ state of C_2H_2, plotted against $J(J+1)$. Levels of e symmetry are shown as squares, and levels of f symmetry are shown as circles. In the color version, levels of e symmetry are coloured red, and levels of f symmetry are coloured blue. The sizes of the symbols roughly represent the intensities of the lines in Fig. 4-4. The $3^36^1, K' = 1$ state interacts with the $B^5, K = 2$ (II) state and (more weakly) with a number of background triplet levels. A third set of energy levels (dashed line) is assigned to the $2^2B^1, K = 4$ (II) state. The S-shaped pattern of the upper set of levels should be noted; it arises from strong Coriolis coupling between the $B^5, K = 2$ (II) and $B^5, K = 3$ (I) states, as illustrated in Fig. 4-6.

there is a $J = 3$ level blended with $B^5, K = 2, J = 3$. We offer no assignment if the upper state has $K = 3$, but for $K = 4$ there is a good match with the 2^2B^1, $K = 4$ (II) state, which is calculated to lie near 44952 cm^{-1}, only 8 cm^{-1} above.

Detailed examination of the spectrum in Fig. 4-4 shows that Fig. 4-5 is not the whole story. In Fig. 4-4 the components of the lines with $J' = 2$ are marked with tie-lines. The low frequency components correspond to the $J' = 2, K' = 2$ levels shown at the bottom of Fig. 4-5. However the Q(2) and P(3) groups contain an additional line for which there is no counterpart in the R(1) pattern. These additional lines turn out to belong to a $K' = 3$ state, which is interacting with the $K' = 2$ state.

As Fig. 4-1 shows, the only polyad that could give perturbing states in this region is B^5. The pattern of its states can be predicted from the constants for the B^n polyads given in [41]. The observed and predicted level structure in this region, plotted against $J(J + 1)$, is shown in Fig. 4-6. (An offset of 3 cm^{-1} has been added to the predictions since the extrapolation from the polyads with lower $n = v_4 + v_6$ is not exact.) The levels from Fig. 4-5, but without the triplet structure, appear at the top of this figure. Figure 4-6 shows that the B^5, $K' = 2$ (II) state interacts strongly with the B^5, $K' = 3$ (I) state, just below. At $J' = 3$ the separation of the $K' = 2$ and 3 states is calculated to be 7.8 cm^{-1}, which suggests that the additional lines in the Q(2) and P(3) patterns of Fig. 4-4 (which are 7.1 cm^{-1} apart) are R and Q lines going to the $K' = 3$ state. Combination differences confirm this assignment. Some higher-J Q lines going to the $K' = 3$ state are also marked in Fig. 4-4; the observed $K' = 3$ levels shown in Fig. 4-6 correspond to them.

Immediately below the $K' = 3$ state is the B^5, $K = 1$ (II) state. The curvature of its plot in Fig. 4-6 shows that it is also involved in the interaction scheme. It gives rise to quite intense bands at 45931 cm^{-1} in both the ν_3'' and $(\nu_3 + \nu_4)''$ double resonance spectra, showing that the goodness of the quantum number K is severely compromised by Coriolis effects. Some of the lines shown as dashed in Fig. 4-4 are lines of its R branch.

The parabola-like energy level pattern given by the $K' = 2$ and 3 states in Fig. 4-6 is characteristic of a b-axis Coriolis (J-dependent) interaction between two states that

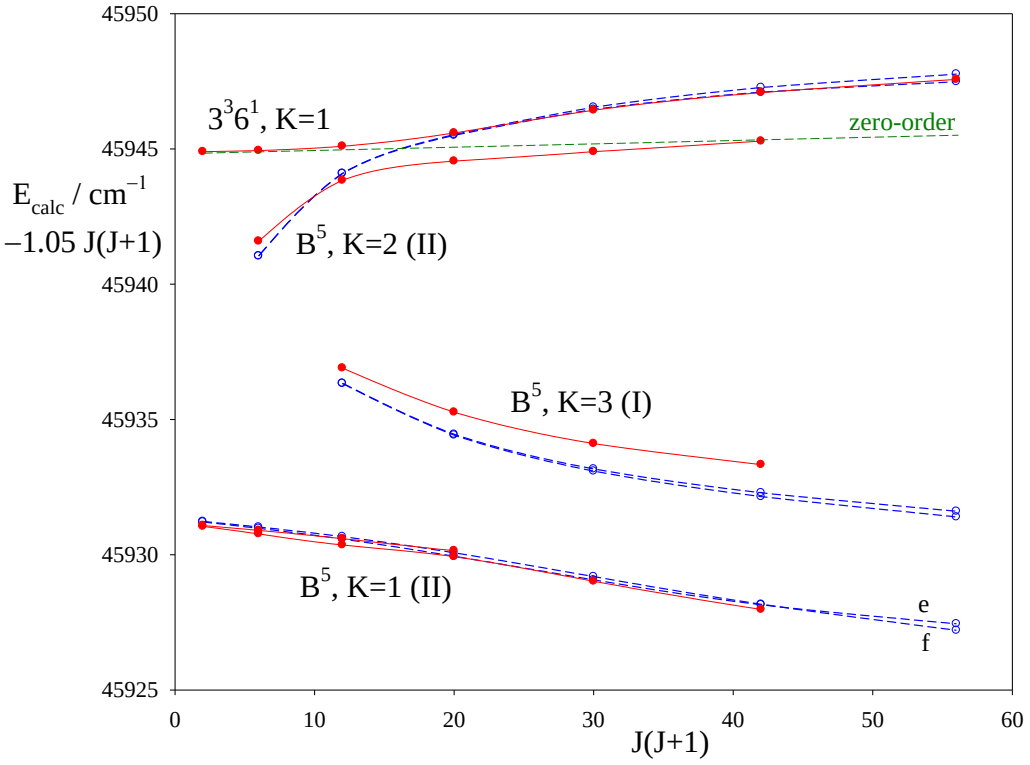

Figure 4-6: Observed and calculated energy levels of the $\tilde{A}\ ^1\mathrm{A}_u$, B^5 polyad of C_2H_2 in the neighbourhood of the $3^36^1, K = 1$ state, plotted against $J(J + 1)$. Observed levels are shown as full circles joined by solid lines; calculated levels are shown with open circles joined by dashed lines. In the online version, observed levels are also coloured red, and calculated levels are also coloured blue; the zero-order position of the $3^36^1, K = 1$ state is shown in green. The calculations are based on the parameters of [16], with an offset of 3 cm^{-1} added. The $3^36^1, K = 0$ state lies at 45937 cm^{-1}, but is not shown.

are almost degenerate in zero-order. In this case the interaction is strong because the $K' = 2$ (II) and $K' = 3$ (I) states belong to nominally different vibrational components of the polyad, as indicated by the Roman numerals.

We note that the $1 - 2$ cm^{-1} splitting of the $J \geq 2$ levels of the $3^3 6^1, K' = 1$ state reported in previous work [46, 91] is not the result of triplet perturbations, but represents an avoided crossing with another vibrational level within the S_1-trans state. There are triplet perturbations in addition to the avoided crossing, but these are much smaller, and are centred on the $3^3 6^1, K = 1$ state rather than its perturbing partner, B^5, $K = 2$ (II). The interaction between the $3^3 6^1, K = 1$ and B^5, $K = 2$ (II) states is an extremely high-order resonance, representing a difference of at least seven quanta of vibration between the interacting states; consistent with this, the matrix element is only about 0.5 cm^{-1}.

Although there are no other avoided crossings among the states in this energy region, there are some interesting near degeneracies. For example, the $2^1 B^3$, $K = 2$ (III) and B^5, $K = 1$ (I) states, near 45896 cm^{-1}, lie only 0.4 cm^{-1} apart at zero rotation. Clearly they interact quite strongly, apparently by a b-axis Coriolis mechanism, because the rotational levels are already 2.8 cm^{-1} apart at $J = 5$. Because they belong to different polyads they should not interact at all, but the fact that they do is a result of Fermi resonance. This particular resonance occurs also between the $2^1 3^1 B^1$ and $3^1 B^3$ polyads, where the interaction parameters were determined by least squares [43] to be $k_{244} = -7$ cm^{-1} and $k_{266} = 8.7$ cm^{-1}. No attempt has been made to fit the two polyads simultaneously in the present instance, but it should be possible to refine the Fermi resonance parameters from the data for these states.

The same type of Fermi resonance occurs between the $K' = 0$ states belonging to $2^1 B^3$ and B^5 near 45900 cm^{-1}; this was described in Section 4.4.1. Surprisingly, the $2^1 B^3$, $K = 0$ A_u and B_u states give very much weaker bands than the B^5, $K = 0$ A_u and B_u states, despite the resonance. By contrast, the nearby $21 B^3$, $K = 2$ (III) state gives reasonably strong bands, in spectra from both $(\nu_3 + \nu_4)''$ and ν_3'', though it is possible that its intensity is enhanced by the b-axis interaction with B^5, $K = 1$ (I) just described. Throughout the spectra the relative intensities of the various bands are

not always easy to understand. An important contributing factor appears to be the interference between vibrational transition moments that occurs when the vibrational wave functions are far from harmonic as a result of the Coriolis and Darling-Dennison resonances. The Fermi resonances seem to be a less important factor, though their effects are unpredictable in the presence of the other resonances. Predissociation also begins to affect the intensities midway through this region.

The $3^3 6^1, K' = 2$ state (at 45972 cm^{-1}) displays extensive triplet perturbations, but without the complication found in the $K' = 1$ state of an avoided crossing within the S_1 state. In all cases where triplet perturbations are seen in our spectra it is found that at low J' values a nominal-S_1 line is split into a few well-separated components, with spacings of typically 0.2 cm^{-1}. With increasing J' the number of components grows; they become closer together, and quickly coalesce into a single broad line. This represents the increasing density of the background triplet levels with increasing J'. At higher J values the lines become apparently sharper, as interactions with triplet levels within the line profile dominate, though weak outliers have been observed as much as 0.4 cm^{-1} away. This is the pattern found in the $3^3 6^1, K' = 2$ state. The $J' = 2$ level has four recognizable components for both parities, but the splitting patterns are not the same. The $J' = 3$ lines have at least five components, though they are not well resolved, while the $J' = 6$ features look like single lines.

It has been possible to assign nearly all the observed lines in this region by combining data obtained via ν_3'' and $(\nu_3 + \nu_4)''$. A few weaker lines remain unassigned, particularly in among the very intense bands from $3^3 6^1$, as seen via $(\nu_3 + \nu_4)''$. Predictions of the expected structure show that some of these lines must be Coriolis-induced transitions to $K' = 3$ states, but the severe blending has made it impossible to obtain secure assignments.

4.4.4 $K' = 0 - 2$ levels in the region 46000 − 46250 cm^{-1}

The region $46000 - 46250$ cm^{-1} contains the $K' = 0 - 2$ states from the $3^3 4^1$ [46] and $3^1 5^1$ [39] vibrational levels, together with eight states from the B^5 polyad. Bands from two cis vibrational levels, cis-6^2 and cis-$3^1 6^1$ are also found; the cis-6^2 $K = 0$

and the cis-3^16^1 bands have already been described in [11], but the cis-6^2, $K = 1$ band is new.

The 3^34^1 vibrational level gives the most intense bands in this region. In contrast to the 3^36^1 vibrational level, which suffers from exceptionally large numbers of perturbing triplet states, the 3^34^1 vibrational level is only mildly perturbed by triplets. Surface electron ejection by laser-excited metastables (SEELEM) spectra have recently documented [8] the perturbations in both of the $K' = 0$ states, but perturbations have not been found previously for the $3^34^1, K' = 1$ and 2 states. [46, 91] Our spectra show that all three states with $K' = 0 - 2$ are perturbed at low J. The $K' = 0$ state gives only a Q branch in double resonance via $(\nu_3 + \nu_4)''$, but extra lines are seen in our spectra accompanying the Q(1)−Q(3) lines, consistent with the SEELEM results. The $K' = 1$ state gives a weak band fragment in double resonance via $(\nu_3 + \nu_4)''$, but an intense band via ν_3''. Although the two parity components of the $J' = 1$ level appear at first sight to give single sharp lines, least squares fitting shows that they are both out of place. Weak extra lines can then be identified, lying within 0.4 cm^{-1} of the main lines. The extra e symmetry levels lie above their main level, but the extra f level lies below its main level. The $3^34^1, K' = 2$ state (46105 cm^{-1}) also shows extra lines and other small irregularities which become obvious in the least squares fitting. The analysis is quite complicated because, for zero rotation, this state lies less than 0.5 cm^{-1} above the $3^15^1, K = 1$ state, which is itself perturbed by triplet levels. In the $(\nu_3 + \nu_4)''$ spectra the complications are compounded by an overlapping one-photon artifact, but the details are clearer in the ν_3'' spectra.

The triplet perturbations found in the 3^15^1 vibrational level affect just the $K = 1$ $J = 5e$ level, which is split into at least four components spread over more than 0.7 cm^{-1}. Every triplet perturbation found so far in the S_1 state appears in a level where ν_3 is involved, but this is the first example of a triplet perturbation in a level involving ν_5 (the antisymmetric CH stretching vibration).

It is interesting that the IR-UV double resonance spectra of the 3^15^1 level recorded by Tobiason et al. [39] via the $3\nu_3''$ overtone level show no sign of the bands from the $3^34^1, K = 2$ level or the B^5, $K = 1$ (V) level, which lie close by in our spectra taken via

the ν_3'' fundamental, and have comparable intensity. One of the contributing factors must be that the composition of the two ground state levels is different, despite the similarity of their names. The ν_3 fundamental is involved in an anharmonic resonance with $\nu_2+\nu_4+\nu_5$, such that the eigenfunction of the 3295 cm^{-1} level (which we used as the intermediate state in the present work) is an almost 50:50 mixture of the two basis functions. [92] The mixing of the two bending vibrations, ν_4 and ν_5, into the wave function must enhance the probability of transitions to bending levels of the upper state according to the Franck-Condon principle. On the other hand the nominal $3\nu_3''$ level at 9640 cm^{-1} has 62% ν_3 character and 28% $2\nu_1+\nu_3$ character, [92] so that there is very little bending character in its eigenfunction. This phenomenon was noted in Ref. [38], where (1112^00) was used instead of $3\nu_3$ as a $J'' < 8$ intermediate for studying ν_4'/ν_6', but this was not necessary for ν_5' or 3^15^1.

Contributing to the ν_3'' spectrum in this region are bands from two further states, B^5, $K = 1$ (V) at 46112 cm^{-1}, and cis-6^2, $K = 1$ at 46120 cm^{-1}. The B^5 state is unexceptional, but the cis-6^2 state is very interesting, because it provides a second example of K-staggering in the S_1 electronic state caused by quantum mechanical tunnelling through the barrier to isomerization. [48] The first example of K-staggering was the cis-3^16^1 vibrational level, discussed in [11].

The selection rules for transitions to cis upper states are different from those to trans upper states. Bands involving even-K and odd-K rotational states of cis vibrational levels cannot appear in the same spectrum because different numbers of photons are needed to record them. For an A_1 vibrational level such as cis-6^2, its $K = 0$ state can be observed in one-photon hot band spectra from an $l'' = 1g$ level such as ν_4'' (π_g), but its $K = 1$ state requires IR-UV double resonance via an $l'' = 0u$ level, such as ν_3'' (σ_u^+). Experimentally, the trans-$1^13^1, K = 0$ state at 46114.5 cm^{-1}, as observed in one-photon hot band spectra from ν_4'', was found [11] to undergo an avoided crossing with the cis-6^2, $K = 0$ state, which lies at 46114.0 cm^{-1}. The cis-6^2, $K = 1$ state should then be observable near this energy in IR-UV double resonance spectra via ν_3''. In this work a band with $K' = 1$, which appears at 46120.3 cm^{-1} in IR-UV double resonance via ν_3'', is assigned to cis-6^2. The upper state therefore has

an apparent A$-\frac{1}{2}$(B+C) constant of 6.3 cm^{-1}. The expected value of this quantity is about 13 cm^{-1}, which suggests that the upper state K-structure exhibits an even-odd K-staggering, which is one of the results of tunnelling through the barrier to isomerization. [48] The cis-6^2 $K' = 0$ and 1 bands, as observed in a one-photon hot band from ν_4'' and in IR-UV double resonance via ν_3'', respectively, are illustrated in Fig. 4-7. Both bands are overlapped by other structure.

Two $K' = 2$ states, one from B^5 and the other from 2^1B^3, are expected at 46059 cm^{-1}, but only one very weak band is found. It is provisionally assigned to B^5, since this polyad generally gives stronger bands than 2^1B^3. Of the 43 upper states with $K' = 0 - 2$ expected in the $45800 - 46250$ cm^{-1} region, only three have not been identified, although their positions can be predicted to within a very few cm^{-1}.

4.4.5 The 3^2B^3 and $2^13^2B^1$ polyads (46250 - 46550 cm^{-1})

The next bands in the IR-UV double resonance spectra, in order of increasing energy, lie in the region $46250 - 46550$ cm^{-1}. Although the region contains only seven vibrational levels from the trans manifold, accidental overlapping of bands from two polyads, 3^2B^3 and $2^13^2B^1$, produces some surprisingly complicated structures. The other states contributing to the region are 2^15^1, B^5 and the new cis levels 3^2 and 4^16^1. Nearly all the structure from the B^5 polyad lies in the regions described above, but the Darling-Dennison resonance effects in it are so large that its highest $K' = 1$ and 2 states are several hundred cm^{-1} above its lowest states. The highest-energy $K' = 1$ state appears at 46292.3 cm^{-1}, 4 cm^{-1} below its predicted [41] position, and the highest $K' = 2$ state (not found) is predicted to lie at 46424 cm^{-1}.

Figure 4-8 gives an overview of the region, in the form of a stick spectrum of the $K' = 0 - 2$ levels. When two quanta of ν_3 are excited, the very large cross-anharmonicity between ν_3 and ν_6 starts to break up the bending polyads. Even though the two bending fundamentals, ν_4 and ν_6, are only 3 cm^{-1} apart, [38] the result in the 3^2B^3 polyad is that the nominal 3^26^3 (B_u) level lies 110 cm^{-1} below the nominal 3^24^3 (A_u) level. The Darling-Dennison resonance pushes the combination levels $3^24^16^2$ (A_u) and $3^24^26^1$ (B_u) more than another 100 cm^{-1} higher still, so that

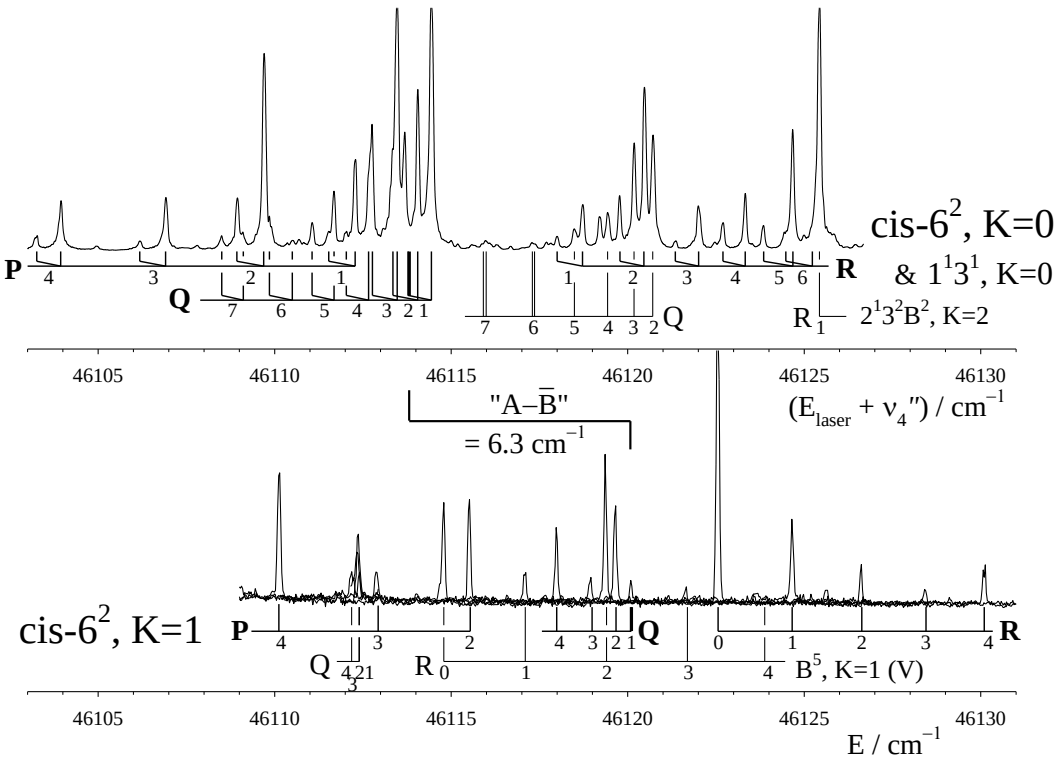

Figure 4-7: Upper spectrum: the interacting cis-$6^2, K = 0$ and trans-$1^1 3^1, K = 0$ states, as seen in one-photon hot band spectra via the ν_4'' (π_g) fundamental. These two states lie less than 1 cm^{-1} apart, and are linked in the figure with a single set of tie-lines for each J value. The calibration for this spectrum is not exact; a small correction equal to $[\mathrm{B}(\nu_4'') - \mathrm{B}(v'' = 0)]\ J''(J''+1)$ should be applied for each line. Lower spectrum: the cis-$6^2, K = 1$ state, as seen in IR-UV double resonance via the ν_3'' (σ_u^+) fundamental. This spectrum consists of five superimposed plots taken via the rotational levels $J'' = 0 - 4$ individually. No correction needs to be applied to the calibration of this spectrum. The tie-lines for the cis-6^2, Q(1) lines in the two spectra of this figure are shown thickened, in order to emphasise that the $K' = 1$ state lies only 6.3 cm^{-1} above the $K' = 0$ state. This quantity corresponds to the rotational constant $\mathrm{A}-\frac{1}{2}(\mathrm{B}+\mathrm{C})$, less the amount of the K-staggering which results from quantum mechanical tunnelling through the barrier to isomerisation. Since $\mathrm{A}-\frac{1}{2}(\mathrm{B}+\mathrm{C})$ is expected to be about 13 cm^{-1}, the K-staggering has lowered the $K' = 1$ state, relative to the $K' = 0$ state, by about 7 cm^{-1}.

the four $K = 0$ levels are spread over 250 cm^{-1}. The Coriolis effects are then not strong enough to cause re-ordering of the low-K energy levels, such as is seen in the 1^1B^1 and 2^1B^3 polyads, except in the third of the four vibrational levels (in order of energy). The K-structure is more like that of a slightly perturbed asymmetric top, though the lowest $K = 0$ and 1 levels lie very close in energy, which (as we see below) can lead to interesting effects. The $2^13^2B^1$ polyad behaves in similar fashion, except that there is no Darling-Dennison resonance. The predicted positions of the states of these polyads (following Eq. (1)) are given in Table 4.2. The agreement between the observed and calculated positions is not as good as for the B^5 polyad, though it is still adequate to allow assignment of the bands.

Table 4.2: Observed and predicted level energies (cm^{-1}) for the 3^2B^3 and $2^13^2B^1$ polyads. Observed band energies are in Roman type, predicted energies in italic type.

$K =$		0	1	2
3^2B^3	B_u	46287.0	46291.0	46321.7
		46291.9	*46298.6*	*46319.6*
	A_u	46397.8	46413.8	46430.1
		46399.7	*46411.3*	*46430.9*
	B_u	46511.0	46479.6	46500.8
		46512.9	*46483.4*	*46498.6*
	A_u	46531.1	46598.5	46696.3[(a)]
		46532.3	*46595.2*	*46694.9*
$2^13^2B^1$	B_u	∼46359[(b)]	46358.8	46380.3
		46356.3	*46359.8*	*46380.4*
	A_u	46387.0	46415.8	46476.1
		46395.6	*46418.1*	*46475.1*

(a) Assignment not secure. An alternative assignment to a $K = 2$ state at 46707.7 cm^{-1} is possible.
(b) See text and Fig. 4-10 for further details.

The lowest $K' = 0$ and 1 levels of the 3^2B^3 polyad give rise to weak bands near 46290 cm^{-1}. There is no direct coupling between them, but transferred b-axis Coriolis interaction causes both of them to appear in double resonance spectra via both ν_3'' and $(\nu_3 + \nu_4)''$. The lower $K' = 0$ and 1 levels of the $2^13^2B^1$ polyad (nominally

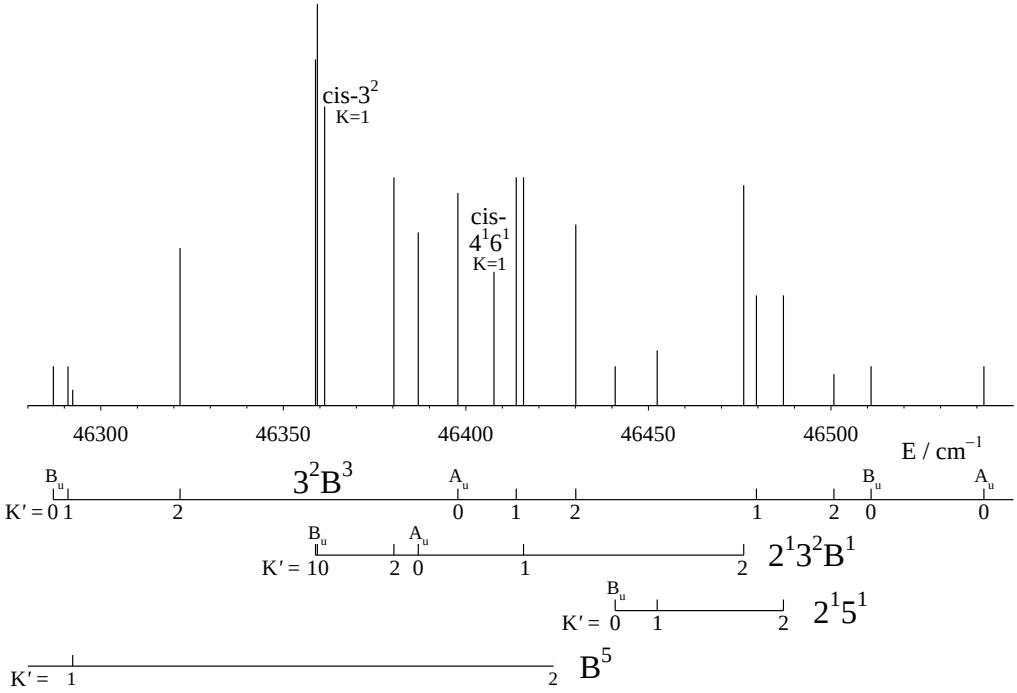

Figure 4-8: Stick diagram of the *ungerade* $K' = 0 - 2$ levels of the $\tilde{A}\ ^1\mathrm{A}_u$ state of C_2H_2 in the region $46280 - 46550$ cm^{-1}, with their assignments, as recorded using IR-UV double resonance via the ν_3'' (σ_u^+) and $(\nu_3 + \nu_4)''$ (Π_u) vibrational levels of the ground state. The spectra recorded from the two intermediate levels have been combined into a single plot. Approximate intensities are indicated by the heights of the sticks. States that could not be found are marked with dotted lines at their predicted positions. The highest $K' = 1$ and 2 states of the 3^2B^3 polyad are not shown; bands at 46598.5 and 46696.3 cm^{-1} are provisionally assigned to them.

$2^1 3^2 6^1$, B_u) lie at 46359 cm^{-1}. They are almost degenerate, and since the nominal $2^1 3^2 4^1$, A_u, $K = 1$ level, to which they are both Coriolis-coupled, lies only 28 cm^{-1} higher, there is strong interaction. The spectrum, as seen in double resonance via the very sharp Q branch head of $(\nu_3 + \nu_4)''$ (Π_u), where the $J'' = 1f - 5f$ levels are populated simultaneously by the IR laser, is illustrated in Fig. 4-9. It is unexpectedly complicated. According to the rotational selection rules, there should be two sets of R and P branches, one going to the $K' = 0f$ state, and the other to the f symmetry levels of the $K' = 1$ state as a result of the Coriolis interaction. Instead three strong R-P branch pairs are seen, together with two weak Q branches in the gap between them. This implies that three sets of excited state f symmetry rotational levels and two sets of e symmetry levels are present. Given that the unperturbed $K' = 1e$ levels may give rise to a weak Q branch if other suitable interactions occur, it is clear that an extra vibrational state must be present. The upper state energy levels are shown, plotted against $J(J + 1)$, in Fig. 4-10. The parabola-like appearance of this figure is reminiscent of Fig. 4-6, and for the same reason. In fact the branch intensities, and the existence of a $J' = 0$ level for the middle set of f symmetry levels, show that the zero-order $2^1 3^2 6^1, K' = 0$ and 1 states correspond to the three lowest sets of levels. The two sets of f symmetry levels, $K' = 0f$ and $1f$, repel each other, while the $K' = 1e$ set, which is unaffected, lies in between them. Further interactions between the f symmetry levels then transfer the curvature of the plot to the upper set of f levels in the figure. A small perturbation in the topmost f level appears to be caused by an unidentified $K' = 4$ state. The pattern of upper state energy levels is confirmed in detail by the double resonance spectrum via ν_3'', where the f symmetry levels give Q branches, and the e symmetry levels give R and P branches.

There is no place in the S_1-trans manifold for the upper $K' = 1$ state, which presumably belongs to the S_1-cis manifold. *Ab initio* calculations of the cis vibrational structure [53] predict that the cis-2^1 and 3^2 levels should both lie close to this energy. These vibrational levels both have the correct symmetry (A_1) to give $K' = 1$ bands in the ν_3'' double resonance spectrum, but the ab initio calculations [10] indicate that the cis-3^2 level should interact much more strongly than the cis-2^1 level with the

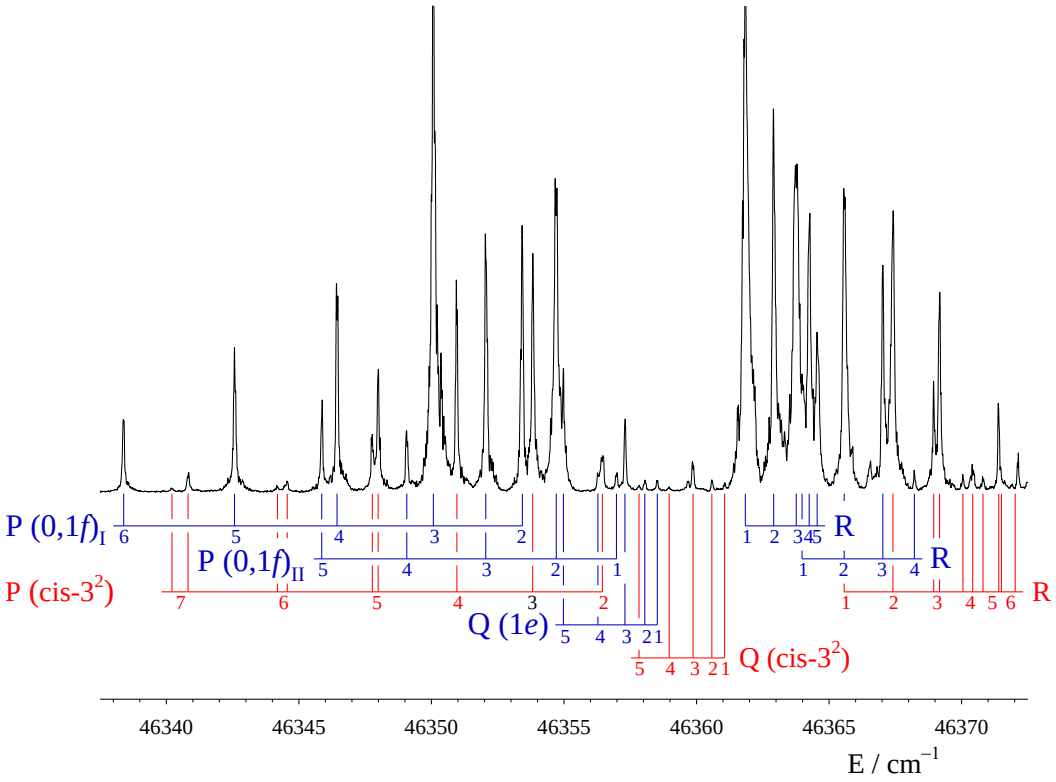

Figure 4-9: IR-UV double resonance spectrum of C_2H_2 near 46359 cm^{-1}, recorded via the Q branch of the $(\nu_3 + \nu_4)''$ (Π_u) combination level. The three sets of R and P branches represent the $K' = 0f$ and $1f$ levels of the $2^1 3^2 6^1$ state, which are almost degenerate, together with the f levels of another $K' = 1$ state at 46361.3 cm^{-1}, which is assigned as cis-3^2. All three sets of f levels are strongly Coriolis-coupled. The two Q branches represent the unperturbed e symmetry levels of the two $K' = 1$ states. In the color version, lines going to the cis-3^2 state are marked in red, and lines going to the $2^1 3^2 6^1$ state are marked in blue.

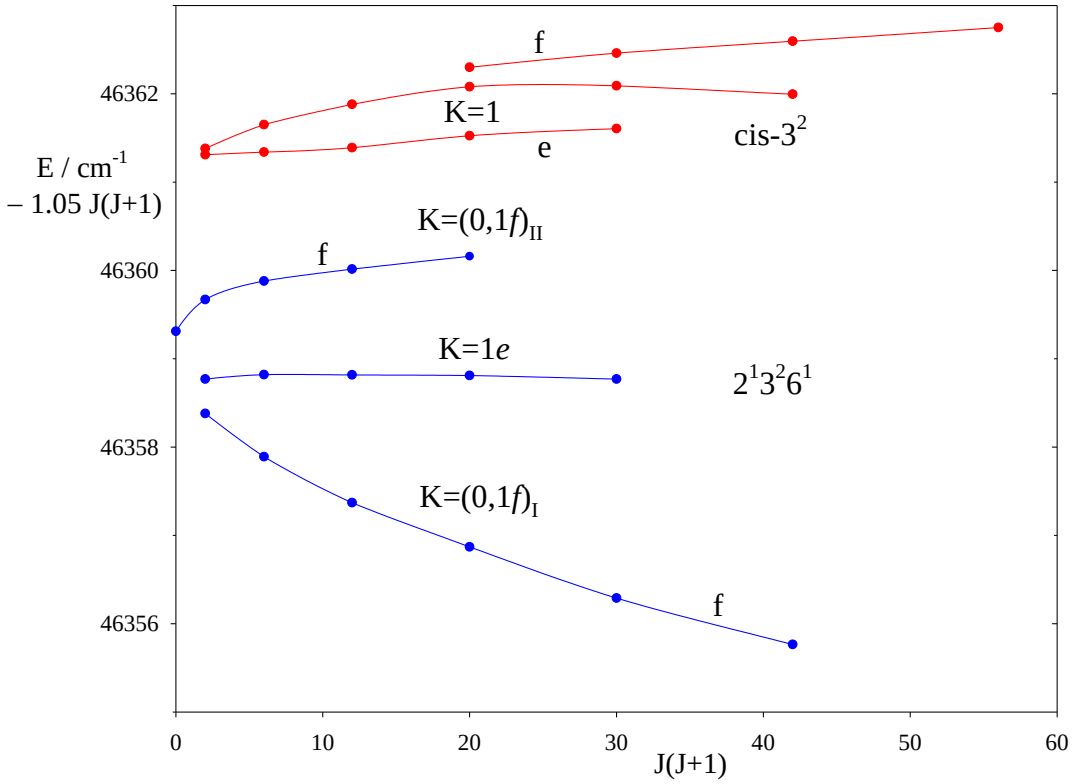

Figure 4-10: Observed energy levels in the 46359 cm^{-1} region of the ungerade manifold of the S_1 state of C_2H_2, plotted against $J(J+1)$. The three lowest levels (two of f symmetry and one of e symmetry) belong to the S_1-trans $2^1 3^2 B^1, K = 0f$ and 1 states, which are almost degenerate in zero-order and interact by indirect b-axis Coriolis coupling. The state near 46361 cm^{-1} is assigned as cis-3^2, $K' = 1$, perturbed at $J' \geq 4$ by an unidentified state. In the color version, levels of e symmetry are coloured red, and levels of f symmetry are coloured blue.

trans manifold and have greater intensity via ν_3''. In view of these calculations, we provisionally assign the new $K' = 1$ state as cis-3^2.

The next region of complexity occurs about 50 cm^{-1} higher, where three close-lying $K' = 1$ states occur at 46408, 46414 and 46416 cm^{-1}. All three have comparatively large asymmetry splittings (see Table 4.1) in the sense f above e, which is consistent with A_u vibrational symmetry. Predictions of the K-rotational structures of the 3^2B^3 and $2^13^2B^1$ polyads would place $K' = 1$ states with A_u symmetry at 46411 and 46418 cm^{-1}, respectively. Unfortunately the predictions are not accurate enough to identify the observed states with particular polyads securely, though it seems that the states at 46414 and 46416 cm^{-1}, which give the strongest bands, belong to these two polyads. However the third state, which gives a much weaker band, is not predicted, and presumably belongs to the S_1-cis electronic state, where its vibrational symmetry would be B_1. Vibrational B_1 states are rare among the low-lying levels of the S_1-cis state, as they require odd quanta of both ν_4 (a_2) and ν_6 (b_2). At this very low vibrational energy of approximately 1500 cm^{-1} the only logical assignment is the combination level cis-4^16^1.

There are only a few triplet perturbations in this region. Most of them take the form of a doubling of the $J' = K'$ lines of a band, but more extensive perturbations occur in the 3^2B^3, $K = 1$ (IV) state at 46598 cm^{-1}, where several J levels are affected; the $J = 5e$ level of this state is split into four components. Where the vibrational assignments of the perturbed states have been established, it is found that they all belong to the 3^2B^3 polyad.

The 2^15^1 vibrational level lies in the middle of this region, at 46441 cm^{-1}, and has been observed previously. [93] It is not subject to Coriolis effects, and is a normal asymmetric top level. Our rotational constants for it are given in Table 4.3.

4.5 Discussion

This work gives the details of the ungerade vibrational levels of the S_1-trans state of acetylene in the energy range $45800 - 46500$ cm^{-1}, as observed in IR-UV double

Table 4.3: Rotational constants from least squares fitting of the $K' = 0 - 2$ levels of the $2^1 5^1$ vibrational state. Values in cm^{-1}.

T_0	46440.894	$\pm$	0.028
A	12.587		0.041
B	1.115		0.0039
C	1.0206		0.0040
r.m.s.	0.016		

resonance. The complete vibrational level structure of this electronic state has now been established up to a vibrational energy of 4300 cm^{-1}. The aim has been to understand the S_1-trans state in sufficient detail that any vibrational states that do not fit into its energy level pattern can be assigned to the S_1-cis isomer. Four such states were identified previously, [11] and the present work has provisionally found two more.

The barrier to isomerization in the S_1 state is calculated [10] to lie around 5000 cm^{-1} above the S_1-trans zero-point level, which means that the signatures of cis-trans isomerization should already be observable in some of the levels studied in this work. The most characteristic effect will be an even-odd staggering in the K-structure of a vibrational level where tunnelling through the barrier is possible. [48] This effect should be largest in those vibrational levels that carry the shape of the molecule along the isomerization pathway from the equilibrium structure of the trans isomer to the half-linear structure at the saddle point. Those vibrational levels are combinations of ν_3 and ν_6, which in the trans isomer are, respectively, the trans-bend and the cis-bend. (The forms of the vibrations are reversed in the cis isomer.) It is difficult to observe the K-staggering in levels of the trans isomer because the Coriolis and Darling-Dennison interactions between ν_6 and ν_4 (torsion) perturb the K-rotational structure so severely that the effects of the tunnelling are masked. The interaction between ν_4 and ν_6 is less important in the cis isomer, so that the K-staggering can be observed. The cis-$3^1 6^1$ level was recently found [11] to have its $K' = 1$ state shifted up by 3.9 cm^{-1} relative to its $K' = 0$ and 2 states. From the present work, the cis-6^2 level appears to have a staggering of about 7 cm^{-1} in the opposite sense.

Nevertheless, trans-levels in the same energy region as these cis levels should show comparable staggerings, and the 3^2B^3 polyad, in the region $46250 - 46550$ cm^{-1}, should offer good examples. It may be that hints of their existence can already be seen. It was found [41] that the vibrational and K-rotational structures of the pure bending polyads, $B^n,\ n = 1-3$, can all be reproduced to within a very few cm^{-1} by a single set of anharmonicity and interaction parameters; the present work confirms that this finding applies also to the states of the B^5 polyad. A similar finding applies to the various bending polyads in combination with symmetric levels such as 3^1, and forms the basis for extending the vibrational assignments to higher energy. [43] On the other hand, this approach works less well for predicting the structure of the 3^2B^3 polyad, perhaps indicating that staggerings are present, but are less completely masked by the intra-polyad interactions. It will be interesting to follow the level patterns to higher energies, where the bending polyad structure is essentially destroyed by the anharmonicity, so that the effects of the barrier should be more clearly seen.

Now that the structures of the trans polyads in this region have been established, it should be possible to analyze the region near the expected transition state energy, located approximately one bending quantum higher. The information gained from the present analysis of the 1^1B^1 and 2^1B^3 polyads has already helped with the analysis of that energy region in our not yet published one-photon spectra, which contain candidates for additional cis levels and the barrier-proximal levels 3^36^2 and 3^46^2. The analysis of these levels, and the information about the transition state energy that can be derived from it, will be discussed in a future paper.

Chapter 5

Anharmonic force fields of *cis*- and *trans*-S_1 C_2H_2

Abstract

We calculate second order vibrational perturbation theory (VPT2) anharmonic force fields for the *cis* and *trans* conformers of S_1 C_2H_2, and compare the results to experiment. The vibrational assignments of recently observed levels belonging to the *cis* well are of particular interest. A refined estimate of the *cis* origin position (44870 ± 10 cm^{-1}) is proposed, and preliminary low-energy fits to the global J=K=0 *trans* level structure are also described. The performance of perturbation theory in this isomerizing system is examined, and both surprising successes and failures are encountered. We examine these and their causes, and offer practical suggestions for avoiding the pitfalls of applying perturbation theory to systems with large amplitude motions.

The results in this chapter, aside from some minor updates, have been published in the FASE special issue of Molecular Physics [53].

5.1 Introduction

The determination of the potential energy surfaces (PES) of polyatomic molecules is a subject of considerable chemical interest. Most often effort is directed at characterizing the stationary points of the PES, since these largely determine the thermodynamics and kinetics of the molecular system. In the S_1 state of C_2H_2, we find

ourselves in the unique position of possessing high resolution spectroscopic information that samples all of the chemically relevant stationary points on a PES that supports *cis*-*trans* isomerization: the *trans* and *cis* minima, and the half-linear transition state [26] that lies between them. In particular, due to the long and intense study of the lower-lying $\tilde{A}\ ^1\mathrm{A}_u$ *trans* conformer, complete vibrational assignments have been made nearly up to the expected transition state energy.

Despite the amount of attention the $\tilde{A}\ ^1\mathrm{A}_u$ state has received, to date few attempts have been made to treat the *trans* conformer in a global sense. Although many workers have contributed significantly to the understanding of the vibrational level structure [35–39, 46], progress was initially made only in a piecemeal fashion, with perturbations and irregular rovibrational structures often explicitly noted. The sole exception was the determination of the harmonic force field by Tobiason *et al.* [72], but unfortunately that work was done before the ν_1 fundamental had been observed [42]; furthermore, a harmonic force field has little predictive power. The work in recent years by Merer *et al.* [40–43], based primarily on a new understanding of the bending (B^n) polyads that arise from strong Darling-Dennison resonance and Coriolis effects, established the *trans* level structure to an extent that allowed several bands belonging to the S_1-*cis* conformer to be identified. [11]

The goal of the present work is to calculate the anharmonic force fields of both the *cis* and *trans* conformers of the S_1 state, in order to be able to extend the comprehensive *trans* assignments in the increasingly congested regions approaching the transition state energy, and to anticipate where additional states of the *cis* conformer might be found. An accompanying paper [88] has already made use of this information in analyzing an extended complicated region of the IR-UV double resonance spectrum, where many interacting *trans* levels, some affected by previously unknown anharmonicities, are located. Two new *cis* vibrational levels have also been discovered, and their vibrational assignments (3^2 and 4^16^1) are based on the calculations presented here. This brings the observed total to six out of an expected ten *cis* levels below 46500 cm^{-1}, where the complete *trans* assignments currently end.

The anharmonic force fields described in this paper are calculated using standard

second order vibrational perturbation theory (VPT2) [94]. Effective use of this convenient and accurate approach for electronically excited S_1 C_2H_2 requires high level quantum chemistry, for which we choose the EOM-CCSDT level of theory [61]. We demonstrated previously that this method obtains excellent optimized geometries and harmonic frequencies for the S_1 state [10], but there the quantities calculated *ab initio* were not easily compared to experiment. Here, where a more direct and quantitative juxtaposition is possible, the performance of this high level method is even more impressive.

A relevant question is whether a perturbation theory approach is appropriate for an isomerizing system, where large amplitude motions are clearly possible. While obviously there are aspects of interest that cannot be addressed by perturbation theory approaches that focus on a single minimum in the PES, for example, K-staggering [48] or intensity borrowing [10] due to tunneling, the good agreement obtained with experiment for many of the results demonstrates that perturbation theory is still useful for many features of such systems. The specific instances where the VPT2 treatment appears unsatisfactory or misleading in this particular molecule will be discussed explicitly.

The extensive literature on the $\tilde{A}\ ^1A_u$ vibrational level structure provides much raw material for assessing the *trans* force field results. In order to focus on the vibrational parameters and avoid the pervasive perturbations as much as possible, we have elected to make use of J=K=0 term values. A compilation of these term values can be found in Appendix 5.A.

5.2 Methods

All *ab initio* calculations were performed with the CFOUR program package [81], employing the MRCC program [82] for analytic gradients, and using the NASA Ames ANO1 basis set [95] with the EOM-CCSDT method. Core electrons were not correlated. VPT2 forcefields were calculated by numerical differentiation of the analytic first derivatives, which were computed in parallel. For the *cis* conformer, harmonic

frequencies were also computed using the ANO2 basis set, but these frequencies were used only for the vibrational term value calculation.

One dimensional torsional Discrete Variable Representation (DVR) calculations were carried out as described previously [10] in order to obtain values for the torsional fundamentals of both conformers. For these calculations, a single crude torsional potential curve was constructed by taking the lower of the two electronic energies obtained using *cis* and *trans* equilibrium values for R_{CC}, R_{CH}, and ∠CCH at values of the torsional angle $\tau = 0 : 12 : 180°$, where $\tau = 0°$ and 180° correspond to planar *cis* and *trans* geometries, respectively. This procedure sufficed to splice together the appropriate potentials at the two minima. The two-fold symmetry of the torsional angle was used to extend the potential over the entire 360° range of the DVR calculation. In the calculation of the kinetic energy, the values of R_{CC}, R_{CH}, and ∠CCH were interpolated between the *cis* and *trans* equilibrium values so that the G matrix elements have the appropriate values in the vicinity of the minimum of each conformer.

5.3 Results

We previously reported [10] *ab initio* harmonic frequencies for both conformers, and found them to be in excellent agreement with experimental values, where those have been determined or estimated. Here we focus on the calculation of vibrational fundamentals, and the determination of the x_{ij} parameters important for the prediction of the level positions of combination bands and overtones.

5.3.1 *cis*-S_1

5.3.1.1 Vibrational Parameters

At present, only six vibrational levels localized in the *cis* well have been observed [11, 88], which limits our ability to assess the *cis* VPT2 results. In particular, without the observation of the *cis* origin, we are left without the natural starting point for such

a discussion; the calculated *cis* harmonic and fundamental frequencies are listed in Table 5.1, but there are no experimental results yet for direct comparison. Fortunately, a relatively precise estimate of the *cis* origin can be made by noting that two of the observed *cis* levels are 3^1 K=1 and 3^2 K=1, with their spacing $46361 - 45624 = 737$ cm^{-1} in good agreement with the *ab initio* value of $\nu_3 + 3x_{33} = 742$ cm^{-1}. (The calculated *cis* x_{ij} are tabulated in Table 5.2.) Extrapolating back one quantum to the *cis* origin gives its position as 44870 ± 10 cm^{-1}, where the sources of uncertainty include not only x_{33} but also the unknown A rotational constants (assumed to be 14 cm^{-1} here) and any K-staggering that affects these levels [48]. This estimate is in excellent agreement with our previous *ab initio* calculation [10] of 44856 and experimental estimate [11] of 44900 cm^{-1}.

Table 5.1: Harmonic and Fundamental Frequencies for *cis*-S_1 C_2H_2

	ANO1		ANO2
	Harmonic	Fundamental	Harmonic
ν_1	2997.14	2789.11	3003.71
ν_2	1583.23	1501.05	1584.79
ν_3	806.10	748.61	796.94
ν_4	817.30	826.53	827.92
ν_5	2941.72	2734.89	2948.44
ν_6	571.72	576.25	579.81

Frequencies in cm^{-1}. The structural parameters from the ANO2 geometry optimization are $R_{CH} = 1.0970$ Å, $R_{CC} = 1.3390$ Å, and $\angle$CCH = 132.75°.

Until more *cis* levels are located, it would be premature to discuss the accuracy of the x_{ij} individually. Quite a few are unusually large, which is perhaps not unexpected when the potential well is only 2300 cm^{-1} deep. Overall, the agreement with experiment by adding the VPT2 energies to the present estimate of the cis origin (Column 2 of Table 5.3) seems unimpressive. However, if we correct ν_4 and ν_6 upwards by 28 and 23 cm^{-1}, respectively, based on the errors for 4^1 and 6^2, then the agreement for the combination levels 3^16^1 and 4^16^1 becomes quite good as well. Corrections of this kind are justifiable if there is cause to suspect that theory has difficulty treating these particular modes; as we will see in much greater detail with the results for the *trans*

Table 5.2: Anharmonicities for *cis*-S_1 C_2H_2

	x_{11}	-42.06	
	x_{22}	-6.93	
	x^*_{33}	-2.03[a]	
	x^*_{44}	15.42[b]	
	x_{55}	-47.29	
	x_{66}	14.57	
x_{12}	-4.67	x_{13}	-7.89
x_{14}	-7.31	x_{15}	-212.48
x_{16}	-15.47	x^*_{23}	-5.02[a]
x^*_{24}	-58.50[b]	x_{25}	-0.23
x_{26}	-43.15	x_{34}	-33.61
x_{35}	-6.11	x_{36}	-54.23
x_{45}	-6.65	x_{46}	62.84
x_{56}	0.97		

Constants in units of cm^{-1}.

[a]The VPT2 result is weakly affected by Fermi resonance between 2^1 and 3^2. Near-zero energy denominators were removed to calculate this value. Ordinarily an effect of this magnitude could safely be neglected, but we have accounted for it because of the role of x_{33} in our estimate of the *cis* origin position. $\phi_{233} = -14.26$ cm^{-1}.)

[b]The VPT2 result is strongly affected by Fermi resonance between 2^1 and 4^2. Near-zero energy denominators were removed to calculate this value. $\phi_{244} = 203.43$ cm^{-1}.

Table 5.3: Level List for *cis*-S_1 C_2H_2

State	Expt. [11, 88]	VPT2	Calc.−Obs.	Corrected
0^0		44870		
6^1		45455		45477
3^1	45610	45610	0	
4^1	45735	45707	-28	45735
6^2	46114	46068	-46	46114
$3^1 6^1$	46175	46141	-34	46164
3^2	46347	46346	1	
2^1		46373		
$4^1 6^1$	46394	46354	-40	46405
$3^1 4^1$		46414		46442

Energies in units of cm^{-1}. The ANO2 harmonic frequencies listed in Table 5.1 were used to calculate the VPT2 term values. See text for derivation of the 44870 value used for the VPT2 zero point level.

conformer, this seems to be the case in this molecule. Returning briefly to the x_{ij}, the good agreement with $3^1 6^1$ and $4^1 6^1$ after these empirical corrections suggests that the values for x_{36} and x_{46}, which are among the largest, are not unreasonable.

To summarize, the *cis* results are difficult to compare to experiment, because of the combination of uncertainties in the (not yet observed) *cis* zero-point level position, the VPT2 *cis* vibrational state energies, and finally any shifts caused by *cis-trans* interactions. [10, 48] Nevertheless, these refinements over simple harmonic predictions have already proven useful in the location and assignment of additional *cis* levels. [88] As shown in Table 5.3, six out of an expected ten levels have now been found, below the energy at which the *trans* assignments are complete. Based on the simulated spectra from Ref. [10], it seems understandable that *cis*-2^1 is not observed, despite the recent discovery of *cis*-3^2 presumably nearby, since the predicted intensity ratio is approximately 10^4 in favor of *cis*-3^2.

5.3.1.2 Rotational Parameters

The vibrational dependence of the rotational constants is an important source of evidence for vibrational assignments. Table 5.4 presents the calculated rotational constants as well as their shifts upon single quantum excitation, and compares them to the fitted rotational constants for the *cis* levels that have been observed.

We should note that the experimental rotational constants are known to be affected by tunneling staggerings [11, 48, 88] and possibly also by the *cis-trans* interaction(s) that allow these nominally forbidden levels to appear in the spectrum. [10] These types of effects cannot be treated by the methods used here, and so the utility of these numbers is limited until sufficient data is available to obtain deperturbed rotational constants. In assessing the reliability of these calculated rotational parameters, it is perhaps useful to inspect the *trans* rotational parameters, where a more direct and comprehensive comparison can be made to experiment. These are shown in Sec. 5.3.2.2 (Table 5.7) and agree very well with the experimentally derived values.

Table 5.4: *cis* Rotational Constants and Vibrational Shifts

	A	B	C
B_e	13.881	1.136	1.050
B_0	13.883	1.133	1.038
α_1	0.410	0.002	0.0042
α_2	0.049	0.007	0.0070
α_3	-0.889	0.183	0.0011
α_4	-1.162	-0.184	-0.0004
α_5	0.403	0.002	0.0035
α_6	1.492	-0.002	0.0069

	Expt. [11, 88]			VPT2		
State	A	B	C	A	B	C
3^1	13.95[a]	1.118	1.045	14.327	1.134	1.038
4^1	15.135	1.185	1.02[a]	13.732	1.133	1.038
6^2	-[b]	1.1353	1.0349	14.439	1.136	1.024
$3^1 6^1$	14.019	1.1258	1.037	15.05	1.136	1.03
3^2	-	1.120	1.038	15.66	1.137	1.036
$4^1 6^1$	-	1.0934	1.027	13.86	1.136	1.031

Constants in units of cm^{-1}. Two pairs of the *cis* α values are large and correlated, $\alpha^A_{4,6}$ and $\alpha^B_{3,4}$, indicating the presence of Coriolis effects. Recomputed values that remove the effects of these near-resonant terms ($\alpha^A_4 = 0.301$, $\alpha^A_6 = -0.278$, $\alpha^B_3 = -0.002$, $\alpha^B_4 = -0.001$) have been used to calculate the state-specific constants (including B_0). The relevant Coriolis constants are $\zeta^a_{4,6} = -0.7371$ and $\zeta^b_{3,4} = -0.6350$. The rotational constants from the ANO2 geometry optimization are (in cm^{-1}): $A_e = 13.975$, $B_e = 1.140$, and $C_e = 1.054$.

[a]Fixed.

[b]The apparent $A - \overline{B}$ for *cis* 6^2 is 6.33 cm^{-1}, which presumably is strongly affected by K-staggering. Without an observation of $K = 2$, a reasonable value for A cannot be determined.

5.3.2 *trans*-S_1

5.3.2.1 Vibrational Parameters

In contrast to *cis*-S_1, the $\tilde{A}\ ^1A_u$ state of acetylene has been studied for over 60 years with almost 100 vibrational levels assigned, and complete assignments up to 4300 cm^{-1} above the zero point level. All of the fundamentals have been observed, and are compared to the *ab initio* results in Table 5.5. The agreement is excellent for the stretching modes, but deteriorates for the lower frequency bending modes. (The value obtained for ν_4 is anomalously bad; it will be shown later on in Sec. 5.4 that this is due to the use of rectilinear coordinates.)

Table 5.5: Harmonic and Fundamental Frequencies for *trans*-S_1 C_2H_2

	Harmonic	Fundamental	Expt. [35, 38, 39, 42]
ν_1	3053.52	2884.76	2880.08
ν_2	1424.63	1383.23	1386.90
ν_3	1106.12	1062.04	1047.55
ν_4	757.87	730.65	764.90
ν_5	3033.45	2860.52	2857.4
ν_6	780.63	755.30	768.26

Frequencies in cm^{-1}.

Almost all of the diagonal anharmonicities have been or can be determined from experimental data. These are seen to agree well with the VPT2 values in the first two sections of Table 5.6. Some of the x_{ij} were previously calculated [40] at the CCSD/TZ2P level of theory, and are slightly improved upon by those reported here. A few of the x_{ij} were determined only very recently [88], and that analysis was greatly facilitated by prior knowledge of their *ab initio* values. The x_{ij} that remain to be determined are irrelevant until much higher energies and are expected to be calculated very accurately by theory (x_{11}, x_{55}, x_{15}).

Although the *ab initio* parameters are not sufficiently accurate to permit prediction of the vibrational level structure at higher energies, fortunately their deficiencies can be identified and remedied by fitting to the extensive set of known J=K=0 levels, which is listed in the Appendix 5.A. By supplementing the experimental constants

with those from theory and using only the parameters $\{\omega_i, x_{ij}, K_{4466}\}$, one can fit the *trans* J=K=0 level structure up to greater than 3000 cm^{-1} above the zero-point level with residuals of 3 cm^{-1} or less. The parameters thus obtained do not deviate significantly from the experimental values listed in Table 5.6. It is important to note that two anharmonicities involving ν_3, x_{34} and x_{36}, are not well determined, but for different reasons. As discussed in Ref. [41], Coriolis effects make a surprisingly large contribution to anharmonicities such as x_{46}. These Coriolis effects depend strongly on A, which in turn increases rapidly [35] with v_3. Although it has not been done in the present work, this effect can be taken into account in J=K=0 fitting by the addition of a y_{346} term, but the values of x_{46} and x_{34} then change significantly. The difficulty for x_{36} arises because the *cis-trans* isomerization path is a combination of these two normal modes, and their combination levels are extremely anharmonic [10, 43, 46]. The value of x_{36} therefore becomes steadily more negative as more and more levels are added to the fit, until the simple model fails completely.

5.3.2.2 Rotational Parameters

The rotational constants of all of the *trans* vibrational fundamentals have been determined experimentally. Table 5.7 compares these values with the *ab initio* results, and the agreement is quite good. Unfortunately, the *trans* rotational parameters are less useful for assignment purposes because of the very strong Coriolis and Darling-Dennison effects found in the ν_4/ν_6 polyads. [40, 41, 43]

5.4 Discussion

Overall, the performance of vibrational perturbation theory is surprisingly good for both conformers of S_1 C_2H_2, given that many manifestations of isomerization appear in their spectra at fairly low energies. Particularly for the *cis* conformer, where the 3^1 and 3^2 levels observed must be delocalized into the *trans* well in order to appear in the spectrum, it is unexpected that the *ab initio* calculations treat them accurately and even quantitatively, insofar as they have been experimentally

Table 5.6: Anharmonicities for *trans*-S_1 C_2H_2

	VPT2	Expt. [39, 41–43, 88]
x_{11}	-36.40	[a]
x_{22}	-10.79	-11.35
x_{33}	-6.59	-8.70
x_{12}	-1.09	-1.07
x_{13}	-6.41	-10.55
x_{23}	-0.13	-0.24
x_{44}	3.63	0.19
x_{66}	-2.65	-4.23
x_{46}	11.82	11.39
x_{14}	-16.09	-16.7
x_{24}	-25.98	-13.29
x_{34}	-22.59	(-11.04)[b]
x_{16}	-9.76	-11.6
x_{26}	-10.39	-7.7
x_{36}	-24.58	(-33.45)[b]
x_{55}	-38.46	[a]
x_{15}	-158.57	[a]
x_{25}	-2.07	-0.98
x_{35}	-8.12	-10.77
x_{45}	-16.12	-16.81[c]
x_{56}	-7.14	-8.98[c]

Constants in units of cm^{-1}.

[a]These anharmonicities cannot be determined from the currently known J=K=0 data, since they require observation of the very high-lying states 1^2, 5^2, and 1^15^1.

[b]Not well determined; see accompanying text for discussion. In the fit performed here $K_{4466} = -51.15$, in good agreement with the value of -51.68 from Ref. [41].

[c]The sum of x_{45} and x_{56} was estimated at -25 cm^{-1} in Ref. [43]. The values listed here are based on unpublished least squares fits of the 5^1B^2 polyad by A. J. Merer.

Table 5.7: Observed and Calculated *trans* Rotational Constants and Vibrational Shifts. For each constant, the experimental value is listed above the *ab initio* value.

	A	B	C
B_e [a]	12.957	1.120	1.031
	12.839	1.1232	1.0329
α_1 [b]	0.385	0.0497	0.0555
	0.347	0.0016	0.0032
α_2 [c]	0.155	0.0091	0.0074
	0.139	0.0088	0.0073
α_3 [c]	-0.961	-0.0015	0.0032
	-0.808	-0.0015	0.0036
α_5 [d]	0.303	0.0004	0.0022
	0.304	0.0013	0.0031

Constants in units of cm^{-1}. Constants related to ν_4 and ν_6 are omitted because of the strong Coriolis effects that distort the rotational structure. [38, 41]

[a]Ref. [73].

[b]Ref. [42]. The values listed here are from the deperturbation of the $1^1/2^1B^2$ interaction, and the values of B and C are presumably correlated with other fit parameters.

[c]Ref. [35].

[d]Ref. [39].

characterized. There are a few distinct failures of the *ab initio* VPT2 forcefields that we now discuss. In particular, the *trans* ν_4 fundamental is an illustrative example.

Compared to the good agreement for the other *trans* vibrational fundamentals (3–15 cm^{-1}), the 35 cm^{-1} error in *trans* ν_4 is unusually large. The possible sources of error are the execution of the VPT2 calculation, the quantum chemistry methods used to evaluate the force constants, and the rectilinear internal coordinates implicit in this approach.

We validate the execution of the VPT2 calculation by performing the same calculation on *trans* N_2H_2, where the $\tilde{X}$ state is electronically analogous to the $\tilde{A}$ ^1A_u state of C_2H_2. The agreement with earlier calculations and experiment is excellent (Table 5.8); the largest error is -7.5 cm^{-1} for ν_6. It is interesting to note that the pattern of the deviations from experiment is similar to that for *trans*-S_1 C_2H_2, with the lower frequency bends giving less good agreement.

The next possibility is that the quantum chemical method used fails along the torsional coordinate. We rule out this possibility by performing a 1D torsional DVR

Table 5.8: Vibrational Fundamentals for *trans* $\tilde{X}$ N_2H_2

	This work	Martin *et al.*	Expt.	Error
ν_1	3116.6	3051.0	$(3128)^a$	
ν_2	1579.2	1578.5	1583	3.8
ν_3	1523.2	1528.2	1529	5.8
ν_4	1294.8	1294.2	1288.65	-6.2
ν_5	3119.6	3133.3	3120.29	0.7
ν_6	1323.9	1317.4	1316.41	-7.5

Frequencies in cm^{-1}. The second and third columns are from Ref. [96] and references therein.
[a]Although it is beyond the scope of this paper, the ν_1 assignment is not secure, and additionally the upper level is likely in Fermi resonance with several combination/overtone levels. See again Ref. [96] and references therein, particularly Refs. [9] and [11].

calculation, and find the *trans* ν_4 fundamental to be 780.7 cm^{-1}, which is a deviation from experiment in line with those for the other vibrational modes. (The *cis* ν_4 fundamental found by this method is 845.8 cm^{-1}, to be compared with 827.92 cm^{-1} from VPT2.) We also find that fitting the 1D potential gives an *ab initio* torsional force constant that agrees to 1% with the harmonic force field of Ref. [72].

We are finally left with the conclusion that the rectilinear coordinates used in VPT2 are the primary cause of the poor agreement obtained for the *trans* ν_4 fundamental. This is consistent with all of the evidence: the problems observed in treating ν_4 and ν_6 of both S_1 C_2H_2 conformers, the improved agreement for 1D *curvilinear* DVR calculations using the same quantum chemistry methods, and a qualitatively similar pattern of errors in *trans* N_2H_2, albeit of smaller magnitude because the motions are smaller in amplitude. A well known signature of rectilinear coordinates is that they overestimate the coupling between torsions and stretches; several of the fitted/experimental values of the *trans* x_{i4} are significantly less negative than the corresponding VPT2 result (Table 5.6).

It is surprising that the rectilinear coordinates appear to pose a comparable or even more serious problem for perturbation theory than the extremely large amplitude motions necessary for isomerization. In other words, the torsional modes of both conformers are treated less well by VPT2 than the $\{\nu_3, \nu_6\}$ modes involved in the lower energy, planar *cis-trans* isomerization path. This is despite the fact that the same

ab initio level of theory gave reasonable results when used in curvilinear but reduced dimension DVR calculations of the type described in this work and in Ref. [10]. It would be interesting to perform a full dimensional curvilinear treatment to assess the consequences of the conventional rectilinear coordinates more completely.

5.5 Conclusion

We have attempted to show here that perturbation theory-based anharmonic force fields can provide useful guidance in analyzing the spectra of systems exhibiting large amplitude motion, using as an example the *cis-trans* isomerization in the S_1 state of C_2H_2. In an accompanying paper [88], the results presented here have already been used to further the analysis of *trans* levels at the frontier of the current assignments, and additionally to aid in the location and assignment of levels belonging to the recently observed *cis* conformer. As the approach to the transition state continues to complicate the spectra, accurate predictions of the level positions of both conformers will be increasingly important.

A number of experiments are in progress to resolve the open questions about the level structures of both S_1 conformers, in addition to continuing higher toward the expected transition state energy. Although much of the *ab initio* error seems to stem from the rectilinear coordinates implicit in the VPT2 approach, we are undertaking calculations of greater sophistication in order to predict the *cis* vibrational parameters as accurately as possible. We are also pursuing theoretical curvilinear treatments that will improve upon this work and that of Ref. [10].

Finally, we alluded earlier to fits of the *trans* $J{=}K{=}0$ level structure. We have achieved some preliminary success in fitting the $J{=}K{=}0$ levels beyond 3000 cm^{-1}, and indeed up to the limit of the current assignments; the additional parameters in such a model and their relationship to the transition state energy will be discussed in a future paper.

Acknowledgments

This work was supported at MIT by DOE Grant No. DE-FG0287ER13671. AJM thanks Academia Sinica, Taiwan, for financial support and the University of British Columbia for some travel funding. JFS also wishes to acknowledge support from the US National Science Foundation (Grant CHE - 1012743).

5.A J=K=0 Level List for *trans*-S_1 C_2H_2

Table 5.9: *trans* J=K=0 Level List

State	T_0	$T_0 - T_{00}$	σ	Ref.
0^0	42197.57	0.00	0.01	[35]
4^1	42962.47	764.90	0.06	[38]
6^1	42965.83	768.26	0.09	[38]
3^1	43245.12	1047.55	0.01	[35]
2^1	43584.47	1386.90	0.01	[35]
B^2 (I) a_g	43700.85	1503.28	0.01	[41]
$4^1 6^1$	43732.13	1544.56	0.1	[41]
B^2 (III) a_g	43752.57	1555.00	0.01	[41]
$3^1 6^1$	43983.1	1785.53	0.5	[46]
$3^1 4^1$	43996.89	1799.32	0.5	[46]
3^2	44275.28	2077.71	0.01	[35]
$2^1 4^1$	44336.46	2138.89	0.02	[43]
$2^1 6^1$	44345.9	2148.33	0.02	[43]
B^3 (I) b_u	44449.15	2251.58	0.03	[41]
B^3 (II) a_u	44457.26	2259.69	0.03	[41]
B^3 (III) b_u	44547.04	2349.47	0.03	[41]

Table 5.9 – continued

State	T_0	$T_0 - T_{00}$	σ	Ref.
B^3 (IV) b_u	44547.77	2350.20	0.03	[41]
$2^1 3^1$	44631.78	2434.21	0.01	[35]
$3^1 B^2$ (I) a_g	44692.84	2495.27	0.03	[43]
$3^1 4^1 6^1$	44749.61	2552.04	0.3	[43]
$3^1 B^2$ (III) a_g	44764.96	2567.39	0.03	[43]
2^2	44948.68	2751.11	0.01	[42]
$3^2 6^1$	44976.33	2778.76	0.08	[46]
$3^2 4^1$	45015.64	2818.07	0.1	[46]
5^1	45054.97	2857.40	0.1	[39]
$2^1 B^2$ (I) a_g	45067.23	2869.66	0.02	[42], [43]
1^1	45077.67	2880.10	0.02	[42]
$2^1 4^1 6^1$	45108.33	2910.76	0.23	[42], [43]
$2^1 B^2$ (III) a_g	45119.83	2922.26	0.02	[42], [43]
B^4 (I) a_g	45172.55	2974.98	0.1	[41]
B^4 (II) b_g	45206.9	3009.33	5.0	[41]
B^4 (III) a_g	45239.8	3042.23	5.0	[41]
3^3	45285.71	3088.14	0.02	[35]
B^4 (IV) b_g	45361.6	3164.03	5.0	[41]
$2^1 3^1 6^1$	45362.99	3165.42	0.05	[43]
B^4 (V) a_g	45363.2	3165.63	5.0	[41]
$2^1 3^1 4^1$	45369.48	3171.91	0.05	[43]
$3^1 B^3$ (I) b_u	45397.81	3200.24	0.05	[43]
$3^1 B^3$ (II) a_u	45444.27	3246.70	0.05	[43]
$3^1 B^3$ (III) b_u	45538.5	3340.93	0.05	[43]

Table 5.9 – continued

State	T_0	$T_0 - T_{00}$	σ	Ref.
3^1B^3 (IV) a_u	45545.87	3348.30	0.05	[43]
3^2B^2 (I) a_g	45644.14	3446.57	0.02	[43]
$2^1 3^2$	45662.69	3465.12	0.01	[35]
$2^2 4^1$	45687	3489.43	5.0	[43]
$2^2 6^1$	45702.85	3505.28	0.05	[43]
$3^2 4^1 6^1$	45736.07	3538.50	0.24	[43]
3^2B^2 (III) a_g	45766.67	3569.10	0.02	[43]
$4^1 5^1$	45804	3606.43	10.0	[43]
2^1B^3 (I) a_u	45810.66	3613.09	0.02	[88]
2^1B^3 (II) b_u	45810.86	3613.29	0.04	[88]
$5^1 6^1$	45814	3616.43	5.0	[43]
$1^1 4^1$	45825.88	3628.31	0.05	[88]
$1^1 6^1$	45834.26	3636.69	0.03	[88]
B^5 (I) b_u	45890.08	3692.51	0.02	[88]
2^1B^3 (III) a_u	45902.93	3705.36	0.01	[88]
2^1B^3 (IV) b_u	45906.07	3708.50	0.02	[88]
B^5 (II) a_u	45919.28	3721.71	0.05	[88]
$3^3 6^1$	45937.76	3740.19	0.01	[46], [88]
$2^2 3^1$	45995.65	3798.08	0.01	[40]
B^5 (III) b_u	46007.58	3810.01	1.0	[88]
$3^3 4^1$	46016.36	3818.79	0.03	[46], [88]
B^5 (IV) a_u	46022.34	3824.77	0.01	[88]
$2^1 3^1 B^2$ (I) a_g	46058.69	3861.12	0.01	[43]
3^1B^4 (I) a_g	46075.38	3877.81	0.02	[43]

Table 5.9 – continued

State	T_0	$T_0 - T_{00}$	σ	Ref.
$3^1 5^1$	46091.75	3894.18	0.03	[39], [88]
$1^1 3^1$	46114.65	3917.08	0.02	[40]
$2^1 3^1 4^1 6^1$	46116	3918.43	7.0	[43]
$2^1 3^1 B^2$ (III) a_g	46129.50	3931.93	0.06	[43]
$3^1 B^4$ (II) b_g	46153.3	3955.73	0.1	[43]
B^5 (V) b_u	46190.69	3993.12	0.01	[41], [88]
B^5 (VI) a_u	46191.01	3993.44	0.01	[41], [88]
$3^1 B^4$ (III) a_g	46209.7	4012.13	0.02	[43]
3^4	46270.52	4072.95	0.02	[36]
$3^2 B^3$ (I) b_u	46287.045	4089.475	0.02	[88]
2^3	46290.94	4093.37	0.05	[42]
$3^1 B^4$ (IV) b_g	46343	4145.43	7.0	[43]
$3^1 B^4$ (V) a_g	46347	4149.43	7.0	[43]
$2^1 3^2 6^1$	46359.31	4161.74	1.0	[88]
$2^1 3^2 4^1$	46386.95	4189.38	0.04	[88]
$3^2 B^3$ (II) a_u	46397.83	4200.26	0.04	[88]
$2^2 B^2$ (I) a_g	46412	4214.43	5.0	[42], [43]
$2^1 5^1$	46440.89	4243.32	0.02	[88]
$2^2 4^1 6^1$	46453	4255.43	10.0	[42], [43]
$1^1 2^1$	46460.58	4263.01	0.01	[42], [43]
$2^2 B^2$ (III) a_g	46467.84	4270.27	0.01	[42], [43]
$3^2 B^3$ (III) b_u	46510.97	4313.40	0.03	[88]
$3^2 B^3$ (IV) a_u	46531.11	4333.54	0.03	[88]

Table 5.9 – continued

State	T_0	$T_0 - T_{00}$	σ	Ref.

All quantities are given in cm^{-1}. Vibrational states in bending polyads are labelled with B^n notation, where $n = v_4 + v_6$, when Darling-Dennison resonance has mixed the zero-order states. Roman numerals indicate ascending energy order within a polyad, regardless of vibrational symmetry, which is also listed. The σ values tabulated here reflect r.m.s. error in rotational fits or measurement uncertainty. We have estimated uncertainties when such values are unavailable or unreliable, and also when the term value given here has been calculated based on other data. It should be mentioned that $J{=}K{=}0$ data exists for additional levels above 4300 cm^{-1}, both unpublished and in the literature, for example in Ref. [37].

Chapter 6

Spectroscopic Characterization of Transition States

Abstract

We demonstrate a method for extracting saddle point energies from a novel pattern found in frequency domain spectra of isomerizing systems. This new pattern, a dip in the vibrational level spacings, is explained based on analysis using the concept of effective frequency, ω^{eff}. Crucially, the desired information is encoded in a subset of special barrier-proximal vibrational states. The method is applied to *cis-trans* isomerization in the S_1 state of C_2H_2, and the results are in good agreement with previous *ab initio* calculations. We show that it is possible to distinguish between modes that actively involved in the isomerization process and those which are passive bystanders. Extensions of the method to differentiate between isomerization pathways and obtain additional information about the saddle point are also discussed.

The work described in this chapter was performed with P. B. Changala, and also owes much to collaborations with Profs. A. J. Merer and J. F. Stanton. In particular, P. B. Changala developed the semiclassical frequency toolkit that led to the empirical ω^{eff} fitting formula and its interpretation. [97]

6.1 Introduction

The central concept of the transition state in kinetics is familiar and intuitive to every student of chemistry. Since its inception by Arrhenius [98] and later develop-

ment into a full theory by Eyring, Polanyi, and Evans [99–101], the idea that the rate depends primarily on the highest point along the lowest energy path from reactants to products has persisted essentially unchanged. This is due at least in part to the paucity of experimental observations of activated complexes, as compared with stable molecules. A few notable exceptions are state-resolved kinetics measurements [102], and "transition state spectroscopy", which includes ultrafast and negative ion photoelectron spectroscopies [103]. Even these techniques, however, cannot provide the detailed characterization attainable by high resolution frequency domain spectroscopy. In order to extend frequency domain spectroscopy to chemically relevant regions of the potential surface, it is necessary to discover new paradigms to supersede the traditional models used for low energy spectra, which are no longer adequate. Our purpose here is to report the observation of a novel vibrational pattern, a dip in the trend of quantum level spacings, which occurs at the energy of the saddle point. This phenomenon is expected to be quite general, leading to a new, high quality method for revealing the characteristics of transition states. Experimental evidence for this concept is drawn from our study of a prototypical system, *cis-trans* isomerization in the first electronically excited singlet state of acetylene.

6.2 Effective Frequency and the Isomerization Dip

We must first define *effective frequency*, ω^{eff}, the central quantity in our proposed model for the spectra of isomerizing systems. In a one-dimensional system, the effective frequency is the derivative of the energy with respect to the quantum number n

$$\omega^{\text{eff}}(n) = \frac{\partial E}{\partial n} = \frac{\Delta E}{\Delta n} \tag{6.1}$$

where ω^{eff} is evaluated discretely for the case of a quantized system. Unlike more familiar frequencies (harmonic ω, or fundamental ν) found as molecular constants, ω^{eff} is a dynamic quantity that can change with increasing excitation. As such, it is a very useful diagnostic of the qualitative behavior of the system.

Consider the series of cases illustrated in Fig. 6-1. For the harmonic oscillator,

$$\omega^{\text{eff}} = \frac{\partial}{\partial n}[\omega(n + \frac{1}{2})] = \omega, \tag{6.2}$$

and

$$\frac{\partial \omega^{\text{eff}}}{\partial n} = 0, \tag{6.3}$$

indicating that the dynamics of the system never change as a function of energy.

For a Morse oscillator, where the potential is $V(r) = D[1 - e^r]^2$,

$$\omega^{\text{eff}} = \frac{\partial}{\partial n}[\omega(n + \frac{1}{2}) + x(n + \frac{1}{2})^2] = \omega + x + 2nx, \tag{6.4}$$

and

$$\frac{\partial \omega^{\text{eff}}}{\partial n} = 2x. \tag{6.5}$$

This linear change of ω^{eff} with n (always a decrease for the Morse oscillator), reflects the outward migration of the Morse wavefunctions towards the softer outer turning point, compared to the harmonic oscillator. This trend terminates at the dissociation limit, which illustrates the profoundly different dynamics available to the Morse and harmonic oscillators.

Analytic expressions for ω^{eff} and $\frac{\partial \omega^{\text{eff}}}{\partial n}$ cannot be derived for the other cases in Fig. 6-1, but they illustrate the most important feature even more clearly: the effective frequency goes to zero whenever the energy of a stationary point on the potential is reached. This can be understood simply by imagining releasing a ball to roll on a double minimum potential surface, but changing the initial height of release. At most heights, as with a harmonic oscillator, the ball will roll down and subsequently return to the initial release point at a certain frequency. But, when the ball is released at exactly the height of a local maximum, the ball will reach that stationary point with zero kinetic energy and stop. Because the ball never returns, the period is infinite and the frequency therefore is zero.[1] We can immediately see that this applies to

[1]As illustrated in Fig. 6-1, the quantum level spacings follow the classical ω^{eff} curve closely, except for slight deviations near the stationary point. See Refs. [104, 105], and also the discussion about K-staggerings below.

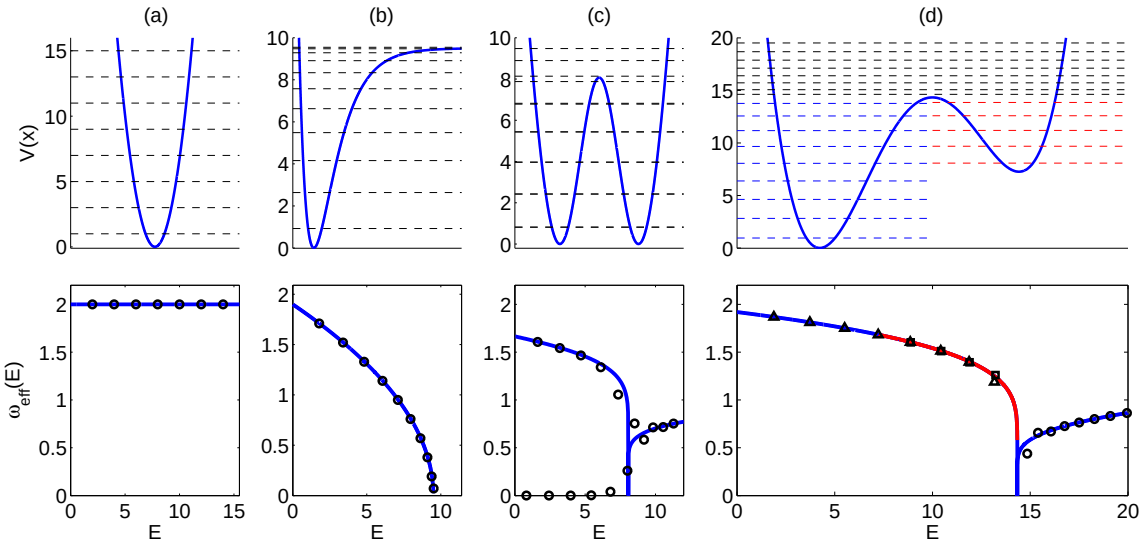

Figure 6-1: Effective frequency plots (bottom row) for a series of model potentials (top row). From left: a) harmonic oscillator, b) Morse oscillator, c) symmetric double minimum potential, and d) asymmetric double minimum potential. In the top panels, the quantum energy levels are marked with dashed lines. In the bottom row, the classical ω^{eff} is shown as a solid line, with the quantum level spacings plotted vs. $\overline{E}$ as open circles. In (c), the upper and lower series of circles correspond to the vibrational level spacings and tunneling splittings, respectively. In (d), the ω^{eff} curve and energy levels for the second minimum are shown in red, and the quantum level spacings are overlaid on the ω^{eff} curve as triangles and squares.

the Morse oscillator as well - ω^{eff} reaches zero at the dissociation limit, which is a horizontal asymptote. In fact, the simple physical insight behind this phenomenon suggests that it should be quite general, e.g. zeros or abrupt changes in ω^{eff} signal important changes in the dynamics of the system. For our purposes it suffices that this behavior provides a marker of the chemically relevant transition state energy, as we demonstrate with experimental data in the next section.

It remains to discuss how best to extract the desired saddle point energy from spectroscopically measured quantities. From the spectrum we measure the term energies of a series of quantized vibrational levels, and take the average $\overline{E}$ and difference ω^{eff} of adjacent level energies to obtain a set of $(\overline{E}, \omega^{\text{eff}})$ data points.[2] A plot of this data reveals directly any trend in ω^{eff}, either constant, linear, or nonlinear. If a stationary point is present within the data range of $\overline{E}$, the plot will dip to a minimum as the energy of the stationary point is approached, but in a bound system there will never be a point with $\omega^{\text{eff}} = 0$. There may be a low density of points due to the quantized nature of the system, and if so the energy of the saddle point may only be approximately determined from a plot of the experimental $(\overline{E}, \omega^{\text{eff}})$ data.

In order to address this sampling rate issue, we propose the following semi-empirical formula for ω^{eff} as a function of $\overline{E}$:

$$\omega^{\text{eff}}(\overline{E}) = \omega_0 \left(1 - \frac{\overline{E}}{E_{TS}}\right)^{1/m} \tag{6.6}$$

where ω_0 is an effective zero-energy frequency for the progression being analyzed, E_{TS} is the energy of the transition state, and m is an empirical barrier shape parameter. For the simplest possible example, a Morse oscillator, $m = 2$ analytically [104], $E_{TS} = D$, the dissociation energy, and $\omega_0 = \omega + x$, the fundamental frequency. Eq. 6.6 can be regarded as a generalization of the Morse formula by simply allowing m to take values other than 2. The formula also exhibits the required physical behavior of a limiting frequency ω_0 at low energy and $\omega^{\text{eff}} = 0$ at $\overline{E} = E_{TS}$.

[2] A word about ω^{eff} vs. $\overline{E}$ as opposed to vs. n: using n simplifies derivations, but $\overline{E}$ is more practical for actual use.

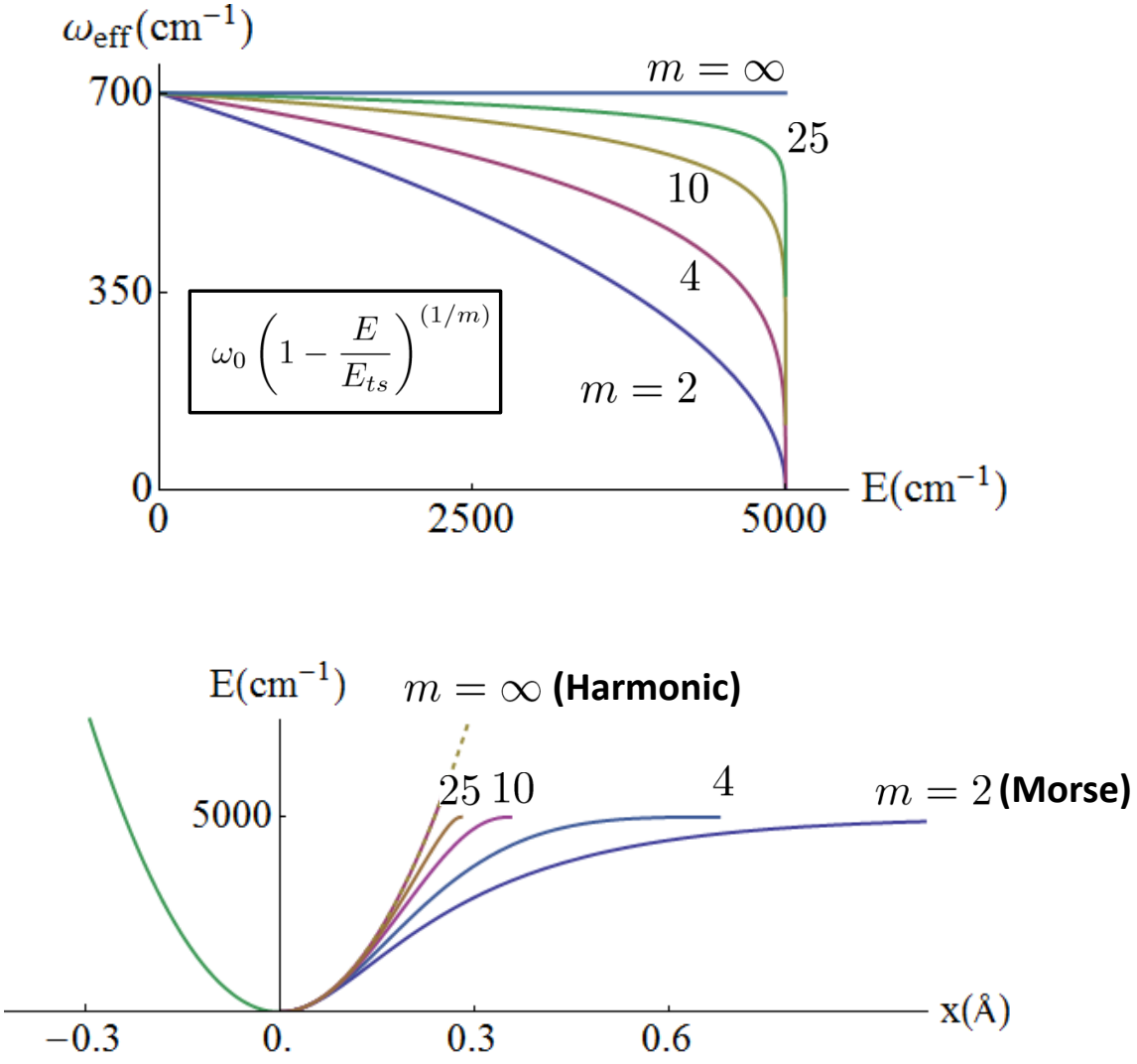

Figure 6-2: Effective frequency curves and the corresponding inverted potentials as a function of the shape parameter m. [97]

The dependence of the m parameter on potential shape is illustrated in Fig. 6-2 [97]. One limit is $m = 2$, the Morse oscillator, where the local maximum is approached infinitesimally with x. The other limit is an abrupt discontinuity in the potential at the local maximum, so that ω^{eff} instantly drops to zero, and in such a case $m = \infty$.

A final important point is that the physical arguments presented here regarding the behavior of ω^{eff} vs. $\overline{E}$ (and therefore Eq. 6.6) pertain *only* up to $\overline{E} = E_{TS}$. Above that energy ω^{eff} can either remain at zero for an unbound system (as with the Morse oscillator), or rise again (in a bound system). The above-barrier behavior of ω^{eff} depends on the outer walls of the potential, and is not predicted by Eq. 6.6. As pointed out to us by Prof. N. Moiseyev, the mth root form of Eq. 6.6 suggests the presence of a "branch point" at E_{TS}, which separates the above-barrier and below-barrier eigenspectra into two distinct sets [106].

6.2.1 Background

The spectroscopic importance of effective frequency has been recognized for a long time. Birge and Sponer first applied it to estimating the dissociation energies of diatomic molecules [107], using the relation $D_0 = \int_{n=0}^{n_D} \omega^{\text{eff}} \mathrm{d}n$ to create the well-known Birge-Sponer plot of ΔG_n vs. n. This idea was subsequently refined by LeRoy and Bernstein to take into account the required long-range shape of the potential near the outer turning point, which gave very accurate D_0 values by dealing effectively with non-linearities in ω^{eff} at high n [108].

Another class of spectroscopic problems where ω^{eff} has been employed is quasi-linear molecules. Dixon [109] performed a numerical calculation for a cylindrically symmetric potential comprised of a harmonic oscillator with a Gaussian bump in the center. The solutions to such a Hamiltonian can be assigned vibrational (v) and rotational (K) quantum numbers, despite the fact that the molecule begins bent and eventually straightens (hence "quasilinear").[3] When the eigenvalues were arranged

[3]Due to the cylindrical symmetry of the system, the K rotational quantum number of the bent molecule can also be thought of as ℓ, the vibrational angular momentum of the linear molecule. Here we follow the notation used by Dixon for consistency with the literature.

in a Birge-Sponer type plot $\left(\Delta G(v,K) \text{ vs. } \frac{1}{2}\{G(v,K)+G(v+1,K)\}\right)$, each K series exhibited a distinct dip at the height of the central local maximum in the potential. Interestingly, the depth of the "Dixon dip" decreases with increasing K, because angular momentum forces the wavefunctions to avoid the center of the potential where the maximum is located.

An example even more closely related to the subject at hand is that of bond-breaking internal rotation in HCP [110]. A beautiful paper on quantum and semiclassical analysis of highly excited states of HCP by Jacobson and Child [111] mentions a dip in ω^{eff} as the signature of an approach to a saddle point. Since the HCP↔HPC potential energy surface exhibits some very unusual features, and cannot strictly be termed an isomerization [110], the observed ω^{eff} trend was categorized as a peculiar example of a "Dixon dip", rather than recognized as the more universal phenomenon proposed here for isomerizing systems.

More generally, the behavior of systems as they encounter stationary points has been investigated from other perspectives as well. The topics of quantum monodromy [112] and excited state quantum phase transitions [113] have been studied in molecular systems, with a focus on the topology of the potential or phase change properties of the system Hamiltonian. The concept of a "branch point" from non-Hermitian quantum mechanics, mentioned above, is also related. Similar dip patterns have been observed in model Hamiltonian calculations of acetylene-vinylidene isomerization [114], where they are understood in terms of a classical separatrix in phase space.

6.3 The Example of S_1 C_2H_2

Our test case for the experimental demonstration of the isomerization dip is that of the *cis-trans* isomerization in the first electronically excited singlet state of acetylene. Since extensive background on this system has already been given earlier in this thesis, only the salient points will be summarized here. The S_1 state supports *cis* and *trans* conformers, with the *cis* conformer lying approximately 2675 cm^{-1} above the *trans*. The lowest transition state is planar and almost exactly half-linear [26]. The bare

saddle point energy is calculated to be around 5000 cm^{-1} above the *trans* minimum, but with an uncertainty of hundreds of cm^{-1}, even for the most accurate calculations to date [10]. It is worth mentioning that a torsional isomerization path might be assumed on the basis of *cis-trans* isomerizations in other molecules, although this does not appear to be the case here.

The height of the barrier compared to the fundamental frequencies leads us to expect at least some "normal" vibrational structure, even in the shallower *cis* well. Thus far, several *cis* vibrational levels have been identified, in reasonable agreement with the predictions of *ab initio* vibrational perturbation theory calculations [11, 53, 88]. In the *trans* well, over 100 vibrational levels below the barrier have been observed and assigned [53]. Of the six *trans* conformer normal vibrational modes, four are fairly well-behaved: the Franck-Condon active vibrations ν_2, the CC stretch, and ν_3, the *trans* bend, [35], and the CH stretching modes ν_1 and ν_5 [39, 42]. On the other hand, a large portion of the *trans* vibrational manifold can only be understood within the framework of bending polyads $B^{n=v_4+v_6}$ [41], due to the Darling-Dennison and Coriolis interactions between the low frequency *ungerade* bending modes ν_4 and ν_6. These effects are surprisingly large, perhaps due to their origin as a vibrational angular momentum in the ν_5 vibration of the linear form of acetylene, and lead to very complicated rovibrational structures, either in isolated polyads or especially when overlapping polyads interact with one another [42, 43, 88].

Despite the success of the polyad model in reproducing the level structures associated with the bending vibrations, there are disturbing exceptions. As illustrated elegantly in Fig. 13 of Ref. [43], the series of 3^nB^2 polyads exhibits a curious trend, with the energy of the lowest member of the polyad decreasing rapidly relative to the energies of the other polyad members. (Similar data is presented in Fig. 3-4.) This unexpected behavior is associated with an increase in the Darling-Dennison constant K_{4466} and an unusually large anharmonicity between ν_3 and ν_6, among other anomalies [43]. The breakdown of the polyad model forces each polyad to be modeled on an *ad hoc* basis, and more fundamentally calls into question our representation of the vibrational dynamics of S_1 *trans* acetylene.

Similar issues confound any attempt to model the *trans* vibrational manifold globally. Our initial efforts along these lines were mentioned briefly in Ch. 5. There it was possible to use a conventional $\mathbf{H}^{\text{eff}}$ to fit the *trans* J=K=0 term values globally up to 3000 cm^{-1}, with residuals of a few cm^{-1}, which sufficed for the determination of the anharmonic constants. As above, the limiting factor in fitting the energy levels was the 3^nB^2 polyads, since once the 3^26^2 level falls by an extra 100 cm^{-1} and crosses below the 2^13^2 level, the model is unable to cope. It is worth noting that the number of levels included in the successful fit to the low energy vibrational manifold just barely exceeded the number of parameters in the model, which consisted of the harmonic frequencies ω_i, the anharmonicities x_{ij}, and the Darling-Dennison constant K_{4466}. Furthermore, attempts to supplement the model in more traditional ways, e.g. by adding Fermi, Darling-Dennison and/or even higher-order resonances between ν_3 and ν_6, were ultimately unsuccessful.

6.3.1 Guiding Fit Models using $\boldsymbol{\omega}^{\text{eff}}$

The concept of ω^{eff} can be applied directly to the problems encountered modeling the *trans* vibrational level structure. Examining Fig. 3-4, we can see that both

$$\frac{\partial\omega^{\text{eff}}}{\partial v_3} \neq 0 \text{ and } \frac{\partial\omega^{\text{eff}}}{\partial v_6} \neq 0 \tag{6.7}$$

must be true. Using a Dunham-style expansion for the vibrational term values

$$\begin{aligned} E(\{v_i\}) = &\sum_i^{3N-6} \omega_i(v_i+1/2) + \sum_i^{j}\sum_j^{3N-6} x_{ij}(v_i+1/2)(v_j+1/2) \\ &+ \sum_i^{j}\sum_j^{k}\sum_k^{3N-6} y_{ijk}(v_i+1/2)(v_j+1/2)(v_k+1/2) \\ &+ \sum_i^{j}\sum_j^{k}\sum_k^{l}\sum_l^{3N-6} z_{ijkl}(v_i+1/2)(v_j+1/2)(v_k+1/2)(v_l+1/2) \end{aligned} \tag{6.8}$$

and taking second derivatives with respect to v_3 and v_6, we find that the lowest order terms that satisfy the dual requirements of Eq. 6.7 are those with the parameters

z_{3366} or the pair $\{y_{366}, y_{336}\}$.

Adding a z_{3366} parameter to the $\{\omega_i, x_{ij}, K_{4466}\}$ model immediately allows the J=K=0 level structure to be fit up to the limit of the current assignments, as listed in Ref. [53]. The inclusion of y_{346} also substantially reduces the residuals, but is not essential. (As explained in Ref. [53], the importance of the y_{346} term can be understood by considering the Coriolis contribution to x_{46} that depends on the A rotational constant, which in turn increases rapidly with v_3, because of the straightening nature of that vibration.) Specifically, $z_{3366} = -1.05$ and $y_{346} = 4.45$ cm^{-1}, and the residuals are 10 cm^{-1} or less in a fit to the 90 levels up to 4400 cm^{-1}. Typically, the levels with the largest residuals are those not observed directly experimentally, and their predicted J=K=0 term values from rotational fits are consequently de-weighted in the input to the vibrational fit. The addition of the z_{3366} and y_{346} parameters does not lead to any significant changes in the other model parameters, except that $x_{46} = 7.93$ instead of 11.39 cm^{-1}, because of the presence of y_{346}. We should also note here that no other parameters, such as Fermi resonances, are included in the model, even though some are known to be significant [42, 43, 88].

The striking success of the supplemental z_{3366} is encouraging for a few additional reasons. First, it unifies the entire *trans* vibrational manifold in one compact model for the first time in decades of study. Second, it is particularly parametrically parsimonious - the addition of a single parameter more than triples the number of levels that can be fit satisfactorily, in contrast to the low number of degrees of freedom in the fit to the conventional model at low energies. Third, the important K_{4466} parameter remains at its nominal value (as determined by fits to low energy pure bending polyads [41], and in good agreement with *ab initio* calculations [53]), despite the observed increase when rotationally fitting the series of $3^n B^2$ polyads individually [43]. Finally, the success of the z_{3366} $\mathbf{H}^{\text{eff}}$ suggests that ω^{eff} is a good guide to furthering our understanding of this system - which is good news, because the z_{3366} model suffers from fatal flaws.

As with its conventional $\mathbf{H}^{\text{eff}}$ predecessor, the z_{3366} model is incapable of reproducing the level structure up to the saddle point energy. We find this to be true

empirically, as will be described momentarily, but as discussed cogently in Ref. [111], polynomial $\mathbf{H}^{\text{eff}}$ models are intrinsically problematic. The higher order terms are unstable, both for fitting and extrapolation purposes. This argues strongly against simply adding additional, similarly motivated parameters, despite the success of the z_{3366} term. In our case, the addition of z_{3366} moves the goalposts slightly more than half the energy distance to the expected transition state energy. Once again, the primary failure is that the energies of the anomalous 3^n6^2 levels are not predicted accurately, even though many other isoenergetic levels fit satisfactorily. A secondary problem arises because of a new type of rotational perturbation that appears at the onset of isomerization. These K-staggerings, distortions of the rotational structure similar to tunneling splittings, are discussed in Ch. 2.6 and in Ref. [48]. As far as the $J{=}K{=}0$ fitting is concerned, the K-staggerings introduce apparently random shifts into the state energies, which become extremely problematic when they become large enough to reorder vibrational levels, for example. In principle it is possible to deperturb the experimentally observed $J{=}K{=}0$ values, but this requires the observation of more K values.

6.3.2 Considering a Subset of Barrier-Proximal States

At this juncture we refocus our attention on the troublesome series of 3^n6^2 levels. Aside from their prominence as the weakest links in the attempts at $\mathbf{H}^{\text{eff}}$ modeling, in the following we present several reasons why they deserve special consideration.

6.3.2.1 Energetic Considerations

As mentioned earlier, the 3^n6^2 levels do not fit well in normal or even extended $\mathbf{H}^{\text{eff}}$ models, deviating increasingly from their predicted positions along the series. This fact alone suggests that they belong to a special class of levels that may be identified with unusual behavior. The idea of local mode behavior is closely related, wherein certain states in polyads with a distinctive energy level pattern exhibit qualitatively new dynamics. Two well-known examples are stretching overtones in water [115],

where quanta in the symmetric and asymmetric stretching normal modes combine to form states with local bond stretching (and eventually breaking) character, and the pure bending polyads in S_0 acetylene, where the bending normal modes evolve into "local benders" en route to isomerization to vinylidene [6, 7]. In those examples, as in our case, the states at the bottom of the polyads fall lower in energy, and become isolated. Here, however, our special class of states represents a fundamentally different phenomenon. The bifurcation in *trans* S_1 C_2H_2 is not a result of the polyad-forming interaction, but rather caused by a separate effect, which might even be termed "polyad-breaking". The unequivocal evidence for this distinction is that we observe the emergence of the special states *not* as a function of the polyad quantum number, and also because of the apparent change in the size of the K_{4466} matrix element from polyad to polyad in the rotational fits.

6.3.2.2 Wavefunctions

A second clue that the 3^n6^2 levels are special can be found by inspecting their wavefunctions. In Fig. 6-3, *ab initio* wavefunctions from the calculations of Ref. [10] are shown for an array of $\{v_3, v_6\}$ states. Most of the functions have the expected appearance of two-dimensional harmonic oscillator wavefunctions, with only mild perturbations. Levels with increasing quanta in both ν_3 and ν_6, and especially the 3^n6^2 series shown in the bottom row, however, are delocalized across the *trans* and *cis* minima on the potential surface (Fig. 3-1). This begs the question: what is the connection, if any, between the anomalous energy pattern of the 3^n6^2 levels and their delocalized wavefunctions? The answer, of course, is that the 3^n6^2 states are participants in an isomerization dip; they are barrier-proximal, meaning that their wavefunctions have considerable amplitude directed toward the transition state, and that their energies feel the effect of the strongly anharmonic minimum energy isomerization path.

An important point to emphasize is that there is clear precedent for variation in the strength of the dip between different progressions of states. In Dixon's original paper [109], as mentioned above, series of levels with K or $\ell = 0$ dipped most strongly, because the states with $K > 0$ avoid the potential maximum at linearity. Just as

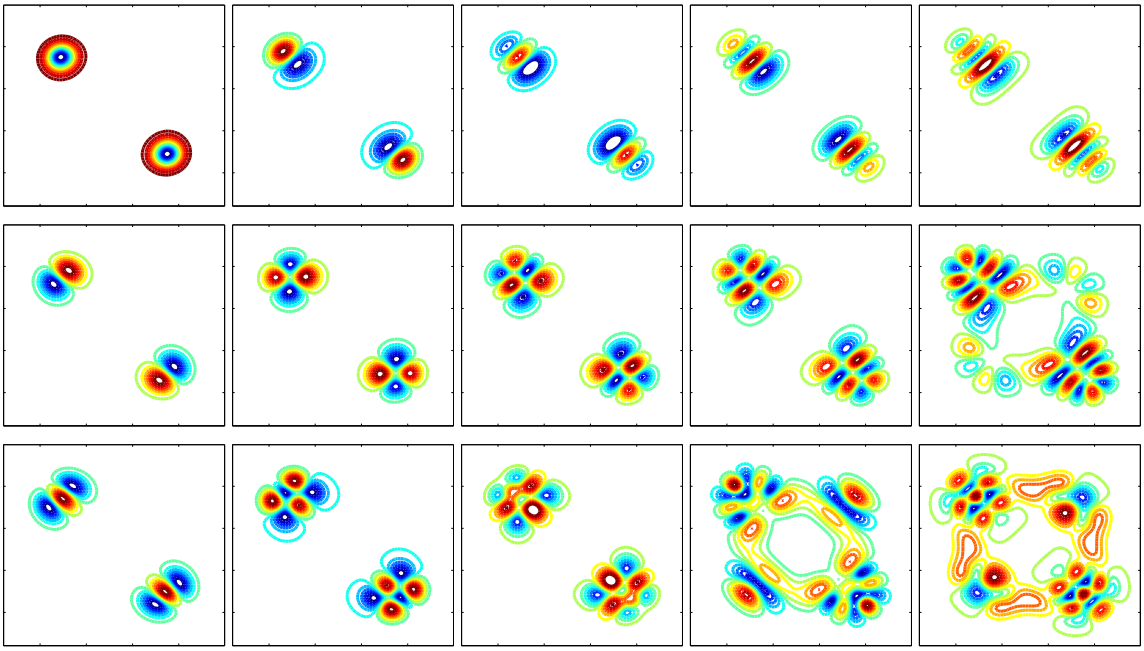

Figure 6-3: An array of *trans* wavefunctions from the calculations in Ref. [10], plotted in the usual two-dimensional ∠CCH plane. The ground state is shown in the upper left, with v_3 increasing to the right, and v_6 increasing in each row. Note the delocalization and nodal pattern distortion that correlates with combined $\{v_3, v_6\}$ excitation.

the $K = 0$ states in the quasilinear case are singularly effective at accessing the stationary point on the PES because of the angular momentum, so too in our case the set of barrier proximal 3^n6^2 levels are the most effective at reaching toward the isomerization transition state. (See Fig. 6-5 below.) In both cases this access to the stationary point is reflected by the sharpest dip as a function of energy for that specific set of levels. We will return to this important topic in the context of the general multidimensional asymmetric double minimum situation.

6.3.3 Determination of the Barrier Height

In this section we show how the isomerization dip idea, and in particular Eq. 6.6, can be applied to the special barrier proximal energy levels discussed in the previous section. Fig. 6-4 shows plots of ω_3^{eff} and ω_6^{eff} for the 3^n6^2 series, where Eq. 6.6 can be seen to fit the observed data very well. It is interesting to note that a plot of ω^{eff} for a one dimensional *ab initio* minimum energy isomerization path potential, similar to Fig. 6-1d, would lie about halfway in between the two experimental ω^{eff} trends; this is because such an *ab initio* calculation uses (approximately) a local bending coordinate, and the two normal modes of the molecule (arising from the combinations of two equivalent local bends) will have higher (ν_3, symmetric) and lower (ν_6, antisymmetric) frequencies. The inputs to and results of the fits are displayed in Tables 6.1 and 6.2 below.

The fitted parameters are very reasonable, and confirm the expectations laid out in the earlier discussion of ω^{eff}. The ω_0 values are in line with the experimentally known ω_3, ω_6 and x_{33}, x_{36}. An m of 2 is obtained for the normal 3^n series, and for the other progressions m falls in a $6-15$ range that seems sensible based on Fig. 6-2. The 3^n6^2 levels are seen to feel the effects of the barrier most strongly, whereas the 3^n levels in particular do not seem to be aware of it at all, because a *combination* of q_3 and q_6 are required to access the transition state geometry. It is worth mentioning here that ω_3^{eff} and ω_6^{eff} can be obtained as a function of v_6 as well, which in a sense involves traversing the array of term values in Table 6.2 horizontally rather than vertically. The same $\{\omega^{\text{eff}},\overline{E}\}$ data are obtained, but in different sets, and we will

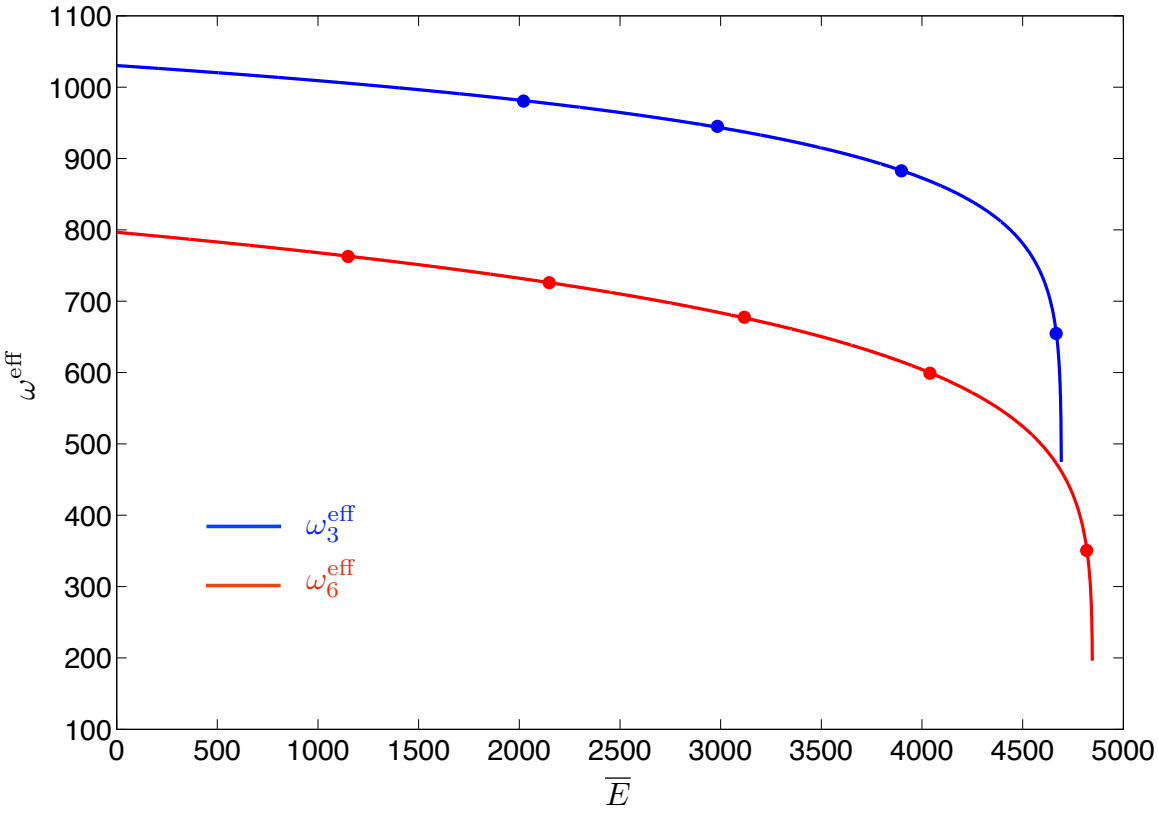

Figure 6-4: Experimental ω^{eff} for the 3^n6^2 levels, shown with fits to Eq. 6.6. ω_3^{eff} is obtained directly from the progression of 3^n6^2 levels, and ω_6^{eff} is derived from the 3^n6^2 and 3^n6^1 levels at a given n_3.

return to this point later on.

Table 6.1: ω^{eff} Fits to 3^n6^m Levels

Fit	ω_0	E_{TS}	m	RMS
ω_3^{eff} : 3^n	1058 ± 21	2e4 ± 2e5	2.3 ± 19	3.4
ω_3^{eff} : 3^n6^1	1039 ± 13	4845 ± 591	14.3 ± 6	0.65
ω_3^{eff} : 3^n6^2	1030 ± 30	4692 ± 33	11.5 ± 3	1.5
ω_6^{eff} : 3^n6^1	777.6 ± 2	5074 ± 83	6.3 ± 0.3	0.48
ω_6^{eff} : 3^n6^2	796.6 ± 4	4846 ± 4	6.3 ± 0.2	0.90

All parameters in cm^{-1}, except m, which is dimensionless. Uncertainties are 2σ. The ω_6^{eff} data sets are constructed by taking the average and difference of the energies of the 3^n6^m series listed and the 3^n6^{m-1} levels.

One particularly exciting outcome of the excellent fits using Eq. 6.6 is the ability to obtain values for E_{TS}. The numbers listed in Table 6.1 for the ω_3^{eff} : 3^n6^2 and ω_6^{eff} : 3^n6^2 fits are consistent with the *ab initio* saddle point energy obtained in Ref. [10] of 4979 cm^{-1}, which has an associated uncertainty of several hundred cm^{-1}. Based on the comparison of the *ab initio* calculation of the *cis* origin at this same level of theory (EOM-CCSDT/ANO1, [10]) to the current experimental value and more accurate *ab initio* calculations [53], one might expect that the 4979 cm^{-1} value is around $150 - 200$ cm^{-1} too high, but this is speculative.

In any case, the agreement with theory and the small uncertainties associated with the fitted E_{TS} values are very encouraging. It is especially promising that this analysis stems entirely from a small subset of the vibrational levels; in other words, it is not necessary to deal with the entire vibrational manifold. Special states exist and encode chemically important information, but we must be able to recognize the patterns with which they communicate it.

6.4 Extensions

Several possibilities suggest themselves when the ω^{eff} analysis outlined above is extended to additional vibrational progressions. The first, shown in Fig. 6-6, is that of differentiating between isomerization pathways. We have seen already that certain

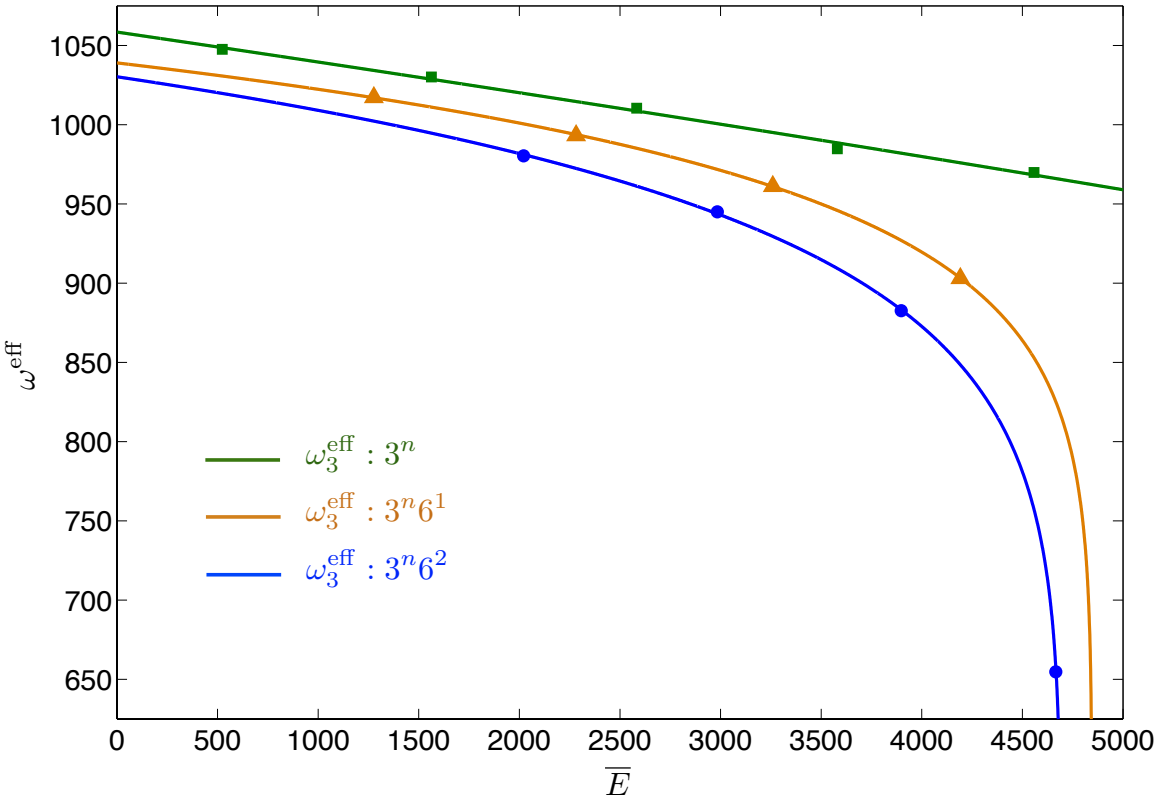

Figure 6-5: Experimental ω^{eff} for the 3^n6^2 levels as compared to ω_3^{eff} for other progressions with varying quanta of ν_6, shown with fits to Eq. 6.6. As mentioned earlier, the 3^n6^2 series has the sharpest dip, in close analogy to the $K = \ell = 0$ series in the Dixon dip [109].

Table 6.2: Term Values Used in ω^{eff} Fits

v_3 \ v_6	0	1	2
0	0	768.26[c]	1531.02[g]
1	1047.55[a]	1785.53[d]	2511.39[h]
2	2077.71[a]	2778.76[d]	3456.38[h]
3	3088.14[a]	3739.98[e]	4339[f]
4	4072.95[a]	4643.11[f]	4993.78[f]
5	5042.78[b]		

All energies in cm^{-1}. T_0 and J=K=0 values used where available. See discussion in Ref. [10].

[a]From Refs. [35, 36]

[b]From Ref. [36], but with a K-staggering of +6.31 factored out. See Ch. 7.

[c]From Ref. [38]

[d]From Ref. [46].

[e]From Ref. [53].

[f]See Ch. 7. The term value for $3^4 6^1$ is based on unpublished IR-UV spectra, with a very large K-staggering of +28 cm^{-1}. The term value for $3^3 6^2$ is based on a $K = 1$ level at 46547 cm^{-1}. The term value for $3^4 6^2$ combines misassigned data from Ref. [36] with unpublished H atom action spectra, and a K-staggering of -6.89 cm^{-1} is factored out.

[g]From Ref. [41].

[h]From Ref. [43].

progressions show no sign of an isomerization dip, such as the 3^n. Here we see that surprisingly, the $3^n 4^2$ levels exhibit the same ω_3^{eff} as the 3^n, from which we conclude that the torsional *cis-trans* pathway is inactive at these energies. This is consistent with the harmonic behavior in ν_4 noted in Ref. [41], but it is nevertheless interesting that, unlike in other molecules, torsion does not play a role in this *cis-trans* isomerization. Furthermore, the very strong Darling-Dennison and Coriolis interactions between ν_4 and ν_6, as well as the inevitable interaction between ν_4 and ν_3 as the molecule straightens and the torsion vanishes, would have led us to predict some kind of nonlinear behavior of the ω_3^{eff} from the $3^n 4^2$ levels. The absence of any such effects implies that the torsion is a "spectator mode", uninvolved in and unaffected by the isomerization occurring in ν_3 and ν_6.

The clear distinction between spectator modes and isomerizing modes has implications for extracting other properties of the saddle point from ω^{eff} analysis. Consider a separable system that consists of an asymmetric double minimum in x, and a har-

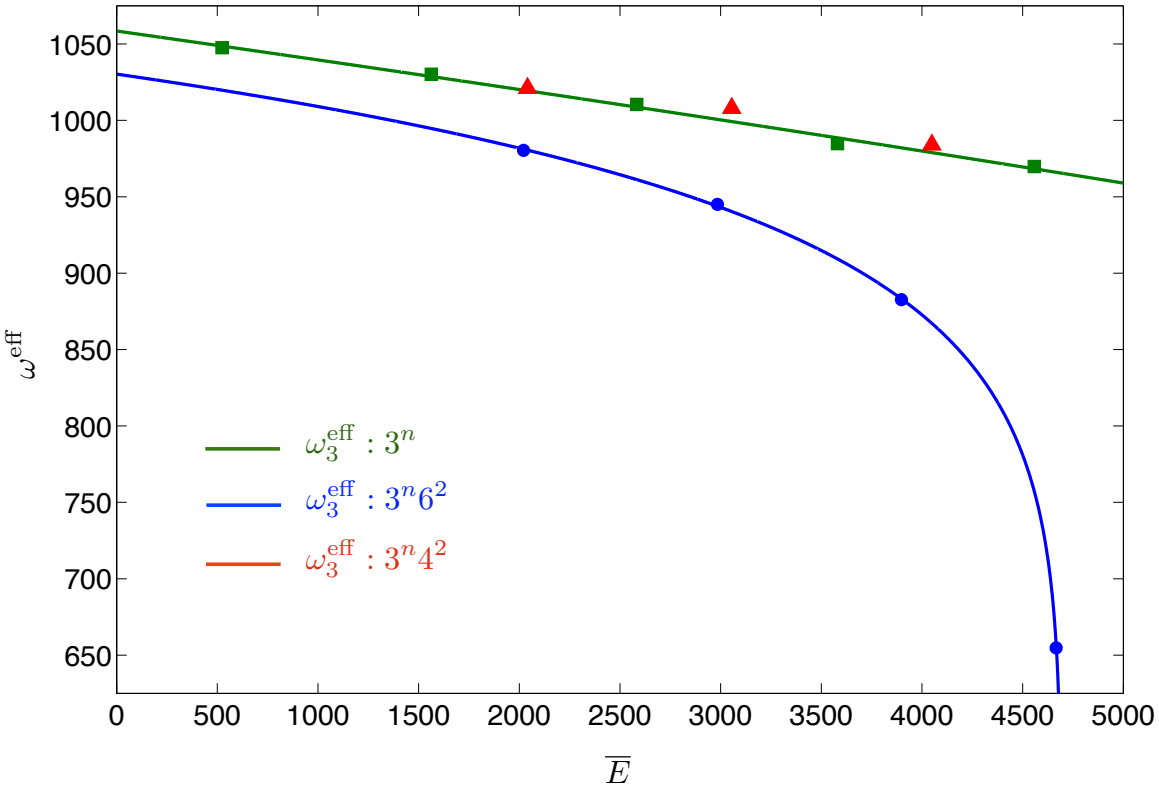

Figure 6-6: ω^{eff} plots for the 3^n, 3^n4^2, and 3^n6^2 progressions. The 3^n4^2 series follows the normal behavior of the 3^n levels, despite the isomerization dip observed in the 3^n6^2 levels. This shows that the torsional mode ν_4 is not involved in the isomerization process at these energies.

monic oscillator in y: $V(x,y) = V(x) + ky^2/2$. Since the Hamiltonian is separable, $E = E(x) + E(y)$, and therefore ω_x^{eff} does not depend on y, similar to how ω_3^{eff} does not depend on v_4 in *trans* S_1 C_2H_2. This means that the ω_y of the transition state is equal to that of the stable species. We can then imagine a case where $\dfrac{\partial^2 V(x,y)}{\partial y^2}$ changes with x. In such a case it should be possible to extract a value for ω_y of the transition state from the spacing of the ω_x^{eff} curves, or by plotting ω_y^{eff} directly. This would require data from levels above the saddle point energy. In a real system there could also be reaction path curvature, such that the normal modes of the minima are not the same as those of the saddle point. Nevertheless, the preceding discussion and examples seem to indicate that modes with a projection along the reaction coordinate will have an ω^{eff} that dips, while those spectator modes unrelated to the isomerization will not, and that it should be possible to obtain information about the curvature of the potential at the saddle point. These transition state frequencies and the saddle point energy are critical inputs to the expression for the rate constant in transition state theory [99].

6.5 Future Work

Directions for future work in developing the isomerization dip concept and the ω^{eff} analysis involve primarily collecting additional experimental data in our model system, but also attempting to refine and generalize the tools introduced above. It would be best to be able to utilize more of the extant data (other J, K term values), and to perform simultaneous fits of multiple vibrational level progressions. Treating an expanded data set should also refine our understanding of the E_{TS} parameters associated with individual progressions. These values may be affected by averaging over the vibrational wavefunctions of the states involved and/or the path they take to the saddle point. It also seems clear that ω^{eff} is in principle a tensorial quantity, and should be amenable to N-dimensional analysis. Plotting finite differences in all dimensions of the N-D array of vibrational state energies vs. $\{v_i\}$ gives a hypersurface, the structure of which is an ordered grid for a harmonic or Morse oscillator,

analogous to a linear plot in $1D$. This structure distorts and "dips" in the dimensions corresponding to isomerizing modes. However, it is not clear how to define $\overline{E}$ in multiple dimensions.

Perhaps the most promising prospect is the application of this methodology to other molecules. It is not too much of an exaggeration to say that little spectroscopy has been done at chemically relevant energies because it was unclear what could be learned, although there are other compelling reasons as well. Our hope is that the concepts and example given here will not only serve as a paradigm for understanding isomerizing systems, but also provide motivation for attacking other chemical problems with spectroscopic tools.

In terms of S_1 C_2H_2 experimental data, additional assignments near and above the transition state energy are needed. Furthermore, observations of higher K values are necessary to deperturb the rotational structures and vibrational term values from K-staggerings. Ongoing efforts in these directions are discussed in the next chapter.

Chapter 7

Ongoing Work

Abstract

In this chapter we describe ongoing experiments that probe the region of the transition state energy for the *cis-trans* isomerization in the S_1 state of C_2H_2. Alternative classes of excitation schemes and detection methods are employed to counteract the problems of K-staggering perturbations and predissociation. Many new subbands and polyads have been observed, although their analysis is still in progress. A few important new findings are summarized briefly.

The work described in this chapter was performed with P. B. Changala, including contributions from J. R. P. Berk, and also owes much to collaborations with Profs. A. J. Merer and J. F. Stanton. We are grateful to B. M. Broderick and Prof. A. G. Suits for their help and advice in setting up the REMPI experiments.

7.1 Introduction

The region of the *cis-trans* isomerization transition state in S_1 acetylene is a difficult one for spectroscopic study. (This region corresponds to the energy range that begins approximately one vibrational quantum below the expected saddle point energy, i.e. around 46400 cm^{-1}.) The state density is rapidly increasing and the rovibrational structures become complicated, but these challenges to standard, pattern-based spectroscopic assignment are expected. Another serious and fundamental problem, which in practice precedes that of spectral complexity, is that of detection. More

and more of the vibrational states become increasingly Franck-Condon forbidden because of growing numbers of quanta in the dark modes $\nu_{1,4,5,6}$, and therefore have low excitation probabilities. In addition, predissociation also reduces the detection efficiency. Above the dissociation limit to $\tilde{X}$ C_2H+H, located at 46074 cm^{-1} [83], the fluorescence quantum yield drops sharply [116–121], making it difficult to use the LIF detection technique that is so effective at lower energies. Once these dual obstacles are overcome (at least partially), as described below, we find a proliferation of the K-staggering perturbations discovered at lower energies, which threatens to derail the normal rotation-vibration classification scheme for energy levels. These K-staggerings reflect the full onset of the *cis-trans* isomerization process and the emergence new dynamics above the barrier, the details of which are not yet understood.

7.2 Experiments

The following experiments have been performed to study states in the region 46400-47250 cm^{-1}:

1. One-photon LIF from $v = 0$ and ν_4'', searching for transitions from 45900-47500 cm^{-1}

2. IR-UV LIF via ν_3'', accessing states with total term energies from 46500-46900 cm^{-1}

3. H atom action and C_2H_2 $1 + 1$ REMPI, searching for transitions from 46250-47250 cm^{-1} region

4. IR-UV double resonance using IR hot bands and a hyperthermal nozzle (proof of principle by P. B. Changala [97]).

7.2.1 One photon LIF from $v = 0$ and ν_4'' (45900-47500 cm^{-1})

In the first of these experiments we used the LIF system described in Ref. [88]. This spectrometer was originally optimized for the detection of states with low fluores-

cence quantum yield. Great care was taken to eliminate scattered light, because the fluorescence lifetime was generally sufficiently short to necessitate gating with a time window that included the laser pulse. Despite this abandonment of the conventional "background-free" advantage of LIF detection, a significant sensitivity improvement was achieved over previous efforts (Fig. 7-1). Many previously unobserved subbands were found, but secure vibrational assignments cannot yet be made in all cases, primarily because of the lack of $K = 0, 2$ data. The new, securely assigned *gerade* levels and polyads include $1^1 3^2, 1^1 B^2, 2^1 B^4$, and $3^3 6^2$, and it seems very likely that the vast majority of the other expected states in this energy region have also been seen ($B^6, 3^1 5^1 B^1, 2^1 3^2 B^2, 2^1 5^1 B^1, 5^1 B^3, 3^2 B^4$, and $3^4 6^2$). The assignments and energies of the $3^{3-4} 6^2$ levels provide particularly important data for the isomerization dip concept discussed in the previous chapter. In several cases, dark perturbers of previously known levels (for example, 3^5 and $3^4 6^2$) are directly observed for the first time. A few subbands in this region appear to be candidates for *cis* well levels, but even tentative assignments would be premature.

7.2.2 IR-UV LIF via ν_3'' (46500-46900 cm^{-1})

The second set of experiments extends the IR-UV LIF spectra, recorded via ν_3'' and reported in Ref. [88], to higher energy. Of the polyads expected in this region, we have securely assigned $5^1 B^2, 3^2 B^3, 1^1 3^1 B^1$, and $3^4 6^1$. Parts of $3^1 B^5$ are also observed, but the $2^2 3^1 B^1$ and $2^1 3^1 B^3$ polyads are not seen at all. Several surprisingly strong subbands near 46650 cm^{-1} are assigned to *cis* $4^2, 6^3$, and $3^1 6^2$, based on the calculations of Refs. [10, 53, 97]. It appears from the *cis* level positions that *cis* y_{666} may be large, perhaps analogously to *trans* z_{3366}, as discussed in Ch. 6, but there are not enough *cis* levels observed yet to be sure. The x_{45}, x_{56} parameters were determined from the $5^1 B^2$ term values and are reported in Table 5.6. Perhaps the most important revelation is the enormous +28 cm^{-1} K-staggering in the $3^4 6^1$ level. This discovery prompted us to examine many other states in this energy region for staggerings, which will be discussed later.

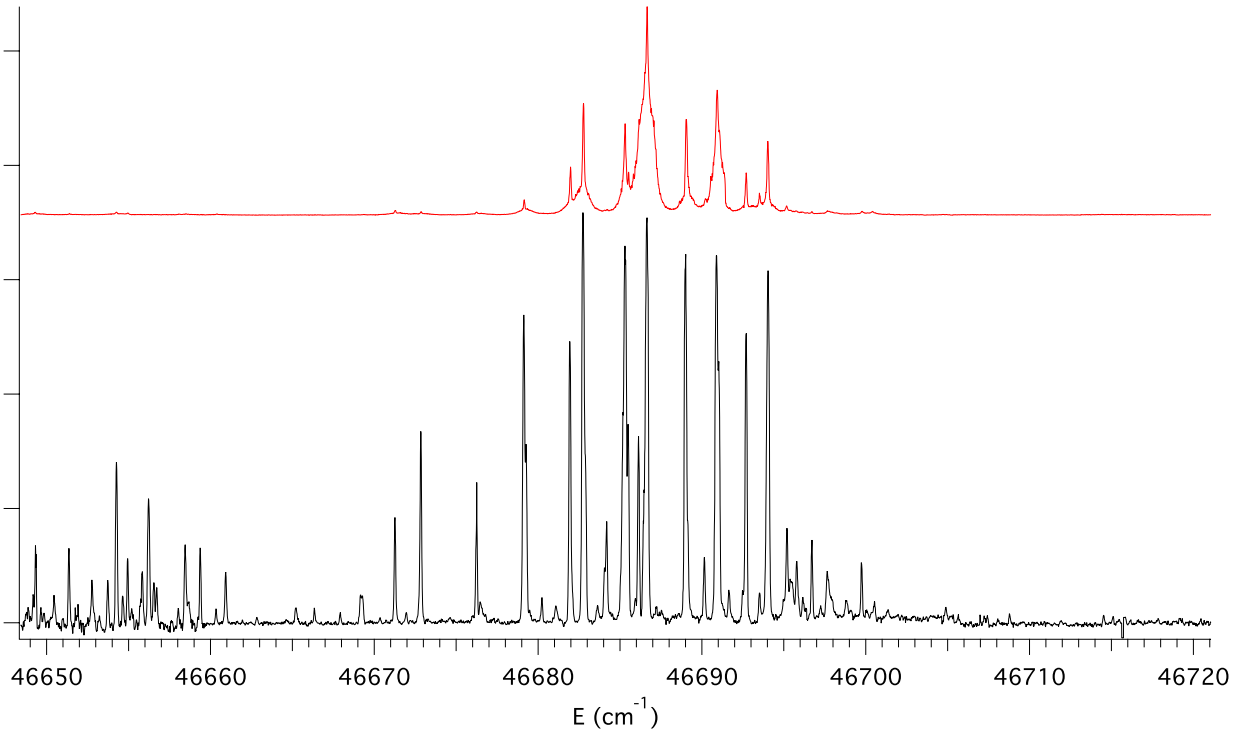

Figure 7-1: Comparison of new C_2H_2 LIF spectra (lower trace, black) with previous spectra (upper trace, red) in the region of the $2^1 3^3$ vibrational state. This represents an increase in signal to background ratio by a factor of at least 10 for severely predissociated states and decreased linewidth by a factor of 3.

7.2.3 H atom action and C_2H_2 $1+1$ REMPI

The obvious course of action when confronted with low fluorescence quantum yield is to resort to an alternative detection technique. We chose to pursue the option of detecting the H atom fragments produced by dissociated states. This technique has been used by many groups to study C_2H_2 dissociation, although there are only previous two reports of $\tilde{A}$-$\tilde{X}$ action spectra [118, 119]. Our implementation here uses the same $2+1$ H atom REMPI process, but our spectral resolution is considerably higher (roughly $\sim 2-5\times$, see Fig. 7-3), both because of the linewidth of our photolysis laser and because we use a skimmed molecular beam. The details of the experimental setup were given in Ch. 1. As noted there, we could simultaneously record H atom action and $1+1$ REMPI spectra of C_2H_2 in this configuration. The H atom action spectrometer is not yet a fully developed tool in our group, and it will definitely be possible to record significantly better spectra than those already acquired. Aside from (in principle) straightforward optimization of the molecular beam and laser alignment conditions, two promising potential improvements are frequency tripling to produce the UV light for photolysis, and a H atom REMPI scheme that ionizes a larger fraction of the Doppler profile of the recoiling H atoms. Currently we use a narrow linewidth laser for $2+1$ REMPI, which captures only $\sim 10\%$ of the H atoms even at low excess energies. An alternative ionization scheme, such as $3+1$ REMPI and/or a broader linewidth laser, would increase the signal by a large factor. Nevertheless, the success of this method in the near-threshold region studied here bodes well for continuing to higher energies, where the H atom yield (and C_2H_2 $1+1$ cross-section) will only increase as the fluorescence quantum yield continues to decrease.

Two prominent early findings from the H atom detected spectra are presented in Figs. 7-2 and 7-3. The first spectrum shows a $\Delta - \Pi$ hot band to the $K' = 2$ level of $3^4 6^2$, which had not previously been seen in LIF or absorption spectra. Based on the positions of this $K = 2$ level and the $K = 0$ (47195 cm^{-1}) and 1 (47206 cm^{-1}) levels, it appears that this vibrational state has a K-staggering of -6.9 cm^{-1}. The second spectrum contains an interesting intensity effect in the triplet splitting of the

R(1) (and P(3), not shown) line of the $2^1 3^3\ \Pi - \Sigma$ subband. Specifically, the relative intensities of the line components are reversed between spectra recorded using the two different detection methods. It is known that triplet states play an important role in the dissociation process, and it would be interesting to survey the lifetimes and dissociation propensities of triplet-mixed eigenstates above the dissociation limit, similar to previous work on acetylene intersystem crossing below the dissociation threshold [52].

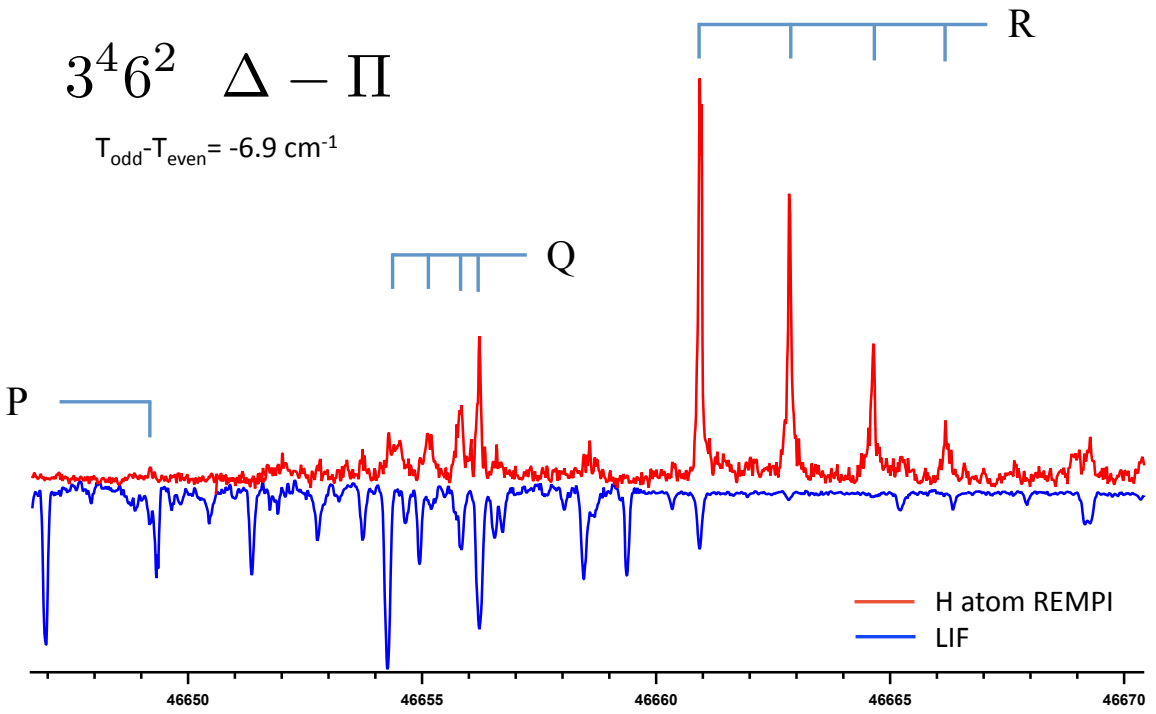

Figure 7-2: The $K = 2$ level of $3^4 6^2$, seen as a $\Delta - \Pi$ hot band detected by H atom action REMPI. The LIF spectrum discussed above (Sec. 7.2.1) is shown for comparison, where these $K' = 2$ lines are not observed.

7.2.3.1 Dissociation Mechanism

The dissociation mechanism of C_2H_2 into $C_2H + H$ deserves a brief digression. The dissociation process has been investigated both theoretically [28, 29, 122] and experimentally [83, 119–121, 123–125], although these references represent only a small

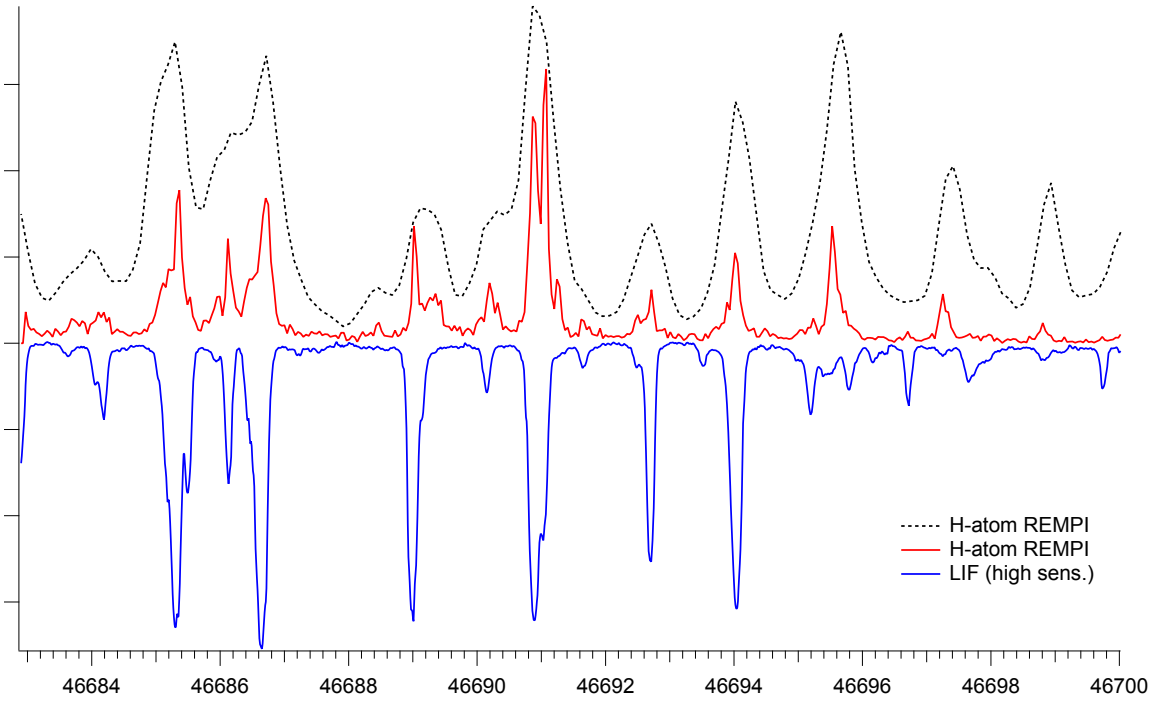

Figure 7-3: Triplet splittings in the $2^1 3^3$ vibrational band, as seen in H atom action and LIF spectra. Shown here is an expanded portion of the region displayed in Fig. 7-2, focusing on the R(1) line of the $2^1 3^3$ $\Pi - \Sigma$ band, which exhibits triplet splittings. The relative intensities of the line components are reversed between our LIF and H atom spectra. The higher resolution of the H atom spectrum is due to the reduced Doppler width in the skimmed beam. The H atom spectrum from Ref. [119] is overlaid as a black dashed line.

fraction of the literature on the subject.[1] The experimental work of Mordaunt *et al.* that determined the D_0^0 value precisely by Rydberg tagging H atom TOF spectroscopy [83] also uncovered evidence for two dissociation channels from the measured photofragment population distributions and their recoil anisotropy [123]. The theoretical calculations of Cui, Morokuma, and Stanton [28, 29] identified several plausible pathways from S_1 C_2H_2 to products. (See Fig. 5 of Ref. [29]. The reader is also referred to the extended discussion in Ref. [123] of the observed channels and their interpretation, which in the following will only be mentioned in passing.) Briefly, one of the predicted channels (S_1 C_2H_2 $\rightarrow T_{3\rightarrow 2\rightarrow 1} \rightarrow \tilde{X}$ $C_2H + H$) was consistent with the characteristics of one component of the observed bimodal distributions ("Channel I"), as well as with other experiments that indicated a T_1 exit barrier of 560 cm^{-1} [118, 121, 124]. However, it was difficult to reconcile any of the *ab initio* pathways with the characteristics of the second component ("Channel II"), which included a higher threshold, promotion by excitation in ν_1, a substantial recoil anisotropy, and a lower rotational temperature. It was therefore hypothesized in [123] that the S_1 *cis-trans* isomerization was the rate limiting step in the Channel II mechanism, since the half-linear structure of the *cis-trans* transition state possessed the necessary attributes to lead to the observed distribution, in combination with a more direct (S_1 C_2H_2 $\rightarrow T_1 \rightarrow \tilde{X}$ $C_2H + H$) process.

As pointed out in Ref. [42], one significant problem with the study of Mordaunt *et al.* was that they based their interpretation on the assumptions of spectroscopic assignments that were later shown to be incorrect. In particular, the revision of the ν_1 frequency meant that the $K = 1$ level at 47206 cm^{-1} did not belong to the $1^1 3^2$ state, and in fact its assignment is now believed to be $3^4 6^2$. Nevertheless, the mechanism proposed by Mordaunt *et al.* for Channel II now seems more likely to be correct, since the $3^4 6^2$ level is intimately involved in the *cis-trans* isomerization.

Since we have significantly expanded the catalog of known vibrational levels above

[1] At the energies discussed in this thesis, only the $\tilde{X}$ $C_2H + H$ channel is available. There is a vast literature on 193 nm photolysis of C_2H_2, where both the $\tilde{X}$ and the $\tilde{A}$ states of C_2H are energetically accessible, as well as on vibrationally mediated photodissociation, but we will not discuss those topics here.

the dissociation limit, and additionally detected several of them by H atom action spectroscopy, it would be very interesting to revisit the question of the dissociation mechanism. It is now possible to use levels for photolysis that possess excitation in any of the S_1 *trans* vibrational modes, states with predominantly *cis* character, and triplet-mixed eigenstates such as those shown in Fig. 7-3, all as functions of J and K. Observing the resulting photofragment distributions produced by a variety of rovibronic intermediate states would generate a rich data set germane to the dissociation process. This ability to select and systematically vary the characteristics of the photolysis intermediate state in combination with new H atom orientation and alignment detection methods [126] is particularly attractive.

7.3 Strategies for K-staggerings

Understanding K-staggerings has recently become a central issue in our study of the S_1 state. The source of these staggerings and the initial examples discovered in *cis* conformer states have already been discussed [11, 48, 88], but a simple illustration may help to explain their importance in the barrier region. Fig. 7-4 shows a toy model calculation of a one-dimensional hindered rotor, where the potential is a cyclic version of the *ab initio* minimum energy isomerization path from the PES of Ref. [10]. An isomerization dip analysis of the energy levels (See Ch. 6) reveals that, in addition to the dip in ω^{eff} at the barrier energy, the degeneracies between identical wells are lifted by tunneling. The resultant tunneling splittings grow larger until the top of the barrier is reached, and then decrease above E_{TS}, but the original energy level pattern does not necessarily return.[2] This complete transformation of the energy level pattern, while very interesting, complicates considerably the essential spectroscopic business of making assignments.

It is important to note that the K-staggerings also present a valuable opportunity

[2]Since the model calculation tends toward a free rotor as $E \gg E_{TS}$, a new pair of degeneracies forms with different partner levels, corresponding to the $\pm m$ degeneracy of the free rotor. It is certainly true that a new above-barrier pattern will emerge in S_1 C_2H_2, but we do not yet know what that pattern might be.

to characterize the chemically important regions of the potential energy surface. In principle the complete shape of the double minimum potential can be obtained when tunneling staggerings or splittings are combined with the vibrational level spacing information discussed in the previous chapter. The staggerings are sensitive to the width and height of the barrier because they are caused by tunneling, and the vibrational level spacings give the widths of the wells and the height of the barrier. Useful discussions of this topic from a semiclassical perspective can be found in Refs. [127–129].

7.3.1 *K*-staggerings Found

In addition to the staggerings found in the *cis* $3^1 6^1$ and 6^2 levels, the spectra discussed in Sec. 7.2.2 reveal a K-staggering of roughly $+28$ cm^{-1} in the *trans* $3^4 6^1$ level. This staggering is several times larger in magnitude than those found previously, and significantly, is substantially larger than the A rotational constant. The existence of a staggering larger than $A - \overline{B}$ means that K subbands can potentially no longer be grouped together by the usual approximate K^2 dependence within a particular vibrational level. This poses a substantial problem for the process of making vibrational assignments, especially since at present we have no way of even approximately predicting K-staggerings in the $\tilde{A}$ state. Usually, when K-staggerings are encountered, they depend only on excitation in a single vibrational mode, such as the torsion in H_2O_2, to pick an example from a similar molecule [130, 131]. In S_1 C_2H_2, the isomerization involves *both* modes Q_3 and Q_6, and therefore there are no *a priori* expected trends of the signs or magnitudes of the K-staggerings.

The discovery of the very large K-staggering in the *trans* $3^4 6^1$ level prompted us to look more closely for staggerings in other isoenergetic levels. In general this requires assignment of $K = 0 - 2$ levels, or at absolute minimum, two K values and a reasonable guess for the A rotational constant. However, a complete set of $K = 0 - 3$ levels is desirable to avoid problems with local perturbations, since it is almost impossible that a local non-K-staggering perturbation would preserve both the $K = 0 - 2$ and $1 - 3$ intervals. We found at least one such case, the 3^5 level,

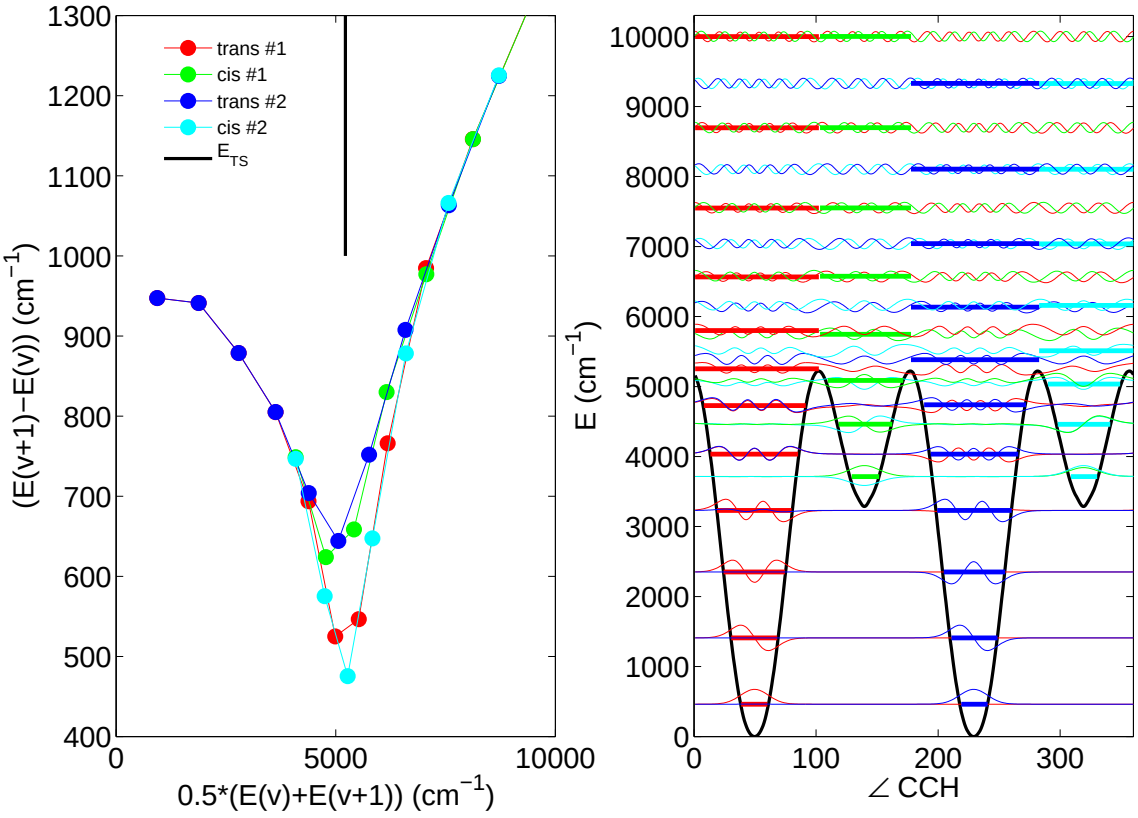

Figure 7-4: K-staggerings for a model one-dimensional minimum energy isomerization path. The cyclic potential is constructed from an *ab initio* MEIP for S_1 C_2H_2, based on the PES calculated in Ref. [10]. The energy level pattern evolves from a symmetric double minimum case at low energy to a free rotor at high energy. An isomerization dip plot is shown in the left panel. The degeneracies at low energy, between levels associated with the two pairs of identical "*trans*" and "*cis*" wells, are broken by tunneling, but new degeneracies (with different partners) re-form above the potential barrier. The high energy case shown here is due to the choice of the simple rotor model for the one-dimensional calculation, and is not expected to reflect the above-barrier S_1 C_2H_2 behavior. The effective frequencies increase linearly with energy above the barrier, because the free rotor energies are proportional to $J(J+1)$, the derivative of which goes like J.

in Table XI of Ref. [36]. There they could observe $K = 3$ levels via $\Phi - \Delta$ hot bands originating from the $2\nu_4''$ level in their non-jet-cooled absorption spectra. A K-staggering in the 3^5 level is somewhat surprising, since without excitation in ν_6, this state would not be expected to isomerize. Nevertheless, the $K = 0 - 3$ data makes the staggering unmistakable. If we divide the $K = 0 - 2$ interval by 4 or the $K = 1 - 3$ interval by 8 to factor out the K^2 dependence, in both cases we obtain $A - \overline{B} \simeq 16.46$ cm^{-1}, a reasonable value. The $K = 0 - 1$ spacing is 22.77 cm^{-1}, and the K-staggering is therefore $22.77 - 16.46 = +6.31$ cm^{-1}. A staggering of similar magnitude, -6.9 cm^{-1}, has been found in the nearby *trans* $3^4 6^2$ level, based on the spectrum shown in Fig. 7-2, and it is also possible that a small staggering of < 1 cm^{-1} exists in the 3^4 level based on data from Refs. [36, 44]. While it is very difficult to extract K-staggering information from *trans* conformer B^n polyads, because of the already complicated rotational structures, we believe that the 3^2B^3 polyad is the first example where this has been done successfully.

On the basis of the growing number of K-staggerings found in the barrier region and their increasing magnitude, it appears necessary to develop new methods for coping with their disruption of the level structure. Experimentally, it would be ideal to record spectra of subbands with higher K' values of 3 or even 4, in order to measure the staggerings and to vibrationally assign the K sublevels definitively. From a theoretical point of view, rovibrational calculations with higher accuracy than those in Ref. [10] are required, and the inclusion of additional coordinates would be desirable as well.

7.3.2 New Calculations and IR-hot-band-pumped IR-UV Double Resonance Spectroscopy

Both of the strategies mentioned above are underway in collaboration with P. Bryan Changala. Since these efforts have either been described in [97] or in manuscripts that are in preparation, only a very brief mention will be made here.

A four-dimensional potential surface that includes the torsional angle, τ, has been

calculated using the methods described in Ref. [10]. Rovibrational variational calculations using this surface or a three-dimensional $\{\angle CCH_1, \angle CCH_2, \tau\}$ PES have achieved excellent agreement with the experimentally observed level structure. The B^n intrapolyad structures appear to be particularly well reproduced. The calculations predict K-staggerings that are in approximate agreement with our observations, which is encouraging [97].

In order to observe higher K' subbands it is necessary to prepare excited vibrational levels of S_0 C_2H_2, since $\ell'' \leq \nu_4'' + \nu_5''$. Our procedure for preparing vibrationally hot, rotationally cold acetylene involves supersonic expansion through a SiC pyrolysis nozzle [132]. This procedure maintains a rotational temperature of ~ 10 K (and certainly less than 40 K [133]), while allowing vibrational temperatures up to 1800 K. Molecules in vibrationally excited states are then excited by IR-UV double resonance in order to avoid complications due to overlapping UV $\tilde{A}$-$\tilde{X}$ hot bands that are also enhanced by the heated nozzle. The IR hot band transition can be chosen to provide an additional unit of ℓ'', if desired. Proof of principle tests of this scheme have been completed successfully.

7.4 Conclusions

The work undertaken in this thesis is aimed at understanding the spectroscopic signatures of isomerizing systems. In particular, a novel pattern that reveals characteristics of the transition state has been identified by experimental investigation of a prototypical system, the *cis-trans* isomerization in S_1 C_2H_2. Significant progress has been made in the study of this isomerization, and acetylene now poses new questions, including those of the above-barrier dynamics and the nature of the dissociation mechanism(s). We have no doubt that the second century of $\tilde{A}$-$\tilde{X}$ acetylene spectroscopy [134] will be at least as enlightening, challenging, and surprising as the first.

Bibliography

[1] C. K. Ingold and G. W. King. Excited states of acetylene. *J. Chem. Soc.*, pages 2702–2755, 1953.

[2] A. D. Walsh. 468. The electronic orbitals, shapes, and spectra of polyatomic molecules. Part III. HAB and HAAH molecules. *J. Chem. Soc.*, pages 2288–2296, 1953.

[3] J. T. Hougen and J. K. G. Watson. Anomalous rotational line intensities in electronic transitions of polyatomic molecules: Axis-switching. *Canadian Journal of Physics*, 43(2):298–320, 1965.

[4] J.K. Lundberg. The SEP Spectrum of Acetylene. In H.L. Dai and R.W. Field, editors, *Molecular Dynamics and Spectroscopy by Stimulated Emission Pumping*, chapter 22, page 791. World Scientific Pub. Co. Inc., 1995.

[5] R. W. Field, J. H. Baraban, S. H. Lipoff, and A. R. Beck. Effective Hamiltonians for Electronic Fine Structure and Polyatomic Vibrations. *Handbook of High-Resolution Spectroscopy*, 2011.

[6] Matthew P. Jacobson, Jonathan P. O'Brien, Robert J. Silbey, and Robert W. Field. Pure bending dynamics in the acetylene $\tilde{X}\ ^1\Sigma_g^+$ state up to 15 000 cm^{-1} of internal energy. *The Journal of Chemical Physics*, 109(1):121–133, 1998.

[7] Matthew P. Jacobson and Robert W. Field. Acetylene at the threshold of isomerization. *The Journal of Physical Chemistry A*, 104(14):3073–3086, 2000.

[8] Kyle L. Bittinger. *Spectroscopic Signatures of Doorway-Mediated Intersystem Crossing*. PhD thesis, Massachusetts Institute of Technology, 2009.

[9] Kyle L. Bittinger, Wilton L. Virgo, and Robert W. Field. Spectral signatures of inter-system crossing mediated by energetically distant doorway levels: Examples from the acetylene s1 state. *The Journal of Physical Chemistry A*, 115(43):11921–11943, 2011.

[10] J. H. Baraban, A. R. Beck, A. H. Steeves, J. F. Stanton, and R. W. Field. Reduced dimension discrete variable representation study of *cis–trans* isomerization in the S_1 state of C_2H_2. *The Journal of Chemical Physics*, 134(24):244311, 2011.

[11] Anthony J. Merer, Adam H. Steeves, Joshua H. Baraban, Hans A. Bechtel, and Robert W. Field. Cis-trans isomerization in the S_1 state of acetylene: Identification of cis-well vibrational levels. *The Journal of Chemical Physics*, 134(24):244310, 2011.

[12] J. H. van 't Hoff. Sur les Formules de Structure dans l'Espace. [On Structural Formulas in Space]. *Archives néerlandaises des sciences exactes et naturelles*, 9:445, 1874.

[13] Johannes Wislicenus. Ueber chlorderivate der krotonsäuren. *Berichte der deutschen chemischen Gesellschaft*, 20(1):1008–1010, 1887.

[14] Johannes Wislicenus. *Abhandl. königl. sachs. Gesell. Wissensch. Leipzig, Math-Phys Classe*, 14:1, 1887.

[15] Aaron J. Ihde. The unraveling of geometric isomerism and tautomerism. *Journal of Chemical Education*, 36(7):330, 1959.

[16] W. Gordy and R. L. Cook. *Microwave Molecular Spectra*. Wiley, New York, 1970.

[17] C. E. Cleeton and N. H. Williams. Electromagnetic waves of 1.1 cm wave-length and the absorption spectrum of ammonia. *Phys. Rev.*, 45:234–237, Feb 1934.

[18] B. Bleaney and R. P. Penrose. Ammonia spectrum in the 1 cm wavelength region. *Nature (London)*, 157:339–340, 1946.

[19] William E. Good. The inversion spectrum of ammonia. *Phys. Rev.*, 70:213–218, Aug 1946.

[20] C. C. Costain. An empirical formula for the microwave spectrum of ammonia. *Phys. Rev.*, 82:108–108, Apr 1951.

[21] E. Schnabel, T. Törring, and W. Wilke. Zum Inversionsspektrum des NH_3. *Zeitschrift für Physik A Hadrons and Nuclei*, 188:167–171, 1965.

[22] Daniel Demoulin and Martin Jungen. Theoretical assignments of the electronic spectrum of acetylene. *Theoretical Chemistry Accounts: Theory, Computation, and Modeling (Theoretica Chimica Acta)*, 34:1–17, 1974. 10.1007/BF00553227.

[23] Hans Lischka and Alfred Karpfen. Ab initio calculations on the excited states of π-systems. I. Valence excitations in acetylene. *Chemical Physics*, 102(1-2):77 – 89, 1986.

[24] Yukio Yamaguchi, George Vacek, and Henry F. Schaefer. Low-lying triplet electronic states of acetylene: cis $^3B_2$ and $^3A_2$, trans ^3B_u and ^3A_u. *Theoretical Chemistry Accounts: Theory, Computation, and Modeling (Theoretica Chimica Acta)*, 86:97–113, 1993.

[25] George Vacek, J. Russell Thomas, Bradley J. DeLeeuw, Yukio Yamaguchi, and Henry F. Schaefer III. Isomerization reactions on the lowest potential energy hypersurface of triplet vinylidene and triplet acetylene. *The Journal of Chemical Physics*, 98(6):4766–4776, 1993.

[26] John F. Stanton, Chang-Ming Huang, and Péter G. Szalay. Stationary points on the S_1 potential energy surface of C_2H_2. *The Journal of Chemical Physics*, 101(1):356–365, 1994.

[27] C. David Sherrill, George Vacek, Yukio Yamaguchi, Henry F. Schaefer III, John F. Stanton, and Jürgen Gauss. The $\tilde{A}\ ^1A_u$ state and the T_2 potential surface of acetylene: Implications for triplet perturbations in the fluorescence spectra of the $\tilde{A}$ state. *The Journal of Chemical Physics*, 104(21):8507–8515, 1996.

[28] Qiang Cui, Keiji Morokuma, and John F. Stanton. Ab initio MO studies on the photodissociation of C_2H_2 from the S_1 (^1A_u) state. non-adiabatic effects and S-T interaction. *Chemical Physics Letters*, 263(1-2):46 – 53, 1996.

[29] Qiang Cui and Keiji Morokuma. *Ab initio* MO studies on the photodissociation of C_2H_2 from the $S_1(^1A_u)$ state. II. Mechanism involving triplet states. *Chemical Physics Letters*, 272(5-6):319 – 327, 1997.

[30] K. Malsch, G. Hohlneicher, R. Schork, and H. Köppel. A quantum dynamical examination of the vibronic structure of singlet and triplet spectra of acetylene. *Physical Chemistry Chemical Physics (Incorporating Faraday Transactions)*, 3:5393–5407, December 2001.

[31] E. Ventura, M. Dallos, and H. Lischka. The valence-excited states T_1–T_4 and S_1–S_2 of acetylene: A high-level MR-CISD and MR-AQCC investigation of stationary points, potential energy surfaces, and surface crossings. *The Journal of Chemical Physics*, 118:1702, 2003.

[32] Bernd Schubert, Horst Köppel, and Hans Lischka. A wave-packet simulation of the low-lying singlet electronic transitions of acetylene. *Journal of Chemical Physics*, 122(18):184312, May 2005.

[33] G. W. King and C. K. Ingold. The bent excited state of acetylene. *Nature*, 169(4313):1101–1102, June 1952.

[34] K. Keith Innes. Analysis of the near ultraviolet absorption spectrum of acetylene. *The Journal of Chemical Physics*, 22(5):863–876, 1954.

[35] J. K. G. Watson, M. Herman, J. C. Van Craen, and R. Colin. The $\tilde{A} - \tilde{X}$ Band System of Acetylene : Analysis of long-wavelength bands, and vibration-rotation constants for the levels $n\nu_4''$ (n = 0-4), $n\nu_3'$ (n = 0-3), and $\nu_2' + n\nu_3'$ (n = 0-2). *Journal of Molecular Spectroscopy*, 95(1):101 – 132, 1982.

[36] J. C. Van Craen, M. Herman, R. Colin, and J. K. G. Watson. The band system of acetylene: Analysis of medium-wavelength bands, and vibration-rotation constants for the levels nν_3' (n = 4-6), $\nu_2' + n\nu_3'$ (n = 3-5), and $\nu_1' + n\nu_3'$ (n = 2, 3). *Journal of Molecular Spectroscopy*, 111(1):185 – 197, 1985.

[37] J. C. Van Craen, M. Herman, R. Colin, and J. K. G. Watson. The band system of acetylene: Bands of the short-wavelength region. *Journal of Molecular Spectroscopy*, 119(1):137 – 143, 1986.

[38] A. L. Utz, J. D. Tobiason, E. Carrasquillo M., L. J. Sanders, and F. F. Crim. The direct observation, assignment, and partial deperturbation of the ν_4 and ν_6 vibrational fundamentals in $\tilde{A}\ ^1A_u$ acetylene (C_2H_2). *The Journal of Chemical Physics*, 98(4):2742–2753, 1993.

[39] J. D. Tobiason, A. L. Utz, and F. F. Crim. The direct observation, assignment, and partial deperturbation of ν_5 and $\nu_3 + \nu_5$ in $\tilde{A}\ ^1A_u$ acetylene (C_2H_2). *The Journal of Chemical Physics*, 99(2):928–936, 1993.

[40] A. J. Merer, N. Yamakita, S. Tsuchiya, J. F. Stanton, Z. Duan, and R. W. Field. New vibrational assignments in the $\tilde{A}\ ^1A_u$–$\tilde{X}\ ^1\Sigma_g^+$ electronic transition of acetylene, C_2H_2: the ν_1' frequency. *Molecular Physics*, 101:663–673, 2003.

[41] Anthony J. Merer, Nami Yamakita, Soji Tsuchiya, Adam H. Steeves, Hans A. Bechtel, and Robert W. Field. Darling–Dennison resonance and Coriolis coupling in the bending overtones of the $\tilde{A}\ ^1A_u$ state of acetylene, C_2H_2. *The Journal of Chemical Physics*, 129(5):054304, 2008.

[42] Adam H. Steeves, Anthony J. Merer, Hans A. Bechtel, Annelise R. Beck, and Robert W. Field. Direct observation of the symmetric stretching modes of $\tilde{A}\ ^1A_u$ acetylene by pulsed supersonic jet laser induced fluorescence. *Molecular Physics*, 106(15):1867–1877, 2008.

[43] A. H. Steeves, H. A. Bechtel, A. J. Merer, N. Yamakita, S. Tsuchiya, and R. W. Field. Stretch-bend combination polyads in the $\tilde{A}\ ^1A_u$ state of acetylene, C_2H_2. *Journal of Molecular Spectroscopy*, 256(2):256–278, 2009.

[44] Anthony J. Merer, Zicheng Duan, Robert W. Field, and James K. G. Watson. Perturbations in the $4\nu_3$ level of $\tilde{A}\ ^1A_u$ state of acetylene, C_2H_2. *Canadian Journal of Physics*, 87(5):437–441, MAY 2009.

[45] J. Cariou and P. Luc. *Atlas du Spectre d'Absorption de la Molécule de Tellure: 21100–23800 cm^{-1}*. CNRS, Orsay, 1980.

[46] Miwako Mizoguchi, Nami Yamakita, Soji Tsuchiya, Atsushi Iwasaki, Kennosuke Hoshina, and Kaoru Yamanouchi. IR-UV double resonance spectroscopy of acetylene in the A^1A_u n$v_3' + v_4'$ and n$v_3' + v_6'$ (n = 2, 3) ungerade vibrational states. *The Journal of Physical Chemistry A*, 104(45):10212–10219, 07 2000.

[47] G. Herzberg. *Electronic Spectra of Polyatomic Molecules*. van Nostrand Inc., New York, 1965.

[48] Jon T. Hougen and Anthony J. Merer. Extended permutation-inversion groups for simultaneous treatment of the rovibronic states of trans-acetylene, cis-acetylene, and vinylidene. *Journal of Molecular Spectroscopy*, 267(1-2):200 – 221, 2011.

[49] Koichi Yamada, Toru Nakagawa, and Kozo Kuchitsu. Correlation between energy levels of linear and bent X_2Y_2 molecules. *Journal of Molecular Spectroscopy*, 51(3):399 – 421, 1974.

[50] Nobuaki Ochi and Soji Tsuchiya. Rovibronic level structure of electronically excited acetylene ($\tilde{A}\ ^1A_u$) in a supersonic jet as studied by laser-induced fluorescence and Zeeman quantum beat spectroscopy. *Chemical Physics*, 152(3):319 – 336, 1991.

[51] Marcel Drabbels, Johannes Heinze, and W. Leo Meerts. A study of the singlet–triplet perturbations in the $\tilde{A}\ ^1A_u$ state of acetylene by high resolution ultraviolet spectroscopy. *The Journal of Chemical Physics*, 100(1):165–174, 1994.

[52] Wilton L. Virgo, Kyle L. Bittinger, Adam H. Steeves, and Robert W. Field. Contrasting singlet-triplet dynamical behavior of two vibrational levels of the acetylene S_1, $2^1 3^1 B^2$ polyad. *Journal of Physical Chemistry A*, 111(49):12534–12537, DEC 13 2007.

[53] Joshua H. Baraban, Anthony J. Merer, John F. Stanton, and Robert W. Field. Anharmonic Force Fields for *cis* and *trans* S_1 C_2H_2. *Molecular Physics*, 110(21-22):2725–2733, 2012. FASE special issue.

[54] Jon T. Hougen. Strategies for advanced applications of permutation-inversion groups to the microwave spectra of molecules with large amplitude motions. *Journal of Molecular Spectroscopy*, 256(2):170 – 185, 2009.

[55] Mihály Kállay and Jürgen Gauss. Calculation of excited-state properties using general coupled-cluster and configuration-interaction models. *The Journal of Chemical Physics*, 121(19):9257–9269, 2004.

[56] Evan Abramson, Carter Kittrell, James L. Kinsey, and Robert W. Field. Excitation spectroscopy of the acetylene $\tilde{A}$–$\tilde{X}$ transition in the 220 nm wavelength region. *The Journal of Chemical Physics*, 76(5):2293–2295, 1982.

[57] P. Dupré, R. Jost, M. Lombardi, P.G. Green, E. Abramson, and R.W. Field. Anomalous behavior of the anticrossing density as a function of excitation energy in the C_2H_2 molecule. *Chemical Physics*, 152(3):293 – 318, 1991.

[58] Daniel Demoulin. The shapes of some excited states of acetylene. *Chemical Physics*, 11(2):329 – 341, 1975.

[59] J.C. Light and T. Carrington Jr. Discrete-variable representations and their utilization. *Advances in Chemical Physics*, 114:263–310, 2000.

[60] Z. Bacić and J. C. Light. Highly excited vibrational levels of "floppy" triatomic molecules: A discrete variable representation—distributed gaussian basis approach. *The Journal of Chemical Physics*, 85(8):4594–4604, 1986.

[61] S. A. Kucharski, M. Włoch, M. Musiał, and R. J. Bartlett. Coupled-cluster theory for excited electronic states: The full equation-of-motion coupled-cluster single, double, and triple excitation method. *Journal of Chemical Physics*, 115:8263–8266, November 2001.

[62] Joseph A. Bentley, Robert E. Wyatt, Michel Menou, and Claude Leforestier. A finite basis-discrete variable representation calculation of vibrational levels of planar acetylene. *The Journal of Chemical Physics*, 97(6):4255–4263, 1992.

[63] Edwin L. Sibert III and Rudolph C. Mayrhofer. Highly excited vibrational states of acetylene: A variational calculation. *The Journal of Chemical Physics*, 99(2):937–944, 1993.

[64] P.R. Bunker and P. Jensen. *Molecular Symmetry and Spectroscopy*. NRC Research Press, 2006.

[65] R. Prosmiti and S. C. Farantos. Periodic orbits, bifurcation diagrams and the spectroscopy of C_2H_2 system. *The Journal of Chemical Physics*, 103(9):3299–3314, 1995.

[66] M.J. Bramley, W.H. Green, and N.C. Handy. Vibration-rotation coordinates and kinetic energy operators for polyatomic molecules. *Molecular Physics*, 73(6):1183–1208, 1991.

[67] E. B. Wilson, J. C. Decius, and P. C. Cross. *Molecular Vibrations: The Theory of Infrared and Raman Vibrational Spectra*. Courier Dover Publications, 1980.

[68] J. C. Decius. A tabulation of general formulas for inverse kinetic energy matrix elements in acyclic molecules. *The Journal of Chemical Physics*, 16(11):1025–1034, 1948.

[69] Salvador M. Ferigle and Arnold G. Meister. Kinetic energy matrix elements for linear molecules. *The Journal of Chemical Physics*, 19(7):982–983, 1951.

[70] D.J. Tannor. *Introduction to Quantum Mechanics: A Time-Dependent Perspective*. University Science Books, 2007.

[71] J. Rheinecker and J.M. Bowman. Ab Initio Calculation of the Low-Lying Vibrational States of C_2H_2 ($\tilde{A}$) in Full Dimensionality. *Journal of Physical Chemistry A*, 110(16):5464–5467, 2006.

[72] J. D. Tobiason, A. L. Utz, E. L. Sibert III, and F. F. Crim. Normal modes analysis of $\tilde{A}$-state acetylene based on directly observed fundamental vibrations. *The Journal of Chemical Physics*, 99(8):5762–5767, 1993.

[73] T. R. Huet, M. Godefroid, and M. Herman. The $\tilde{A}$ electronic state of acetylene: Geometry and axis-switching effects. *Journal of Molecular Spectroscopy*, 144(1):32 – 44, 1990.

[74] D.O. Harris, G.G. Engerholm, and W.D. Gwinn. Calculation of Matrix Elements for One-Dimensional Quantum-Mechanical Problems and the Application to Anharmonic Oscillators. *Journal of Chemical Physics*, 43:1515–1517, 1965.

[75] Viktor Szalay. Discrete variable representations of differential operators. *The Journal of Chemical Physics*, 99(3):1978–1984, 1993.

[76] C. Clay Marston and Gabriel G. Balint-Kurti. The Fourier grid Hamiltonian method for bound state eigenvalues and eigenfunctions. *The Journal of Chemical Physics*, 91(6):3571–3576, 1989.

[77] Daniel T. Colbert and William H. Miller. A novel discrete variable representation for quantum mechanical reactive scattering via the S-matrix Kohn method. *The Journal of Chemical Physics*, 96(3):1982–1991, 1992.

[78] Inbal Tuvi and Y. B. Band. Hermiticity of the Hamiltonian matrix in a discrete variable representation. *The Journal of Chemical Physics*, 107(21):9079–9084, 1997.

[79] Boris Podolsky. Quantum-Mechanically Correct Form of Hamiltonian Function for Conservative Systems. *Phys. Rev.*, 32(5):812–816, Nov 1928.

[80] Hua Wei and Tucker Carrington, Jr. Discrete variable representations of complicated kinetic energy operators. *The Journal of Chemical Physics*, 101(2):1343–1360, 1994.

[81] J. F. Stanton, J. Gauss, J. D. Watts, P. G. Szalay, R. J. Bartlett, with contributions from: A. A. Auer, D. E. Bernholdt, O. Christiansen, M. E. Harding, M. Heckert, O. Heun, C. Huber, D. Jonsson, J. Jusèlius, W. J. Lauderdale, T. Metzroth, C. Michauk, D. R. Price, K. Ruud, F. Schiffmann, A. Tajti, M. E. Varner, J. Vázquez, and including the integral packages: MOLECULE (J. Almlöf and P. R. Taylor), PROPS (P. R. Taylor), ABACUS (T. Helgaker, H. J. Aa. Jensen, P. Jørgensen and J. Olsen). CFOUR, 2005-2008. See http://www.cfour.de.

[82] Mihály Kállay. MRCC, a string-based quantum chemical program suite. See also M. Kállay, P. R. Surján, J. Chem. Phys. **115**, 2945 (2001) as well as: www.mrcc.hu.

[83] David H. Mordaunt and Michael N. R. Ashfold. Near ultraviolet photolysis of C_2H_2: A precise determination of D_0(HCC−H). *The Journal of Chemical Physics*, 101(3):2630–2631, 1994.

[84] Adam H. Steeves. *Electronic Signatures of Large Amplitude Motions*. PhD thesis, Massachusetts Institute of Technology, 2009.

[85] Trygve Helgaker, Wim Klopper, Henrik Koch, and Jozef Noga. Basis-set convergence of correlated calculations on water. *The Journal of Chemical Physics*, 106(23):9639–9646, 1997.

[86] Attila Tajti, Péter G. Szalay, Attila G. Császár, Mihály Kállay, Jürgen Gauss, Edward F. Valeev, Bradley A. Flowers, Juana Vázquez, and John F. Stanton. Heat: High accuracy extrapolated *ab initio* thermochemistry. *The Journal of Chemical Physics*, 121(23):11599–11613, 2004.

[87] Matthew P. Jacobson, Robert J. Silbey, and Robert W. Field. Local mode behavior in the acetylene bending system. *The Journal of Chemical Physics*, 110(2):845–859, 1999.

[88] Joshua H. Baraban, P. Bryan Changala, Anthony J. Merer, Adam H. Steeves, Hans A. Bechtel, and Robert W. Field. The $\tilde{A}\ ^1A_u$ state of acetylene: *ungerade* vibrational levels in the region 45800-46500 cm^{-1}. *Molecular Physics*, 110(21-22):2707–2723, 2012. FASE special issue.

[89] Horst Koppel, Bernd Schubert, and Hans Lischka. Conical intersections and strong nonadiabatic coupling effects in singlet-excited acetylene: An *ab initio* quantum dynamical study. *Chemical Physics*, 343(2-3):319 – 328, 2008. Theoretical Spectroscopy and its Impact on Experiment (in honour of Sigrid D. Peyerimhoff).

[90] W. J. Lafferty and A. S. Pine. Spectroscopic constants for the 2.5 and 3.0 μm bands of acetylene. *Journal of Molecular Spectroscopy*, 141(2):223 – 230, 1990.

[91] N. Yamakita and S. Tsuchiya. Zeeman quantum beat observed by IR-UV double resonance LIF spectroscopy of acetylene in the $\tilde{A}\ ^1A_u$ $3\nu_3' + \nu_6'$ and $3\nu_3' + \nu_4'$ *ungerade* vibrational states. *Chemical Physics Letters*, 348(1):53–59, 2001.

[92] M. Herman, J. Liévin, J. V. Auwera, and A. Campargue. Global and Accurate Vibration Hamiltonians from High-Resolution Molecular Spectroscopy. *Advances in Chemical Physics*, 108:1–431, 1999.

[93] M. A. Payne, A. P. Milce, M. J. Frost, and B. J. Orr. Symmetry-breaking collisional energy transfer in the $4\nu_{CH}$ rovibrational manifold of acetylene: spectroscopic evidence of a quasi-continuum of background states. *Chemical Physics Letters*, 324(1-3):48 – 56, 2000.

[94] I. M. Mills. Vibration-Rotation Structure in Asymmetric-and Symmetric-top molecules. In K. N. Rao and C. W. Mathews, editors, *Molecular Spectroscopy: Modern Research*, chapter 3.2. Academic Press, 1972.

[95] Jan Almlöf and Peter R. Taylor. General contraction of Gaussian basis sets. I. Atomic natural orbitals for first- and second-row atoms. *The Journal of Chemical Physics*, 86(7):4070–4077, 1987.

[96] Jan M. L. Martin and Peter R. Taylor. Benchmark *ab initio* thermochemistry of the isomers of diimide, N_2H_2, using accurate computed structures and anharmonic force fields. *Molecular Physics*, 96(4):681–692, 1999.

[97] P. Bryan Changala. Spectroscopy and Theory of *cis-trans* Isomerization in the S_1 State of Acetylene. Bachelor's thesis, Massachusetts Institute of Technology, 2013.

[98] S. Arrhenius. *Zeitschrift für physikalische Chemie*, volume 2, pages 226–248. Akademische Verlagsgesellschaft Geest & Portig, 1889.

[99] Henry Eyring. The activated complex in chemical reactions. *The Journal of Chemical Physics*, 3(2):107–115, 1935.

[100] H. Eyring and M. Polanyi. Ueber einfache gasreaktionen. *Z. Phys. Chem B*, 12:279, 1931.

[101] M. G. Evans and M. Polanyi. Some applications of the transition state method to the calculation of reaction velocities, especially in solution. *Trans. Faraday Soc.*, 31:875–894, 1935.

[102] Edward R. Lovejoy, Sang Kyu Kim, and C. Bradley Moore. Observation of transition-state vibrational thresholds in the rate of dissociation of ketene. *Science*, 256(5063):1541–1544, 1992.

[103] John C. Polanyi and Ahmed H. Zewail. Direct observation of the transition state. *Accounts of Chemical Research*, 28(3):119–132, 1995.

[104] M. S. Child, M. P. Jacobson, and C. D. Cooper. Scaling laws for strongly anharmonic vibrational matrix elements. *The Journal of Physical Chemistry A*, 105(48):10791–10799, 2001.

[105] Mark S. Child. Quantum states in a champagne bottle. *Journal of Physics A: Mathematical and General*, 31(2):657, 1998.

[106] N. Moiseyev. *Non-Hermitian Quantum Mechanics*. Non-Hermitian Quantum Mechanics. Cambridge University Press, 2011.

[107] R. T. Birge and H. Sponer. The heat of dissociation of non-polar molecules. *Phys. Rev.*, 28:259–283, Aug 1926.

[108] Robert J. Leroy and Richard B. Bernstein. Dissociation energies of diatomic molecules from vibrational spacings of higher levels: application to the halogens. *Chemical Physics Letters*, 5(1):42 – 44, 1970.

[109] R. N. Dixon. Higher vibrational levels of a bent triatomic molecule. *Trans. Faraday Soc.*, 60:1363–1368, 1964.

[110] Haruki Ishikawa, Robert W. Field, S. C. Farantos, M. Joyeux, J. Koput, C. Beck, and R. Schinke. HCP $\leftrightarrow$ CPH isomerization: Caught in the act. *Annual Review of Physical Chemistry*, 50:443–484, 1999.

[111] Matthew P. Jacobson and Mark S. Child. Spectroscopic signatures of bond-breaking internal rotation. II. Rotation-vibration level structure and quantum monodromy in HCP. *The Journal of Chemical Physics*, 114(1):262–275, 2001.

[112] Mark S. Child. *Quantum Monodromy and Molecular Spectroscopy*, volume 136 of *Advances in Chemical Physics*, chapter 2, pages 39–94. John Wiley & Sons, Inc., 2008.

[113] Danielle Larese and Francesco Iachello. A study of quantum phase transitions and quantum monodromy in the bending motion of non-rigid molecules. *Journal of Molecular Structure*, 1006(1–3):611 – 628, 2011.

[114] Shuangbo Yang, Vivian Tyng, and Michael E. Kellman. Spectral Patterns of Isomerizing Systems. *The Journal of Physical Chemistry A*, 107(40):8345–8354, 2003.

[115] M. S. Child and R. T. Lawton. Local and normal vibrational states: a harmonically coupled anharmonic-oscillator model. *Faraday Discuss. Chem. Soc.*, 71:273–285, 1981.

[116] Masaaki Fujii, Akimitsu Haijima, and Mitsuo Ito. Predissociation of acetylene in $\tilde{A}\ ^1A_u$ state. *Chemical Physics Letters*, 150(6):380 – 385, 1988.

[117] Akimitsu Haijima, Masaaki Fujii, and Mitsuo Ito. Predissociation of the acetylene $\tilde{A}\ ^1A_u$ state and its mechanism. *The Journal of Chemical Physics*, 92(2):959–968, 1990.

[118] Nami Yamakita, Sayoko Iwamoto, and Soji Tsuchiya. Predissociation of excited acetylene in the $\tilde{A}\ ^1A_u$ state around the adiabatic dissociation threshold as studied by LIF and H-atom action spectroscopy. *The Journal of Physical Chemistry A*, 107(15):2597–2605, 2003.

[119] Toshinori Suzuki and Nobuhisa Hashimoto. Predissociation of acetylene from the $\tilde{A}\ ^1A_u$ state studied by absorption, laser-induced fluorescence, and H-atom action spectroscopies. *Journal of Chemical Physics*, 110(4):2042–2050, JAN 22 1999.

[120] Nobuhisa Hashimoto, Nobuaki Yonekura, and Toshinori Suzuki. Pump-probe measurements of the predissociation reaction time of C_2H_2 from $\tilde{A}\ ^1A_u$ state. *Chemical Physics Letters*, 264(5):545–550, JAN 17 1997.

[121] Nobuhisa Hashimoto and Toshinori Suzuki. Energy and state dependence in the quenching and predissociation of C_2H_2. *Journal of Chemical Physics*, 104(15):6070–6073, APR 15 1996.

[122] Yoshihiro Osamura, Fujiko Mitsuhashi, and Suehiro Iwata. A theoretical study of the photodissociation of acetylene in its lowest excited singlet state. *Chemical Physics Letters*, 164(2-3):205 – 209, 1989.

[123] David H. Mordaunt, Michael N. R. Ashfold, Richard N. Dixon, Peter Löffler, Ludger Schnieder, and Karl H. Welge. Near threshold photodissociation of acetylene. *The Journal of Chemical Physics*, 108(2):519–526, 1998.

[124] Toshinori Suzuki, Yang Shi, and Hiroshi Kohguchi. Detection of metastable triplet acetylene produced by intersystem crossing from the excited $\tilde{A}\ ^1A_u$ state. *The Journal of Chemical Physics*, 106(12):5292–5295, 1997.

[125] David P. Baldwin, Mark A. Buntine, and David W. Chandler. Photodissociation of acetylene: Determination of D_0^0 (HCC–H) by photofragment imaging. *The Journal of Chemical Physics*, 93(9):6578–6584, 1990.

[126] Bernadette M. Broderick, Yumin Lee, Michael B. Doyle, Oleg S. Vasyutinskii, and Arthur G. Suits. The Velocity Dependence of Hydrogen Atom Spin Polarization. *Nature Physics*, 2013, submitted.

[127] John Archibald Wheeler. *Studies in Mathematical Physics: Essays in Honor of Valentine Bargmann*, page 351. Princeton University Press, 1976.

[128] M. W. Cole and R. H. Good. Determination of the shape of a potential barrier from the tunneling transmission coefficient. *Phys. Rev. A*, 18:1085–1088, Sep 1978.

[129] Petri Pajunen and Mark S. Child. Semiclassical inversion of a symmetric double well potential. *Molecular Physics*, 40(3):597–604, 1980.

[130] J.-M. Flaud, C. Camy-Peyret, J. W. C. Johns, and B. Carli. The far infrared spectrum of H_2O_2. First observation of the staggering of the levels and determination of the cis barrier. *The Journal of Chemical Physics*, 91(3):1504–1510, 1989.

[131] C. Camy-Peyret, J.-M. Flaud, J. W. C. Johns, and M. Noël. Torsion-Vibration Interaction in H_2O_2: First High-Resolution Observation of ν_3. *Journal of Molecular Spectroscopy*, 155(1):84–104, 1992.

[132] Xu Zhang, Anders V. Friderichsen, Sreela Nandi, G. Barney Ellison, Donald E. David, J. Thomas McKinnon, Theodore G. Lindeman, David C. Dayton, and Mark R. Nimlos. Intense, hyperthermal source of organic radicals for matrix-isolation spectroscopy. *Review of Scientific Instruments*, 74(6):3077–3086, 2003.

[133] Peter Chen, Steven D. Colson, William A. Chupka, and Jerome A. Berson. Flash Pyrolytic Production of Rotationally Cold Free Radicals in a Supersonic Jet. Resonant Multiphoton Spectrum of the 3p $^2A_2'' \leftarrow X\ ^2A_2''$ Origin Band of CH_3. *The Journal of Physical Chemistry*, 90(11):2319–2321, 1986.

[134] J. Stark and P. Lipp. The effect of inner molecular relative movement on the intensity of absorption of flourescent by valence electrons. *Zeitschrift Fur Physikalische Chemie–Stochiometrie Und Verwandtschaftslehre*, 86(1):36–50, DEC 1913.